KATHMANDU UNIVERSITY
SCHOOL OF ENGINEERING
DEPARTMENT OF CIVIL ENGINEERING

Final Report

on

NUMERICAL MODELING FOR ANALYSIS AND DESIGN OF TUNNEL SUPPORT IN WEAK GROUND CONDITIONS

Case Studies from Nepal Himalayas

In Partial Fulfillment of the Requirements for the
Master Degree in Civil Engineering

Sujan Karki
*[**Reg. No.**: 017257-14]*

September 2021

Thesis Grant
supported by
Nepal Academy of Science and Technology (NAST)

Copyright © 2021 Sujan Karki

Declaration

This master thesis titled *"Numerical Modeling for Analysis and Design of Tunnel Support in Weak Ground Conditions - Case Studies from Nepal Himalayas"* is submitted to the Department of Civil Engineering for the requirement to partial fulfillment of MS by Research degree in Civil Engineering conducted by Kathmandu University, Nepal. The research work is a genuine work done under the supervision of Dr. Shyam Sundar Khadka and has not been submitted to any other universities or institutions.

This study mainly focuses on the use of numerical modeling technique to design support system in weak rock mass of the Himalayas. Three case studies have been taken for the study and a support guideline has been provided which have been verified by the results of numerical analysis. A methodology has also been provided for two-dimensional modeling of weak rocks which can be adopted for the design of underground constructions in the Himalayan region. All the data and literature referred from other literary works and cited in this study have been duly acknowledged and provided in the references.

I hereby declare that I am the sole author of this thesis and allow Kathmandu University to reproduce the thesis by photocopying or by other means, in total or in part, at the request of other institutions or individuals for the purpose of scholarly research.

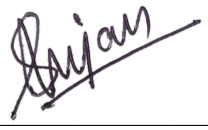

Sujan Karki
Reg. No.: 017257-14
September 2021

Dissertation Evaluation

Numerical Modeling for Analysis and Design of Tunnel Support in Weak Ground Conditions - Case Studies from Nepal Himalayas

by

Sujan Karki

This is to certify that I have examined the above Dissertation thesis and have found that it is complete and satisfactory in all respects, and that any and all revisions required by the thesis examination committee have been made.

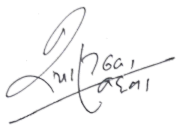

Shyam Sundar Khadka, PhD
Assistant Professor
Supervisor & Head of Department
Department of Civil Engineering

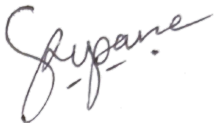

Er. Shri Ram Neupane
External Examiner
Executive Chairman
Megatech Hydro & Infrastructure Pvt. Ltd.

Prof. Manish Pokharel, PhD
Dean, School of Engineering
Kathmandu University

September 2021

Acknowledgment

I express my sincere gratitude to the Department of Civil Engineering and Research Division, Kathmandu University for allowing and supporting me to conduct my research in this field. I am especially thankful to my supervisor and Head of Department, Dr. Shyam Sundar Khadka for his valuable guidance, suggestions and motivation throughout the period of my studies. I would also like to thank my colleague Bimal Chhushyabaga who has helped me academically and professionally during my research. I thank Mr. Cheta Sushling Magar, who aided me during all the laboratory activities from laboratory setup to sample testing. Finally, I thank the Rock Mechanics and Rock Engineering Lab for allowing to conduct all the tests required for my studies.

I have my gratitude towards all the faculties of the Department of Civil Engineering and my seniors and colleagues from Department of Mechanical Engineering for their motivation and support. Also, I am grateful to Dr. Pawan Kumar Shrestha and the entire Hydro Tunnelling and Research team for directly or indirectly supporting me during my studies.

I express my gratitude to Nepal Academy of Science and Technology (NAST) for the financial assistance through 'Master Thesis Grant 2077/78'. Also, I would like to thank Department of Civil Engineering for providing me the opportunity for field visits during my study period through the *ENEP-RENP-II-18-02* project awarded by the Energize Nepal programme, Kathmandu University.

Lastly, I thank my family who have supported me during the duration of my studies, my friends who provided valuable suggestions and all the personnel who have directly or indirectly helped me in completing my thesis.

Executive Summary

Nepal is a country with potential for hydropower development because of its fast flowing rivers and steep terrain. Due to the geological setting of the country, almost all the hydropower required underground structure like tunnels and caverns for efficient development. However, the challenge for underground construction in the country persists due to the weak geology as a result of frequent seismic activities and presence of discontinuities like faults. Recently, the country is developing rapidly in the field of tunneling with its construction for transportation and water ways. Due to the presence of weak geology with high rock cover, problems of squeezing and collapse are frequently encountered. Such problems not only increase the cost of the project but it also severely delays the construction process.

The current practice in the country is to rely on Rock Mass Classification approaches for classification and design of underground supports. These approaches although provide a sound basis for rock classification, they fail to address the support requirement especially for weak geology. In absence of a proper support guideline for the weak rocks, the design relies on the expertise of the engineer and the designer. So, the study aims in providing a support guideline for the weak rocks in the Himalayas. Through the use of numerical modeling technique, stability analysis have been done for three hydropower tunnels in the Lesser Himalayan region of Nepal. Eight sections from poor to exceptionally poor rock mass have been taken for study and support has been designed such that they are able to successfully sustain the ground stress thus providing a safe support system.

Two dimensional finite element modeling has been done to study the effect of support on the stability of the rock mass. A methodology has been prepared for modeling such weak rocks in two dimensional method with the inclusion of face support such as the forepole. Stress distribution around an opening has been studied and support is recommended to sustain those ground stress. Highlight has been made on the sequence of installation support in the numerical model since it plays an important role in the opening stability. Providing support too early or too late can lead to failure of the supports and the excavation in general. Analytical method has been used to determine the location of support installation. The rock model have been developed as elastic plastic and strain softening and Generalized Hoek-Brown failure criteria has been utilized.

Finally comparison of the empirical defined support with the support elements in practice in the country and a support guideline has been prepared utilizing the support elements currently used for underground excavations. For very poor rock mass, yielding support has also been studied. It was found that yielding supports

provide an economic solution for supporting the rock mass during construction by providing robust support for the stability, at the same time providing flexibility for allowing the ground to deform. This solution works well with the extreme squeezing ground as verified from the selected case studies. The results are then used to define a limiting value for the use of yielding support based on the rock mass strength and in-situ stress.

Contents

Acknowledgments i
Executive Summary iii
List of Figures xii
List of Tables xiv

I Introduction **1**
1.1 Background 1
1.2 Tunnels in Nepal 2
1.3 Need of Study 3
1.4 Objectives 4
1.5 Scope of Research 5
1.6 Research Methodology 5
1.7 Organization of Report 8

II Design of Tunnel Support **9**
2.1 Geology of Himalayas 9
2.2 Rock Mass Classifications 11
2.2.1 Terzaghi Rock Mass Classification 11
2.2.2 Rock Quality Designation (RQD) 11
2.2.3 Rock Mass Rating (RMR) 12
2.2.4 Rock Quality Index (Q-System) 15
2.2.5 Geological Strength Index (GSI) 19
2.3 Rock stress redistribution 21
2.4 Design Practice of Hydropower Tunnels 30
2.4.1 Empirical Methods 30
2.4.2 Analytical Method 31
2.4.3 Numerical Modeling 33
2.4.4 Construction Practice 33
2.5 Conclusion 34

III Analysis and Modeling of Supports **37**
3.1 General 37
3.1.1 Development of model 38
3.1.2 Development of equivalent section 39
3.1.3 Equivalent section and Capacity Curve 39
3.1.4 Analysis 42
3.2 Modeling in Weak Rocks 44

3.2.1 Rock Failure Models . . . 45
3.2.2 Selection of Residual Parameters . . . 49
3.2.3 Two-Dimensional modeling of face support . . . 50
3.3 Conclusion . . . 53

IV Description of Case Studies **57**
4.1 General . . . 57
4.2 Chameliya Hydropower Tunnel . . . 57
4.2.1 Introduction . . . 57
4.2.2 Geology of Area . . . 57
4.2.3 Design of Tunnel Support . . . 59
4.2.4 Instability Problems . . . 61
4.3 Kaligandaki 'A' Hydropower Tunnel . . . 62
4.3.1 Introduction . . . 62
4.3.2 Geology of Area . . . 62
4.3.3 Design of Tunnel Support . . . 64
4.3.4 Instability Problems . . . 64
4.4 Khimti Hydropower Tunnel . . . 65
4.4.1 Introduction . . . 65
4.4.2 Geology of Area . . . 66
4.4.3 Design of Tunnel Support . . . 67
4.4.4 Instability Problems . . . 69

V Numerical Modelling **71**
5.1 General . . . 71
5.2 Finite Element Model . . . 72
5.3 Numerical Steps . . . 75
5.4 Analyzed Tunnel Sections . . . 76
5.5 Estimation of Rock Parameters . . . 78
5.6 Procedure of Modeling . . . 81
5.7 Results . . . 84
5.7.1 Case Study: Chameliya Headrace Tunnel . . . 84
5.7.2 Case Study: Kaligandaki A and Khimti I Headrace Tunnel . . . 97
5.8 Analysis and Discussion . . . 102

VI Conclusion **107**

References **118**

Appendix A Empirical approach of rock mass classification **i**

Appendix B Ratings for rock mass classifications ix

Appendix C Rock Mass Parameter selection guidelines xxiii

Appendix D Equations for the analysis of arches made of composite sections xxix

Publications xxxv

List of Figures

Figure 1.1: Work methodology for the study. 7

Figure 2.1: Geological Map of Nepal (Upreti, 1999) 10
Figure 2.2: Example of obtaining RQD for a rock core (Deere & Deere, 1988) 12
Figure 2.3: RMR calculation algorithm (Aksoy, 2008) 14
Figure 2.4: Results of five years of monitoring test-tunnel sections in mudstone, using four different support and reinforcement measures (left) and Representation of the relative stiffness of different support measures (right) Barton (2015) 16
Figure 2.5: Stress distribution in a circular opening in homogeneous, elastic rock mass (Panthi, 2006) 23
Figure 2.6: Effect of plastic zone in tangential stress distribution around a circular opening (Bray, 1967) 24
Figure 2.7: Stress distribution around circular opening after application of support (G. L. Shrestha, 2005) 24
Figure 2.8: Stress concentration around circular tunnel in non-hydrostatic state of in-situ stress (B. Singh & Goel, 2006). 26
Figure 2.9: (a) Effect of radius of opening on K_t for an infinite sheet under tension and (b) Graphical representation of stress concentration on the tip of openings (Schijve, 2009) 27
Figure 2.10: Variation of K_t with radius of curvature in a fillet (Schijve, 2009) 28
Figure 2.11: (a) Distribution of normal stress around the opening in three layered medium (Agarwal & Boshkov, 1968) and (b) Variation of floor stress of openings in a three layered medium of different material properties (Barla, 1970) 29
Figure 2.12: Semi-empirical method for classifying rocks based on strain values (Hoek & Marinos, 2000) 31
Figure 2.13: (a) Cylindrical tunnel of radius R driven in the rock mass, (b) Cross-section of the rock mass at the section A-A' and (c) Cross-Section of the circular support installed at section A-A' (Carranza-Torres & Fairhurst, 2000) 32
Figure 2.14: Design process for estimation of tunnel support (Khakda, 2019) 35

Figure 3.1: Ground loading of circular excavation according to ground support interaction approach. 39
Figure 3.2: Schematic diagram of composite support along with equivalent support. 40
Figure 3.3: Sectional view of (a) S&S beam, (b) R&S beam and (c) RRS Support. 40
Figure 3.4: Distribution of total moment in various liners. 44
Figure 3.5: Thrust-Moment interaction diagram for shotcrete element in composite section. 45
Figure 3.6: Bending moment acting over the individual element in the composite sections. 46
Figure 3.7: Percent distribution of moment in individual elements of the composite supports. 47
Figure 3.8: Post failure characteristics of different quality of rock mass. (Khakda, 2019; Lorig & Varona, 2013) 47
Figure 3.9: Stress – strain curves for Tennessee Marble at different confining stresses. (Wawersik & Fairhurst, 1970) 48
Figure 3.10: Use of spiling bolt support in tunnels from Lesser Himalayas region of Nepal. 51
Figure 3.11: Methodology for pre-support of excavation in weak rock mass. 52
Figure 3.12: Results from RocLab for Chainage 3+190 m of Chameliya headrace tunnel. 53

Figure 4.1: Longitudinal geological map of Chameliya hydropower tunnel along the alignment (Khakda, 2019) 58
Figure 4.2: Orientation of major joint sets and headrace tunnel alignment of Chameliya HEP (NEA, 1997) 58
Figure 4.3: Tunnel support used in Chameliya headrace tunnel (Shah, 2016) 60
Figure 4.4: (a) Squeezing and (b) Mud flow in sections of Chameliya headrace tunnel (Shah, 2016) 62
Figure 4.5: Geological Profile of Kaligandaki 'A' headrace tunnel (Khakda, 2019) 63
Figure 4.6: (a) Orientation of main joint sets and Kaligandaki 'A' headrace tunnel (Panthi, 2006) and (b) Typical tunnel section with applied supports (P. K. Shrestha & Panthi, 2014a) . . 63
Figure 4.7: (a) Collapse due to strength and stress anisotropy and (b) Cracks formed in the lining due to high squeezing pressure (Panthi, 2006) 65

Figure 4.8: Geological profile of Khimti I hydropower project (Panthi, 2006) 66
Figure 4.9: Orientation of main joint sets and headrace tunnel of Khimti I hydropower (Panthi, 2006) 67
Figure 4.10: Tunnel instability (a) collapse after application of support and (b) open and permeable joints within gneiss (Panthi, 2006) 69

Figure 5.1: Two-dimensional modeling approaches (Moldovan & Popa, 2012) 73
Figure 5.2: Circular tunnel in an elasto-plastic rock mass subjected to hydrostatic initial stress field (Sofiano & Nomikos, 2006) . . 74
Figure 5.3: 2D model developed for the analysis of sections *This is a representative model for section at Ch. 3+190 m of Chameliya HRT).* 75
Figure 5.4: Methodology adopted for numerical modeling in *RS2*. 84
Figure 5.5: Longitudinal Deformation Profile for selected sections of Chameliya headrace tunnel. 85
Figure 5.6: (a)Bending moment and (b) Failure region of liners for designed (site provided) support for Ch. 3+190 m of Chameliya HRT. 86
Figure 5.7: Bending moment and failure point for (a) Shotcrete element and (b) RRS element in Q recommended support for Ch. 3+190 m of Chameliya HRT. 86
Figure 5.8: Bending moment and failure point for (a) concrete and (b) steel beam element in modified support for Ch. 3+190 m of Chameliya HRT. 88
Figure 5.9: Bending moment around the liner for different support systems for Ch. 3+190 m of Chameliya HRT. 88
Figure 5.10: Capacity Plot for (a) shotcrete element and (b) RRS element for Q recommended support for Ch. 3+404 m of Chameliya HRT. 89
Figure 5.11: Modified support in Section (a) 3+190 m and (b) 3+404 m. *(All dimensions are in meters unless specified and forepole support has not been shown in the figure but applied in the model)* 90
Figure 5.12: Stress distribution around (a) Horse-shoe and (b) Circular excavation for section at chainge 3+190 m of Chameliya headrace tunnel. 92

Figure 5.13: (a) Schematic diagram showing yielding liner and (b) Sliding gap in steel sets (Hoek & Briceno, 2009) 92
Figure 5.14: Effect of support with and without sliding gap in ground deformation in sections from Chameliya HRT. 94
Figure 5.15: (a) Bending moment and (b) Capacity Plot for liner with sliding gaps for Ch. 3+190 m of Chameliya HRT. 95
Figure 5.16: Capacity Plot for final concrete lining after installation of yielding support in Ch. 3+404 m of Chameliya HRT. 96
Figure 5.17: Squeezing treatment of failed section in Chameliya headrace tunnel (Shah, 2016) 98
Figure 5.18: LDP for study sections of Kaligandaki A and Khimti I HRT. 99
Figure 5.19: (a) Support element with bending moment and (b) Capacity Plot for liners in Ch. 0+763 m of Kaligandaki A HRT. . . . 100
Figure 5.20: Support element for (a) Yielding support in horseshoe excavation and (b) Circular excavation for Ch. 2+167 m of Kaligandaki A HEP. 101
Figure 5.21: Support recommendation for the underground construction in Himalayan rock mass. 104
Figure 5.22: Region for circular excavation and yielding support (with changes made in the original chart from Figure 2.12). 106

Figure A.1: Prediction of squeezing by Singh, Jethwa, Dube, and Singh (1992). vi
Figure A.2: Prediction of squeezing by R. K. Goel, Jethwa, and Paithankar (1995a). vi
Figure A.3: Prediction of squeezing by Jimenez and Recio (2011). vii

Figure B.1: Estimate of GSI based on visual inspection of geological conditions (Cai, Kaiser, Uno, Tasaka, & Minami, 2004) xv
Figure B.2: Examples of Joint wall surface. xviii
Figure B.3: Permanent support recommendation based on Q value (NGI, 2015) xxi

Figure C.1: Guidelines for estimating disturbance factor D (Hoek, Carranza-Torres, & Corkum, 2002) xxiii

List of Tables

Table 2.1: Geomorphic units of Nepal and main types of rocks (Upreti, 1999) 10
Table 2.2: Classification of rocks based on RQD values (Deere & Deere, 1988) 12
Table 2.3: Adjustment of Joint orientation (Bieniawski, 1989) 14
Table 2.4: Design parameter and engineering properties of rock mass (Bieniawski, 1989) 14
Table 2.5: Values of ESR. 18
Table 2.6: Fitness of Q system in various types of ground behavior in tunnels (Palmstrom & Broch, 2006) 19

Table 3.1: Ground parameters used for modelling 38
Table 3.2: Properties of elements in a composite section. 42
Table 3.3: Thickness and modulus of equivalent section for different composites. 42
Table 3.4: Reduction in peak GSI for determining the residual GSI value. (Khakda, 2019) 50

Table 4.1: Details of squeezing section from chainage 3+172 to 3+820 m in Chameliya headrace tunnel (Basnet, 2013; Khakda, 2019) . 59
Table 4.2: Rock mass classification and support pattern for Chameliya hydropower tunnel based on the Q-system (Khakda, 2019) . . 61
Table 4.3: Recommended tunnel support for Khimti hydropower project (for tunnel width of 4 m and ESR of 1.6) (G. L. Shrestha, 2005) 68
Table 4.4: Supplementary design principles for squeezing ground in Khimti I HEP(G. L. Shrestha, 2005) 69

Table 5.1: Properties of support elements used for the analysis of study sections. 76
Table 5.2: Rock Mass Parameters for study sections from selected case studies. 77
Table 5.3: Q Recommended and Designed Support for selected sections of Chameliya headrace tunnel. 91
Table 5.4: Remedy and tunnel supports used for squeezing ground in Chameliya headrace tunnel (Shah, 2016) 97

Table 5.5: Deformation values with corresponding support: Results from numerical analysis. 103
Table 5.6: Support recommendation for weak rock mass of the Himalayas. 104

Table A.1: Wall factor for various ranges of Q value (Barton, Lien, & Lunde, 1974) i
Table A.2: Correction factor f' for tunnel closure (Singh et al., 1992) . . ii
Table A.3: Correction factor for tunnel closure (R. K. Goel et al., 1995a) iii
Table A.4: Classification of the degree of squeezing (Aydan, Akagi, & Kawamoto, 1993) v

Table B.1: Rock classes given by Terzaghi (Terzaghi, 1946) ix
Table B.2: Rating of strength of intact rocks. xi
Table B.3: Rating for RQD values. xi
Table B.4: Rating for discontinuity spacing. xi
Table B.5: Rating for condition of discontinuity. xi
Table B.6: Guideline for classification of discontinuity condition. xii
Table B.7: Rating for groundwater condition. xii
Table B.8: Characterization of discontinuity orientation related to underground excavation. xii
Table B.9: Guidelines for excavation and support of rock tunnels in accordance to RMR. xiii
Table B.10: Joint set number. xvii
Table B.11: Joint roughness number. xviii
Table B.12: Joint alteration number. xix
Table B.13: Joint water reduction factor. xix
Table B.14: Stress Reduction Factor. xx

Table C.1: Field estimate of Uniaxial Compressive Strength (UCS) (Hoek, 2007) xxiv
Table C.2: Average Uniaxial Compressive strength (q_c) of a varity of rocks. measured on 50 mm diameter samples (Plamstrom, 2000) xxv
Table C.3: Values of constant m_i for intact rock, by rock group (Hoek, 2007) xxvi
Table C.4: Guideline for selection of Modulus Ratio (MR) values based on Deere (1968) and Palmstrom and Singh (2001) xxvii

Chapter I
Introduction

1.1 Background

Nepal covers the central portion of the Himalayas, with its extension of about 880 km from east to west and a width ranging from 150 to 250 km. This mountainous topography of the country creates opportunity and potential for development of underground structures as an economic and viable solution for transportation, storage, water divergence and mining (Panthi, 2004). However, the construction of these structures comes with great challenges as the geology of Himalayas is weak and fragile and subjected to frequent seismic activities. The compressional tectonic stress regime in the Himalaya has resulted in intense deformation of the rock mass, making it highly folded, sheared, fractured and deeply weathered. The presence of faults in the region has also added to the problems in underground construction. The major problems associated with underground construction is: squeezing in weak and deformable rocks and rock burst and spalling in very strong and brittle rocks.

During tunneling accuracy should be maintained from the start of geological investigation, as the results of the investigation plays a crucial role in selection of the tunnel alignment. However, the past tunneling experience in Nepal shows that the accuracy of planning phase geological investigations for underground works has often been rather poor (Panthi, 2008). Considerable discrepancies have been found between predicted and real rock mass conditions, resulting in significant cost and time overrun for most of the tunneling projects (Panthi & Nilsen, 2007). Due to the presence of major fault zones in the country: Main Central Thrust *MCT)*, Main Boundary Thrust *MBT*, Main Frontal Thrust *MFT*; weakness zones are created along the alignment of the tunnels, which, in many cases cannot be avoided. In such conditions, proper design of support systems with regular update and modification to the initially designed supports should be done, based on the encountered geological condition.

The current practice of support design in the country relies in the empirically established methods such as the Q and the Rock Mass Rating RMR systems. These methods, although used worldwide due to its reliability in optimum support recommendation, have in many cases proved to be insufficient for the Himalayan geology. The Himalayas is considered as a tectonically active zone and the nature of rocks here are weak with many discontinuities due to which the empirical methods are unable address all of its uncertainties. Thus, the final support lining design heavily relies on

the judgment of engineers and geologists. This could result in under or over support to the structures. Under estimation of support system leads to failure of the structure while over estimation leads to unnecessary increase in the overall cost of the project. This problem could be solved if a standard guideline, with the necessary changes in existing rock mass classifications, can be developed. However, in the present situation, use of computational technique during the design can help determine safe and economic support. The major challenge in using numerical technique is the reliability of the rock data used for modeling for which laboratory and field tests should be performed.

The present study addresses the need of the numerical technique and focuses on the development of a methodology for design of tunnel openings in weak rock mass conditions. An attempt has been made to establish a support guideline for tunneling in weak rocks through the results obtained via finite element analysis. The presented result is based on analysis of case studies from the Lesser Himalayan region where rock masses are weak, highly jointed, weathered, faulted, folded and tectonically disturbed with high overburden.

1.2 Tunnels in Nepal

Nepal has had a long history of tunnels with the first tunnel built around 1917 A.D. in the *Churiya* range in Hetauda. The 500 m tunnel was built to reduce the travel time between Hetauda and Amlekhganj with a dimension of 2.7 m width and 3 m height (Gartoula, 2019). The tunnel was build in a time when no support techniques or guidelines were available with locally available resources. Since then many tunnels have been build over time with more advances equipment and materials.

In 1978 A.D., the first hydropower tunnel, Tinau Hydroelectric Project situated at Dovan, Palpa District was constructed with joint initiative between their Majesty's Government of Nepal and the United Mission to Nepal *(UMN)*. The tunnel of length 2400 m has a cross-sectional area of 2.1 m^2. The project was commenced on 2022 B.S. (1966 A.D.), taking nearly 12 years for its completion. Similarly, other hydropower project that incorporated tunnel as the waterway is Kulekhani I hydropower project which was commissioned in 1982 A.D. with a tunnel length of 6233 m followed by Kulekhani II HPP of length 5847.8 m (NEA, n.d.). Adhikhola hydropower plant was commissioned on 1991 A.D. with the installed capacity of 5.1 MW. The headrace tunnel of the project is fully concrete lined having a length of 1284 m with the cross-section area of 7.5 m^2, drop shaft of 245 m having the diameter of 4.5 m and at last long a tailrace tunnel with the 1080 m having cross sectional area of 8.5 m^2. It also consists of cavern of size 37 m x 7 m x 10 m with the shotcrete support together with rock bolts (Hydro-Solutions, n.d.). Following them, Jhimruk hydropower Plant

was commissioned in 1994 A.D., located at Pyuthan district, Nepal. It incorporated a headrace tunnel of 1100 m length with the cross-sectional area of 8.5 m^2 and two inclined penstock tunnel of 280 m long (IHA, n.d.).

In transportation sector, Nepal government is constructing the Kathmandu Nijgadh Fast track of 76.2 km length connecting Khokana (Lalitpur) to Nijgadh (Bara). The projects consist of 1.35 km long twin tube tunnel with the purposed tunnel width of 11 m for 2 lanes of roadway and 22 m for 4 lanes of roadway respectively. Similarly, the road tunnel connecting Naubise and Thankot is being constructed by the Nepal government in collaboration with the Japan Government. The tunnel consists of 2.45 km of tunnel with two 3.5 m lanes and 2.5 m shoulder. In water supply and irrigation sector, Nepal government constructed the Melemchi water supply tunnel of length 27 km, one of the longest tunnel in Nepal. The project started operating from 2021 A.D. and supplies water from Melemchi river to Kathmandu Valley. While the Bheri Babai Diversion Multipurpose Project consist 12 km headrace tunnel structure which is constructed using the Tunnel Boring Machine (TBM) in the western region of Nepal.

1.3 Need of Study

The geology of Himalayas is highly folded, faulted, sheared and subjected to frequent seismic activities. This creates major challenges during the construction of underground structures in the region. The presence of weak rock mass along with the high rock cover creates another problem of excess inwards movement of the excavation boundary during the construction process. It is thus necessary to explore these challenges and design optimum and safe support systems to withstand them. In case of weak rock mass, the support system must be designed such that it provides safe working environment to the workers at the same time allowing some amount of inwards movement of rocks to allow relaxation of the stress. Allowing relaxation of the stress around the excavation offers economic solution to tunnel support design. This, however, is seldom practiced in the country. The design philosophy in the country is based on the empirically established Q system of rock mass classification. The problem with adopting the system is that the system was originally designed for hard rocks subjected to rock burst phenomena, which is not as seldom in the Himalayas. Although this empirical system offers flexible support (steel fiber reinforced shotcrete) compared to the tradition wire mesh shotcrete, the support estimate has proved to be inadequate in many cases for the Himalayan geology. The responsibility then lies in the engineer to estimate the required support for which they provide heavy, robust support in the weak regions.

In the absence of a proper support guideline for weak rock mass of the Himalayas,

the designers and engineers usually provide closely spaced steel ribs, covered by thick concrete lining as final supports upon encountering weak zones. This support combination, although overcomes the problem of squeezing ground in most cases, it unnecessarily increases the cost of the project. If the designers are to use numerical solutions instead of modifying the empirical guidelines, more economic and optimum support can be obtained. The use of numerical solutions allows to study the behavior of the rock mass subjected to the additional stress, created by the excavation process, more precisely. By use of visual graphs and stress distribution patterns, numerical solutions can provide designers the flexibility to design support as per the need of the rock mass condition. Behavior of the support to the ground conditions can be studied prior to installing the support in-situ, which allows saving time, money and life of the workers.

Only recently, the use of numerical modeling technique has been increasing in the Nepalese tunneling community and not all people are fluent in using the platform. There is thus a need to define a certain methodology that allows practitioner to follow and design supports for the weak rock mass condition. This study aims to fulfill the gap by designing a methodology for modeling of support in such rock mass condition by taking case histories of failed hydropower tunnels from the Nepal Himalayas. In the past, extreme squeezing was encountered in the Chameliya headrace tunnel despite providing heavy support linings and several other reports of failure of tunnel sections has been recorded. Thus, the methodology developed in this study is designed for weak ground conditions where the empirically determined support seems insufficient and is aimed at obtaining flexible and economic solution of underground support for such zones of failures. By studying the stress redistribution around the excavation, finite element modeling technique has been applied to design support system. The finite element software *RS2*, developed by *RocScience*, has been used to model a two-dimensional plain strain model and the study of interaction of rock mass and support system has been done to achieve the objective of the study.

1.4 Objectives

Primary Objective

- To analyze and design tunnel supports through numerical modeling for weak ground condition.

Secondary Objective

- To study stress distribution mechanism in underground structure.
- To review the rock mass classifications put in practice in Nepal Himalaya.

- To develop methodology for two-dimensional numerical modeling for weak grounds.
- To provide support recommendations for tunneling in weak rock masses.

1.5 Scope of Research

Underground construction has always been a challenge due to the presence of weak rock mass and high cover. Empirical methods are used for design of support linings in the region and since the methods have proved to be inadequate in several cases, necessary changes are made based on the decision of the engineers and geologists. Only recently, the use of numerical modeling is put into practice for tunnel design in the country. However, the difficulty lies in modeling of weak rocks by use of two-dimensional modeling techniques. In this regard, this study aims to address the gap by answering the following questions:

i Study the distribution of stress around an opening.
ii Define a methodology for tunnel support in weak rock mass condition through two-dimensional numerical modeling.
iii To compare the support lining practice in the country with the empirically recommended supports.
iv Provide support recommendation for tunneling in weak ground in the Himalayas.

In Nepal, due to lack of practice of proper data recording, it is difficult to obtain all the rock mass parameters required for modeling. For this, the case studies have been selected for which laboratory and field recorded data, information on rock mass quality logs and tunnel support details are available.

Despite these, the modeling has been done within the limits of two-dimensional, plain strain finite element method. Regarding the effects of dynamic loading, tectonic effect has been considered while obtaining the in-situ stress condition and other dynamic effects have not been considered. Similarly, the modeling has been done only considering the weak rocks and no faults and discontinuities has been included in the model, however, the rock strength parameters has been reduced to incorporate the weakening effects of the discontinuities. The effect of the groundwater has not been considered in the study assuming dry excavation by extracting the groundwater before the excavation process.

1.6 Research Methodology

The study and analysis of weak rock mass has been carried out in two stages. In the first stage a methodology has been created to model the support linings in the weak rock mass. Along with it, different supports has been analyzed for comparative study

of its behavior and performance. With the methodology defined, in the second stage (enclosed in the dashed box), different support combinations has been applied for the selected section of the case studies. With this, a support guideline has been created for weak rock mass. Three case studies from the Lower Himalayan Region has been selected for the study. The case studies have been selected based on the geological condition (preferably weak rocks), the availability of the rock mass parameters and information on tunnel supports. The overall work methodology has been shown as a flow chart given in Figure 1.1.

The meet the research objectives, the following tasks have been carried out:

i *Literature review* on
- Geology of the Nepal Himalayas
- Rock Mass Classifications and support design method
- Modeling and excavation in weak rock mass

ii *Data Collection*: Selection of case studies based on availability of rock mass data, tunnel logs and support details has been done. Necessary data on tunnel deformation, failure and support design was collected for the selected case studies from various sources like internet, field reports, research articles and academic reports.

iii *Modeling in weak rocks*: Based on empirical, analytical and numerical methods, support modeling for underground excavation has been done. Necessary rock mass parameters have been calculated and the parameters have been used to develop rock models for the selected sections. A methodology for face support in two-dimensional model has been created.

iv *Numerical Modeling*: Based on selected rock models, finite element modeling of the rock sections have been done using the commercially available software *RS2*. A methodology has been developed for modeling in the weak rock mass from which the results are validated against measured values.

v *Support Recommendations*: The support linings obtained from numerical modeling is compared with the lining recommendations from empirical method. Final lining recommendations are provided based on current practice and modeling results for the weak rocks in the Himalayas.

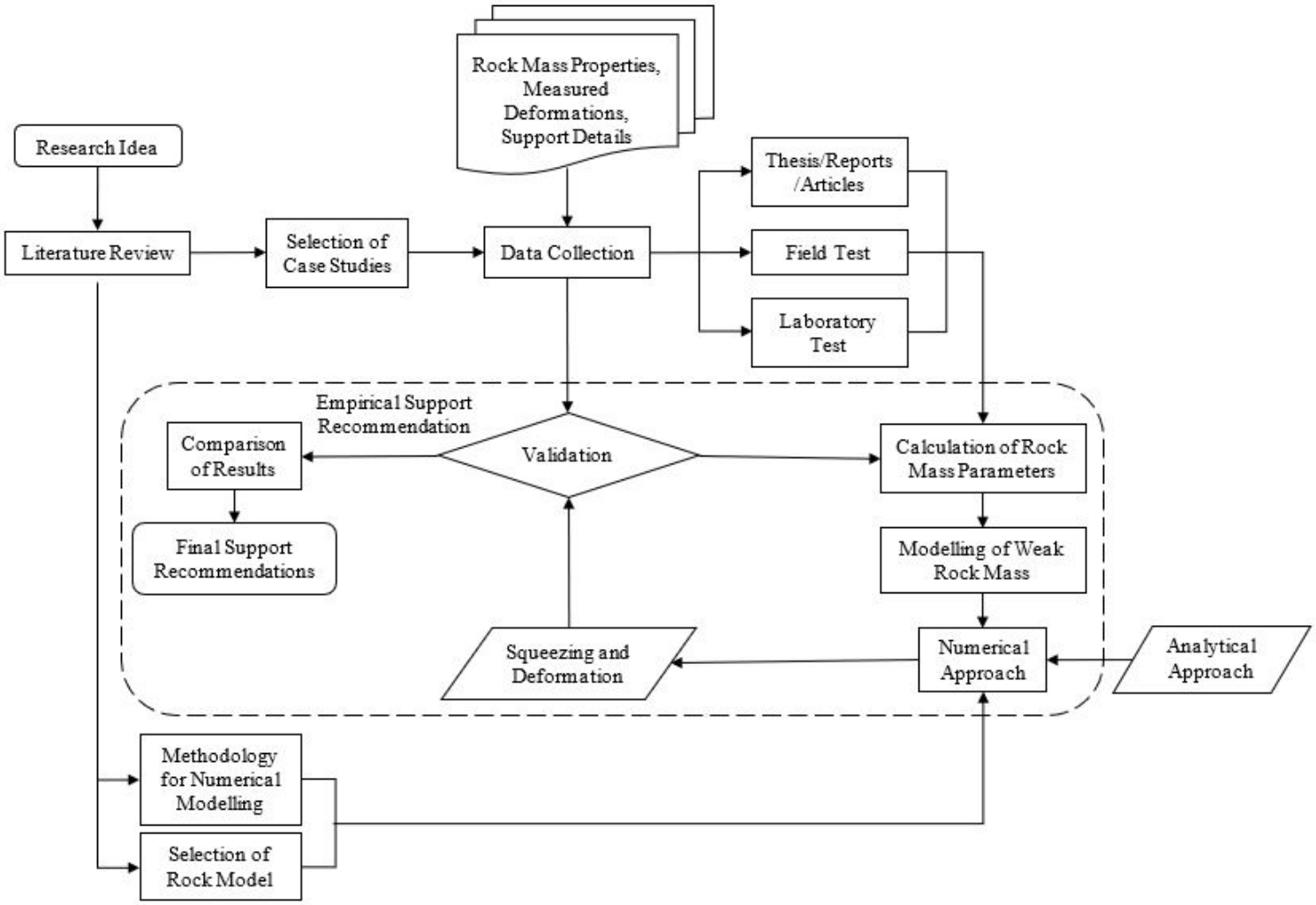

Figure 1.1: Work methodology for the study.

1.7 Organization of Report

This report is divided into six chapters with each chapters describing individual aspects in detail. The first chapter explains the objective and scope of the study along with the overall methodology implemented to conduct the study for this research.

The second chapter talks in detail about the different approaches for tunnel design. The chapter begins with the introduction to the Himalayan geology and goes on to explain the rock mass classification techniques for design of tunnel supports along with their limitations and shortcomings. Further the rock stress distribution around an underground excavation has been explained for various stress and ground condition.

Chapter three compares the performance of support elements with respect to their capacity and load distribution. The support elements are those used in the weak ground and later the chapter talks about the various rock models available to model the rock mass. The chapter concludes by providing a methodology for implementing face support via two dimensional numerical model.

Chapter four talks in detail about the selected case studies. It cover the geology of the selected hydropower tunnels along with the support system used during their design. Rock mass parameters have been provided for the cases in the chapter and the chapter also covers the instability problems encountered during the construction.

Chapter five covers the numerical modeling section with the details of the methodology implemented for modelling weak rocks. Results from two dimensional modeling of the selected section from the case studies have been discussed and the implementation of different supporting techniques has been talked about in this chapter. The chapter concludes by providing a support guideline and the criteria for the implementation of different supporting techniques.

Chapter six concludes the report by highlighting important results and findings of the study along with few recommendations for further study.

Chapter II
Design of Tunnel Support

2.1 Geology of Himalayas

The Himalayas covers the major portion of the geology of Nepal. The Himalayan range, formed by the collision of Indian Plate and the Eurasian plate, is 2500 km in length with width varying from 200-300 km. Nepal lies around the central section of this arc starting from the west at the *Mahakali* river and ending at the east by the *Mechi* river. Different authors have classified the Nepal's geology in different ways. Dhakal (2014) has classified Nepal Himalayas in five geological units: Indo-Gangetic Plane, Sub-Himalays, Lesser-Himalayas, Higher Himalayas and Inner Himalayas while Upreti (1999) has classified it into eight physiographic units: Terai, Siwalik, Dun Valleys, Mahabharat Range, Midland, Fore Himalayas, Higher Himalayas and Inner and Trans Himalayas. The geomorphic units of Nepal's geology is shown in Figure 2.1. The major types of rocks found in the Nepal, as summarized by Upreti (1999) is given in Table 2.1. The geomorphic units defined in Table 2.1 is separated by major fault systems. These faults creates a weakness zones in the geology which cause problems and difficulties during underground constructions. The major faults in the Himalayas and their arrangement from North towards South is listed below:

- Tibetan Tethys Zone
  - *South Tibetian Detachment System (STDS)*
- Higher Himalayas
  - *Main Central Thrust (MCT)*
- Mahabharat Range (Lesser Himalayas)
  - *Main Boundary Thrust (MBT)*
- Siwaliks (Churia)
  - *Main Frontal Thrust (MFT)*
- Gangetic Plane (Terai)

Along with the faults, the tectonic activity is also one of the major problems of Himalayas. Himalayas being one of the most tectonically active range, is subjected to frequent seismic activities. Along with it, heavy rainfalls has created several problems like rock failure, shallow landslides and debris flows. All these challenges make underground construction a challenge in the Himalayas.

Table 2.1: Geomorphic units of Nepal and main types of rocks (Upreti, 1999)

Geomorphic Unit	**Width (km)**	**Altitude (m)**	**Main rock types**
Gangetic Plane (Terai zone)	20–50	100–200	Alluvium deposits, coarse gravel in the north near the foot of mountains.
Siwaliks (Churia group)	10–50	200–1000	Sandstone, mudstone, shale and Conglomerate, etc.
Lesser Himalayan Zone	70–165	1000–5000	Schist, Phyllite, Gneiss, Quartzite, Granite, Marble and Dolomite
Higher Himalayan Zone	10–60	> 5000	Gneisses schists and Marbles
Tibetan-Tethys Zone	-	2500-4000	Gneisses schists and marbles of Higher Himalayan Zone and Tethyan sediments (limestone, shale, sandstone, etc.)

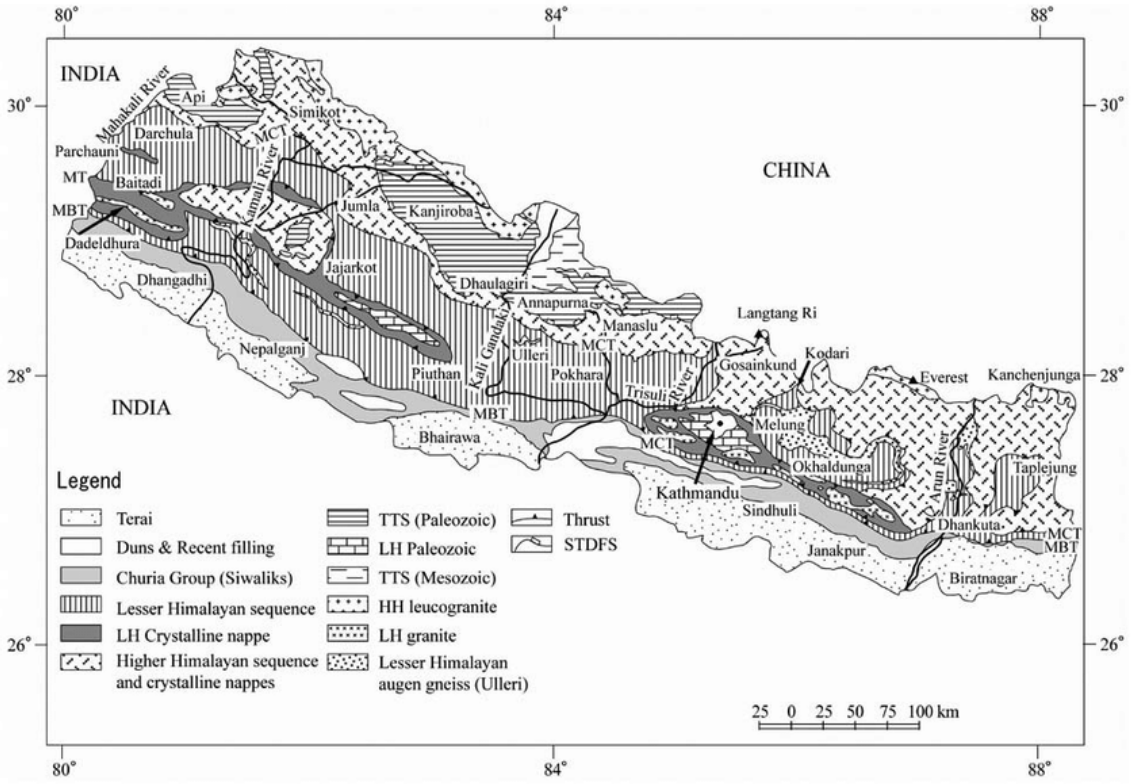

Figure 2.1: Geological Map of Nepal (Upreti, 1999)

2.2 Rock Mass Classifications

The support provided in the underground structures must be safe and economic. Providing the same support throughout the length of the opening not only increases the cost of the project but in some cases, can lead to failure due to accumulation of large amount of stress around the boundary. Some flexibility must be provided to the support such that some amount of stress is released. The support must thus be provided based on the quality and strength of the rocks. This leads to various support within sections of the same structure. The support to be provided in the tunnel can be determined from the rock mass classification system such as Rock Mass Rating *(RMR)*, Rock Quality Index *(Q)* or the Rock Mass Index *(RMi)*. The Geological Strength Index *(GSI)* also classifies the rock based on the geological structure but it does not provide information on type of support to be used. *GSI* is used in conjunction with *RMR* and *Q* system to determine the support required.

2.2.1 Terzaghi Rock Mass Classification

The Rock Mass Rating (RMR), Rock Quality Index (Q) and the Rock Mass Index (RMi) system was developed later compared to the descriptive classification provided by Terzaghi in 1946 (Terzaghi, 1946). He used rock mass characteristics that dominate the rock mass behavior, particularly in situations where gravity constitutes the dominant driving force and classified rocks into nine different classes from hard and intact rock to swelling rocks as given in Table B.1 (Terzaghi, 1946).

2.2.2 Rock Quality Designation (RQD)

The Rock Quality Designation index (*RQD*) was developed by Deere in 1964 to provide a quantitative estimate of rock mass quality from drill core logs. The *RQD* is a modified percent core recovery that incorporated only sound pieces of core that are 100 mm (4 in) or greater in length along the core axis. The core should be at least NW size (54.7 mm or 2.15 inches in diameter) and should be drilled with a double-tube core barrel. Equation (2.1) gives the relation for obtaining the *RQD* value in percent.The correct procedures for measurement of the length of core pieces and the calculation of *RQD* are summarized in Figure 2.2. The rocks are classified into five categories based on the *RQD* value and is given in Table 2.2.

$$RQD(\%) = \frac{\text{sum of core pieces} \geq 10cm}{totaldrillrun} * 100 \tag{2.1}$$

RQD is a directionally dependent parameter and its value may change significantly, depending upon the borehole orientation. The use of the volumetric joint count

Table 2.2: Classification of rocks based on RQD values (Deere & Deere, 1988)

S.No.	RQD (%)	Rock Quality
1	< 25	Very Poor
2	25–50	Poor
3	50–75	Fair
4	75–90	Good
5	90–100	Excellent

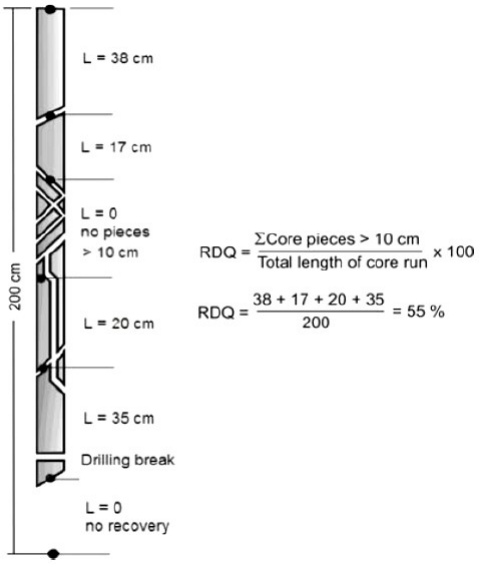

Figure 2.2: Example of obtaining RQD for a rock core (Deere & Deere, 1988)

can be quite useful in reducing this directional dependence. *RQD* is intended to represent the rock mass quality in-situ. When using diamond drill core, care must be taken to ensure that fractures, which have been caused by handling or the drilling process, are identified and ignored when determining the value of *RQD*. *RQD* alone is not sufficient to classify the rock mass as it neglects discontinuity orientation, discontinuity condition, type of discontinuity fillings and other features but forms an important part in other classification system such as *RMR* and *Q-system* (Zhang, 2017).

2.2.3 Rock Mass Rating (RMR)

The geomechanics classification *(RMR)* was initially developed by Bieniawski in 1973 which allowed determining the unsupported span of an underground opening, in shale and clay-bearing rocks, exposed to water and wetting-drying process. Since then, the classification system has undergone several changes: reduction of classification parameters from 8 to 6 in 1974; adjustment of ratings and reduction of recommended support requirements in 1975; modification of class boundaries to even multiples of 20 and involvement of Point Load Strength Index in 1976; adoption of ISRM (Inter-

national Society of Rock Mechanics) in 1979. Changes pertinent to the discontinuity condition and groundwater was made in 1979 and correction factor with regard to the discontinuity orientation was derived for tunnels, foundations and slopes (Bieniawski, 1973, 1974, 1976, 1978, 1979). The latest modifications of *RMR* system done are as follows (Bieniawski, 1984, 1988, 1989)

- "Parameter-score" graphs were introduced for more precise scoring;
- Parameters of discontinuity continuation, discontinuity spacing, roughness, back-fill and degree fo deterioration were specified and scored accordingly to ISRM;
- Correction factors for determining of rock masses, weakened by mining activity impact, were recommended;
- The unsupported-span was re-arranged;

Since there are several versions, it is important to specify which version is used (Bieniawski, 1993).

The following six parameters are obtained to calculate the RMR value for a given rock mass:

1. Uniaxial Compressive Strength (UCS) of intact rock material
2. Rock Quality Designation (RQD)
3. Joint or discontinuity spacing
4. Joint Condition
5. Groundwater condition
6. Joint orientation

Ratings are provided for each of the six parameter according to the rock conditions. The definition of each of the six parameters along with their rating values are provided in the Appendix B. The ratings are then summed to obtain the basic Rock Mass Rating (RMR_{basic}) value which after the adjustment according to the orientation of the discontinuity according to Table 2.3 (Bieniawski, 1989), we obtain the final value of Rock Mass Rating. Moreover, Bieniawski (1989) also proposed a table, regarding the scouring of discontinuity surface and corrections for blasting in tunnelling ans mining activities were also introduced (Laubscher, 1977, 1984). On the basis of the *RMR* values for a given engineering structure, the rock mass is sorted into five classes as shown in Table 2.4 and based on the classified rock, the support is provided to the rock mass. Bieniawski (1989) provided a chart for the support recommendation and the excavation method for different rock classes which is given in in Table B.9 provided in Appendix B. Aksoy (2008) provided a chart (Figure 2.3) to summarize the *RMR* calculation algorithm, including the correction factors, to obtain the final *RMR* value that can be used for estimation of supports.

Table 2.3: Adjustment of Joint orientation (Bieniawski, 1989)

Joint orientation assessment	Very favorable	Favorable	Fair	Unfavorable	Very Unfavorable
Tunnels	0	-2	-5	-10	-12
Raft foundations	0	-2	-7	-15	-25
Slopes	0	-5	-25	-50	-60

Table 2.4: Design parameter and engineering properties of rock mass (Bieniawski, 1989)

S.No.	Parameter/properties of rock mass	RMR (Rock Class)				
		100–81 *(I)*	80–61 *(II)*	60–41 *(III)*	40–21 *(IV)*	< 20 *(V)*
1	Classification of rock mass	Very Good	Good	Fair	Poor	Very Poor
2	Average standup time	20 years for 15 m span	1 year for 10 m span	1 week for 5 m span	10 hours for 2.5 m span	30 min. for 1 m span
3	Cohesion of rock mass (MPa)	> 0.4	0.3–0.4	0.2–0.3	0.1–0.2	< 0.1
4	Angle of internal friction of rock mass	$> 45^0$	$35 - 45^0$	$25 - 35^0$	$15 - 25^0$	$< 15^0$
5	Allowable bearing pressure (T/m^2)	600–440	440–280	280–135	135–45	45–30
6	Safe cut slope (^{0})	> 70	65	55	45	< 40

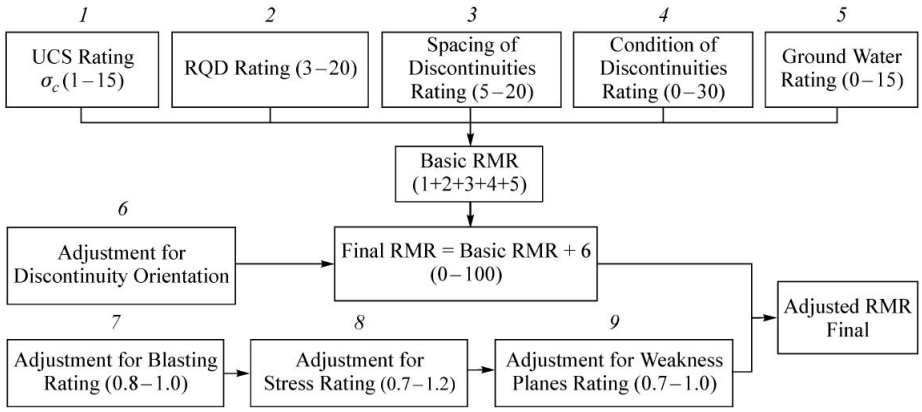

Figure 2.3: RMR calculation algorithm (Aksoy, 2008)

Limitations

One of the major shortcomings of *RMR* system is that it is mainly dependent on the observations, experts' experience and it may result in extremely safe or unsafe conditions. It is thus preferable to apply field observations together with field surveys (Aksoy, 2008). Another limitation is that the *RMR* system disregards the discontinuity orientation for extremely jointed and completely crushed rock masses. Also, while applying *RMR* for slopes, some meaningless results used to appear, thus, a number

of instability models are developed for scoring in order to adjust the discontinuity orientation and to eliminate this situation (R. Singh & Gahrooee, 1989). At previous studies, aimed at prevention of such results, the orientation adjustment equal to (-5) is assumed. Problem also lies in the determination of class ranges in the system for which Ulusay (1991) suggests to set a narrower interval for weak and clay-bearing rocks, in particular, for rock masses where $RMR < 40$.

Rock mass rating system is helpful exclusively for predesign. It is explicit that application of the system involves high-class experience of users. The data, obtained by applying RMR system, should be considered in combination with both analytical and numerical study data. In case of tunnelling with 20 – 25 m roof span, one should be very careful because this tunnel roof level is actually crucial from the carrying load stand point. In practice, there are cases when *RMR* system fails to distinguish heterogenous rock masses (Aksoy, 2008).

2.2.4 Rock Quality Index (Q-System)

Development of the Q-System

The Rock Quality Index (Q-System) was developed as a part of the Norwegian Method of Tunneling and was introduced in 1973 and has undergone several improvements and modifications after its introduction. The method was birthed with around 210 case records with introduction of shotcrete and grouted rock bolts for stabilizing the tunnels and was updated in 1993 with replacement of wire mesh shotcrete S(mr) with fiber reinforced shotcrete S(fr) based on additional 1050 new case records (Barton & Grimstad, 2004). With the addition of further 800 case records from Norway, Switzerland and India, the support chart was further modified with removal of a support category with only 8 categories in the new chart, the minimum thickness of recommended shorcrete was greater than 4 cm and the inclusion of Reinforced Ribs of Shotcrete (RRS) for very poor rock (and below) quality (Barton, 2015). The advantage of the Q-system of classification compared to other classification method as highlighted by Barton (2015) is the use of logarithmic scale, which covers rock quality within six orders of magnitude ($10^{-3} - 10^{3}$), compared to the linear rock mass quality scales of Rock Mass Rating *(RMR)* and Geological Scale Index *(GSI)*, which cannot predict the non linearity and anisotrophy of rock mass. The parameters of the Q-index (J_n/J_r) also allows for predicting of possible overbreaks ($J_n/J_r > 6$) and thus can be used for assessing the working methods of the contractors while blasting. The best use of the method is made when a histogram is provided for every parameters instead of giving a single representative Q value. The variable nature of the rock mass can be best described and interpreted when a range of values is provided as a histogram (Barton, 2015).

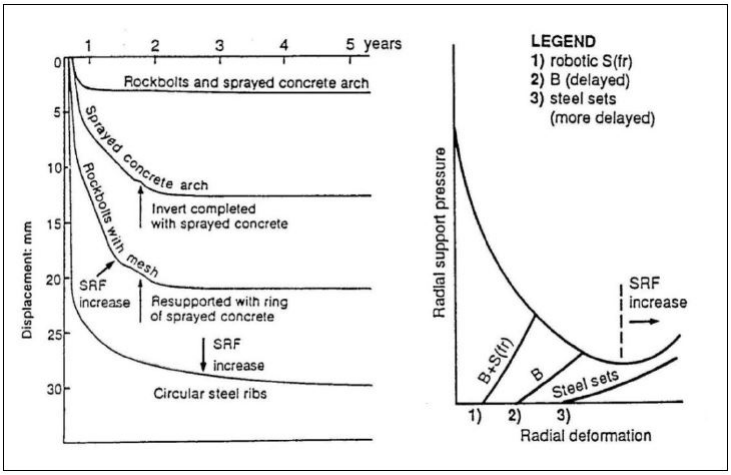

Figure 2.4: Results of five years of monitoring test-tunnel sections in mudstone, using four different support and reinforcement measures (left) and Representation of the relative stiffness of different support measures (right) Barton (2015)

Barton (2015) compares the support requirement defined by the traditional New Austrian Tunnelling Method *(NATM)* method against Q-system of classification. In Norwegian Method of Tunnelling *(NMT)* (Q-system), the temporary support forms a part of the permanent support and the authors argue that the temporary support of *NATM* (lattice girders, S(mr) and temporary steel sets) are inferior to *RRS* defined in the upgraded Q-chart as these are 'soft-supports' compared to *RRS* since they do not resist deformation until they cease to deform elastically. However, the supports of Q -system can be used as a temporary support in the *NATM* if a final concrete lining is planned and the temporary supports can be obtained by increasing the factor in Q chart by '1.5*ESR + 5*Q' (Barton, 2015).

Figure 2.4 from Barton (2015) shows the result of five years of monitoring for different types of support. It can be seen that less deformation measured in case of sprayed concrete and rock bolts while high deformation values for steel sets. From this, we can see the advantages of fiber reinforced shotcrete over wire mesh shotcrete: better bonding, gets in to overbreaks, less corrosion, lower permeability, faster, safer, cheaper per tunnel-meter and the obvious advantages is that it leaves behind no shadows i.e. there lies no gap between the rock and the shotcrete (Barton, 2015). The figure on the right shows the convergence confinement diagram of various supports where the lower gradient in case of steel sets signify its delayed activation to resist the support pressure. This nature of the steel sets makes it insignificant in overcoming the loosening pressures as mentioned by Barton (2015), however, in case of squeezing grounds, this proves to be beneficial. During tunneling in squeezing ground, it is necessary to release the ground pressure before support installation all the while providing safe environment for the workers to work. Providing stiff supports in such grounds could lead to failure of supports as in the case of Chameliya Hydropower

Project (Basnet, 2013) in Nepal and Yacambú-Quibor tunnel in Venezuela (Hoek & Briceno, 2009). Barton (2015) also states the economic advantages of Q support method over *NATM* support. The overall cost of the Q support reduces by one fourth to one fifth than *NATM* support as heavy lining such as concrete lining, steel sets are not required. Also, in hard and brittle rocks, due to overbreaks, more amount of concrete would be required in case of *NATM* while S(fr) being sprayed over the rocks would require minimum amount of shotcrete.

Design of Supports

The Q-value gives a description of the rock mass stability of an underground opening in jointed rock masses. High Q-values indicates good stability and low values means poor stability. Based on 6 parameters the Q-value is calculated using Equation (2.2).

$$Q = \frac{RQD}{J_n} * \frac{J_r}{J_a} * \frac{J_w}{SRF} \tag{2.2}$$

where, RQD is the Rock Quality Designation defined in Section 2.2.2, J_n is the Joint Set Number, J_r is the Joint Roughness Number, J_a is the Joint Alteration Number, J_w is the Joint Water Reduction Factor and SRF is the Stress Reduction Factor. All the parameters have been defined and their values for different types of rocks are provided in Appendix B.

The Q-system can thus be considered a function of three parameters which are approximate measures of:

i Block Size (RQD/J_n): It represents the overall structure of rock masses.
ii Inter block shear strength (J_r/J_a): It represents the roughness and frictional characteristics of the joint walls or filling materials.
iii Active stress (J_w/SRF): is an empirical factor describing the active stress.

Based on the obtained Q value, the rock mass is classified into eight class *(A to G)* from Exceptionally Good to Exceptionally Poor as shown in Figure B.3 (NGI, 2015). The support to be provided is also determined from the same graph. In the chart, on Y-axis the term *ESR* refers to the Excavation Support Ratio which signifies the factor of safety requirement. There will be an increasing need for support with increasing span and increasing wall height and the safety requirement will depend on the purpose of the excavation i.e. a road or underground powerhouse tunnel will require higher level of safety than a water tunnel. A low *ESR* value indicates the need of high level of safety. The values of *ESR* for different excavation is shown in Table 2.5. It is recommended to use $ESR = 1.0$ when $Q \leq 0.1$ for the types of excavation B, C and D. The reason for that is that the stability problems may be severe with such low Q-values, perhaps with risk for cave-in.

Table 2.5: Values of ESR.

	Type of Excavation	ESR
A	Temporary mine openings, etc.	3 - 5
B	Vertical shafts: (i) circular opening (ii) rectangular opening	 2.5 2.0
C	Permanent mine openings, water tunnels for hydro power (exclude high pressure penstocks), water supply tunnels, pilot tunnels, drifts and headings for large openings	1.6
D	Minor road and railway tunnels, surge chambers, access tunnels, sewage tunnels, etc.	1.3
E	Power houses, storage rooms, water treatment plants, major road and railway tunnels, civil defense chambers, portals, intersections, etc.	1.0
F	Underground nuclear power stations, railways stations, sports and public facilitate, factories, etc.	0.8
G	Very important caverns and underground openings with a long life-time, $\approx$ 100 years, or without access for maintenance.	0.5

The ratio of span (or wall height) to *ESR* (Equation (2.3)) gives the *Equivalent Dimension*. The equivalent dimension refers to the opening dimension factored by the required degree of safety for construction.

$$\text{Equivalent Dimension } = \frac{\text{Span or height in m}}{ESR} \tag{2.3}$$

Limitations

The major limitation of the Q-system is that it was originally developed for hard rock mass where the dominant mode of failure is the block failure. This suggested its unacceptability to weak ground subjected to brittle failure and squeezing (Palmstrom & Broch, 2006). Palmstrom and Broch (2006) also states that the Q system is limited by its estimation in input parameters such as *RQD* (Rock Quality Designation), J_w (Joint Water Reduction Factor) and *SRF* (Stress Reduction Factor). The authors suggests that since the value of *RQD* is limited from 10 to 100, the estimated Q value cannot cover all kinds of rocks and suggests the methods is best suited for rocks within range of Very Poor to Good with size of excavation within 3 to 30 m (span or height) which estimated to Q value within 0.1 to 4. The suitability of the methods for various types of ground has been summarized by the authors in Table 2.6. However, Barton (2015) argues that the limiting value of the *RQD* doesn't impact the overall Q value as there is qualitative meaning behind the theoretical numbers and has useful anisotropic and 3D recording abilities. The inadequacy of the Rock

Table 2.6: Fitness of Q system in various types of ground behavior in tunnels (Palmstrom & Broch, 2006)

Types of ground behavior	**Suitability(*)**
Stable	2
Fall of block(s) or fragment(s)	1 - 2
Cave-in	3
Running ground	4
Buckling	3
Slabbing, spalling	2
Rock burst	3 - 4
Squeezing ground	3
Raveling from slaking or friability	4
Swelling ground	3
Flowing ground	4
Water ingress	4

(*) *1: Suitable; 2: Fair; 3: Poor; 4: Not Applicable*

Mass Classification *(RMC)* for estimating supports in weak rock mass has also been shown by Chhushyabaga, Karki, and Khadka (2020); Karki, Karki, Chhushyabaga, and Khadka (2020); Khadka, Karki, Chhushyabaga, and Maskey (2019), and will further be explored in this study through case studies from the Himalayan region. Palmstrom and Broch (2006) also states that the Q system is more suitable during the preliminary estimate of the rock support where detailed description of the rock mass is not available and during construction, the authors suggest to provide qualitative description of the rock mass which can later be used to quantify the required parameters for the Q value. This allows for verification of the estimated parameters at a later time based on the qualitative description. One of the major shortcomings of the the empirical *RMC* approach is that it does account for the disturbances created during the excavation of the the structures. During construction of and excavation of underground structures, disturbances are created which alters the state of the surrounding rock around the perimeter from the natural state. The amount of disturbances and damage is affected by the excavation method and although this is partially covered in the Q system while estimating the Joint Set Number (J_n), the overall damage is not predicted. Palmstrom and Broch (2006) suggests including an excavation damage factor or similar in the empirical methods to account for the damage caused. This damage factor is however accounted for in the numerical methods (by means of plastic radius in the finite element software RS2).

2.2.5 Geological Strength Index (GSI)

Geological Strength Index (*GSI*) was first introduced by Hoek and Brown (1997) for hard and weak rock masses fro classifying the rock mass based on visual inspection of geological conditions. In this classification, there are five main qualitative

classification of rock mass structures:

i Intact/Massive
ii Blocky
iii Very blocky
iv Blocky/Disturbed
v Disintegrated

Further, discontinuities are classified into five surface conditions which are similar to discontinuity conditions in *RMR*.

i Very good
ii Good
iii Fair
iv Poor
v Very poor

A 6 x 5 block in the matrix of Figure B.1 is picked up first according to actual and undisturbed rock mass classification and discontinuity surface condition. Then a corresponding *GSI* is read. According to Hoek (1998) and Marinos and Hoek (2000), a range of values of *GSI* (*or RMR*) should be estimated instead of just a single value. This practice has a significant impact on the design of slopes and excavations in rocks.

The *GSI* chart based on visual inspection has been commonly used by the rock mechanics community since it was developed. However, due to the lack of measurable parameters for describing the rock mass structures and the discontinuity surface conditions, it is possible for different persons to estimate different *GSI* values from the chart for the same rock mass, particularly for engineers with limited experience. Therefore, researchers have attempted to develop quantitative measures of the rock mass structures and the discontinuity surface conditions (Cai et al., 2004; Hoek, Carter, & Diederichs, 2013). Figure B.1 is used judiciously for crushed/disintegrated and laminated/sheared rocks. Similarly, hard, thick laminated rocks in the last row of Figure B.1 may not be applicable, because they may have a higher strength classification.

Cai et al. (2004) used the quantitative block volume V_b and joint condition factor J_C to describe the rock mass structure and the discontinuity surface condition, respectively. The block volume (V_b), affected by the joint set spacing and persistence, can broadly be known by the joint spacing given for six different rock classes in Figure B.1. The value of joint condition factor, J_C, controlled by joint roughness, weathering, and infilling material, can be obtained by Equation (2.4) from Cai et al. (2004).

$$J_C = \frac{J_W J_S}{J_A} \tag{2.4}$$

where, J_W is the large scale joint or discontinuity waviness in meters from 1 to 10 m, J_S is the small-scale smoothness in centimeters from 1 to 20 cm and J_A is the joint alteration factor. With the obtained V_b and J_C, *GSI* can be determined using the quantified *GSI* chart given in Figure B.1 (Cai et al., 2004). The *GSI* can also be obtained empirically using Equation (2.5) given by Cai and Kaiser (2006).

$$GSI = \frac{26.5 + 8.79 ln J_C + 0.9 ln V_b}{1 + 0.015 ln J_C - 0.0253 ln V_b} \tag{2.5}$$

where J_C is dimensionless given by Equation (2.1) and V_b is in cm^3.

Hoek et al. (2013) quantified the *GSI* chart on the basis of joint condition and *RQD*, and proposed a simple expression for estimating *GSI* given by Equation (2.6)

$$GSI = 1.5 JCond_{89} + RQD/2 \tag{2.6}$$

where $JCond_{89}$ is the joint condition rating defined by Bieniawski (1989) and can be determined using Table 2.4 or Table B.6.

When the joint roughness number Jr and the joint alteration number J_a in the Q-system are used to describe the joint condition, the expression given in Equation (2.7) can be used to estimate *GSI* (Hoek et al., 2013).

$$GSI = \frac{52(J_r/J_a)}{1 + J_r/J_a} + RQD/2 \tag{2.7}$$

2.3 Rock stress redistribution

It is important to understand the stress distribution mechanism in rock masses around the excavation for proper and economic design of the structure. The stress distribution and displacement gives valuable insight on the stability of underground openings. Since rocks are initially stressed, any opening causes a change in the initial stress state i.e. the in-site stress are redistributed inducing tangential stresses in the vicinity of the opening (Hoek & Brown, 1980). As soon as the tangential stress exceeds the rock mass strength, instability are induced in the opening that can lead to failure of the structure if not properly addressed. The stress distribution must be studied in the 3 dimension for accurate interpretation but for simplicity, the 3D problem can be reduced to a 2D problem by studying a section of the long tunnel. The principle origin of in-situ stress in the rock mass are gravity, plate tectonics and surface topography (Panthi, 2006). The gravity loading on the opening is obtained as a product of the rock cover and its unit weight (Equation (2.8)) and the horizontal stress on the opening can be obtained by Equations (2.9) (Panthi, 2012) where the effect of the

plate tectonics is also included by the tectonic stress.

$$\sigma_v = \gamma * H \tag{2.8}$$

$$\sigma_h = \sigma_v * \frac{\nu}{1-\nu} + \sigma_{tec} \tag{2.9}$$

where σ_v, σ_h is the vertical and horizontal stress,σ_{tec} is the tectonic stress γ is the unit weight of the rock mass and ν is the Poisson's ratio.

Case 1: Hydrostatic stress in elastic ground

The distribution of stress can be estimated by *Kirsch Solution* who provided linear elastic solution for stresses around a hole in an infinite plate (Kirsch, 1898). This solution for uniaxial tension can be extended to biaxial stress state by principle of superposition, which gives the equation for radial, tangential and shear stress as given in Equation (2.10).

$$\left.\begin{aligned} \sigma_r &= \sigma\left(1-\left(\frac{a}{r}\right)^2\right) \\ \sigma_\theta &= \sigma\left(1+\left(\frac{a}{r}\right)^2\right) \\ \tau_{r\theta} &= 0 \end{aligned}\right\} \tag{2.10}$$

where σ is the far field stress, a is the radius of the opening and r is the radial distance of the element from the center of the opening.

The redistribution of stress around the opening is shown in Figure 2.5a. For a hydrostatic case, the redistribution is such that the maximum tangential stress in the boundary of the opening is two times the in-situ stress (Figure 2.5b) which decreases as the distance from the boundary increases and stabilize to the value of in-situ stress, at a distance approximately equal to the radius of the opening (Nilsen & Palmstrom, 2000). SImilarly, the radial stress is zero at the boundary of opening and stabilizes at a value equal to the in-situ stress far from the boundary. In situation of stress anisotropy, which is usually the case, the tangential stress varies around the periphery of the opening. According to *Krisch solution*, the tangential stress will reach its maximum value ($\sigma_{\theta max}$)where the major principal stress (σ_1) direction is tangent to the contour, and its minimum value ($\sigma_{\theta min}$) where the minor principal stress (σ_3) direction is tangent. The actual value are given by Equation (2.11).

$$\left.\begin{aligned} \sigma_{\theta max} &= 3\sigma_1 - \sigma_3 \\ \sigma_{\theta min} &= 3\sigma_3 - \sigma_1 \end{aligned}\right\} \tag{2.11}$$

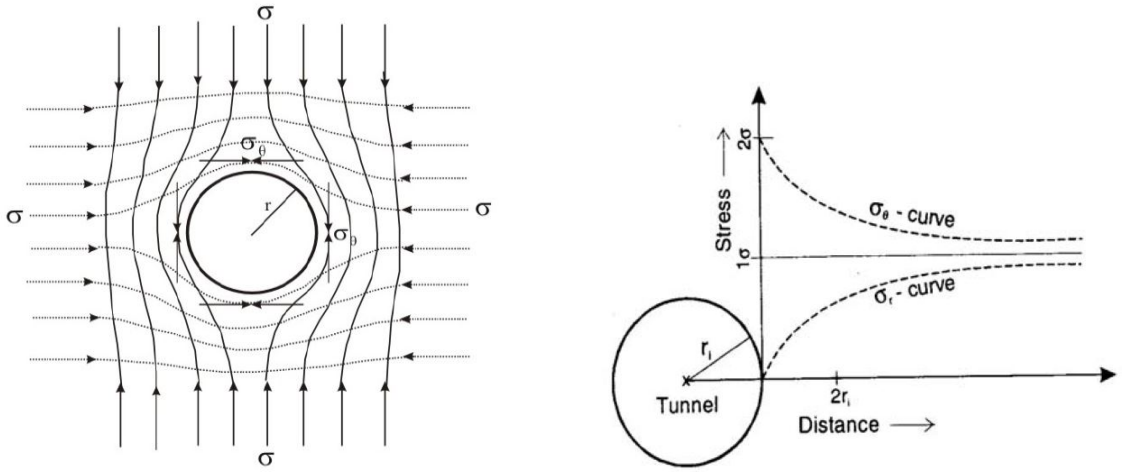

(a) Stress trajectories in rock mass surrounding a circular opening and subjected to a far field stress.

(b) Tangential and radial stress distribution in elastic ground.

Figure 2.5: Stress distribution in a circular opening in homogeneous, elastic rock mass (Panthi, 2006)

The above Equations (2.10) and (2.11) are valid for homogeneous, isotropic and elastic rock mass having widely spaced and tight joints.

Case 2: Hydrostatic stress in elasto-plastic ground

While tunnelling in weak and anisotropic, the rock mass in the immediate vicinity of the opening gets disturbed which causes gradual reduction in its strength. When the tangential stress around an opening exceeds the rock mass strength, cracks begin to form in the rock mass. At large depth, such rock failure can cause violent bursts while in weak rocks, the crack begins at shallow depths. These cracks can initiate new cracking, forming a visco-plastic zone of micro-fractured rock mass and drive the zone of broken rock deeper into the rock mass. This broken zone is called the plastic zone and beyond the plastic zone, the rock mass is in elastic state. Due to the formation of the plastic zone, the induced maximum tangential stresses are moved beyond the plastic zone into the elastic rock mass. Figure 2.6 shows the effect of plastic zone in the distribution of tangential stress around the excavation which was numerically solved by Bray (1967) by taking a random case study as an example. In Figure 2.6 we can see that the tangential stress is maximum around the outer periphery of the plastic zone (i.e. in the elastic rock) and the value is less than twice of in-situ stress and the stress peak is relatively flat (G. L. Shrestha, 2005).

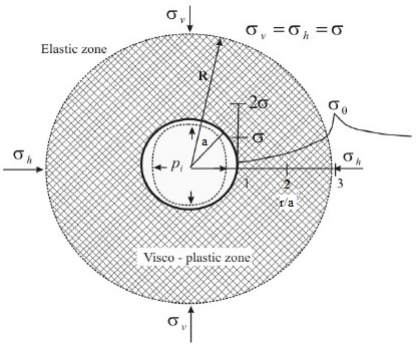

Figure 2.6: Effect of plastic zone in tangential stress distribution around a circular opening (Bray, 1967)

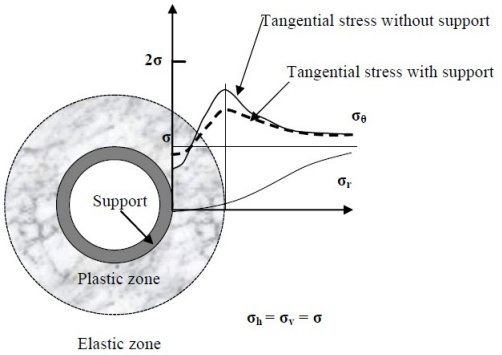

Figure 2.7: Stress distribution around circular opening after application of support (G. L. Shrestha, 2005)

Effect of internal support

The stress condition change with the change in condition of the opening. When support is applied to the tunnel contour, stress redistribution takes place and stress also build up on the tunnel support. In Figure 2.7, the solid line represent the tangential stresses in unsupported while the dotted line represent for supported opening case. The support affects the stress condition in two ways: the stress level at tunnel contour increases and the stress peak level decreases (Goodman, 1989). Support provides confining pressure (P_i) and helps rock mass to take more stress (Mohr-Coulomb criteria). Support activates only after rock mass pushes it. However, the location of the stress peak will be same as in Figure 2.6 as the tunnel lining cannot change the rock mass from plastic to elastic condition (G. L. Shrestha, 2005). When an internal support (P_i) is provided, the tangential, radial and shear stress, for a hydrostatic case, is given by Equation (2.12). Some of the concentrated stress passes through the support as it finds support capable to stand the part of the stress, and hence partial stress relief takes place from the rock mass around the underground opening. Thus with the decrease of the tangential stress peak value, creep rate will reduce or stop, depending on the support strength. Considering these facts, thickness and residual strength of plastic zone need to be assessed for support design (G. L. Shrestha, 2005).

$$\left.\begin{aligned} \sigma_r &= \sigma\left(1-\left(\frac{a}{r}\right)^2\right)+P_i\frac{a^2}{r^2} \\ \sigma_\theta &= \sigma\left(1+\left(\frac{a}{r}\right)^2\right)-P_i\frac{a^2}{r^2} \end{aligned}\right\} \tag{2.12}$$

Case 3: Non-hydrostatic stress

B. Singh and Goel (2006) made the following assumptions in the analysis of elastic rock mass in non-hydrstatic state of in-site stress (Figure 2.8).

1. The rock mass is continuous, homogeneous, isotropic, dry, linearly elastic and infinite medium.
2. The tunnel is circular in cross-sectional shape having radius a and r is the radial distance at any point from the center of the circular tunnel.
3. The in-situ stress field is homogeneous and non-hydrostatic. The vertical stress is σ and the horizontal stress is $k\sigma$. The vertical stress σ is generally assumed equal to the overburden pressure γH, where γ is the unit weight of rock mass and H is the depth of the tunnel.
4. The modulus of elasticity (or deformation E_d) is the same in loading and unloading conditions.

The radial (σ_r), tangential (σ_θ) and shear stress ($\tau_{r\theta}$) in this condition is given by Equation (2.13).

$$\left.\begin{aligned}
\sigma_r &= \frac{\sigma}{2}\left[(1+k)\left(1-\frac{a^2}{r^2}\right)+(1-k)\left(1+\frac{3a^4}{r^4}-\frac{4a^2}{r^2}\right)\cos 2\theta\right] \\
\sigma_\theta &= \frac{\sigma}{2}\left[(1+k)\left(1+\frac{a^2}{r^2}\right)-(1-k)\left(1+\frac{3a^4}{r^4}\right)\cos 2\theta\right] \\
\tau_{r\theta} &= \frac{\sigma}{2}\left[(1-k)\left(1+\frac{2a^2}{r^2}-\frac{3a^4}{r^4}\right)\sin 2\theta\right]
\end{aligned}\right\} \tag{2.13}$$

If the tunnel is internally pressurized, then the solution for the radial and tangential stress is given by Equation (2.14).

$$\left.\begin{aligned}
\sigma_r &= \frac{\sigma}{2}\left[(1+k)\left(1-\frac{a^2}{r^2}\right)+(1-k)\left(1+\frac{3a^4}{r^4}-\frac{4a^2}{r^2}\right)\cos 2\theta\right]+P_i\frac{a^2}{r^2} \\
\sigma_\theta &= \frac{\sigma}{2}\left[(1+k)\left(1+\frac{a^2}{r^2}\right)-(1-k)\left(1+\frac{3a^4}{r^4}\right)\cos 2\theta\right]-P_i\frac{a^2}{r^2}
\end{aligned}\right\} \tag{2.14}$$

Case 4: Effect of opening shape

Most of the analysis is done in circular section, however, in practice circular section is seldom used. Horse-shoe and inverted D excavation are preferred, as it gives a wide flat floor for the equipment used during construction. In weak rocks, this shape is not a good choice because of high stress concentration at the corners where the sidewalls meet the floor or invert. In some cases failures initiating at these corners can lead to severe floor heave and even to failure of the entire perimeter. Large bending moment are generated in the linings at the corners which can be reduced by providing a concave curvature of the floor. This was also seen on analysis of tunnel section of Himalayas by Khadka et al. (2019) where the authors suggested to modify the section at the point of junction of walls and invert by smoothing the angle of curvature or

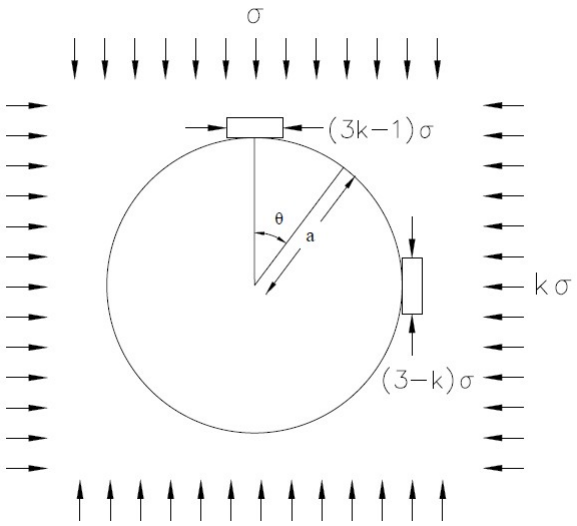

Figure 2.8: Stress concentration around circular tunnel in non-hydrostatic state of in-situ stress (B. Singh & Goel, 2006).

by providing higher thickness of lining. Schijve (2009) studied the effect of curvature on the concentration of stress by gradually increasing the radius of an ellipse. The severity of the stress concentration is visualized by the *Stress Concentration Factor* (K_t), which is defined as the ratio of peak stress to the nominal stress (original in-situ stress). Figure 2.9a (Schijve, 2009) shows the variation of K_t for various radius of the ellipse. In the figure, a and b is the radius along the major and minor axis respectively and the infinite plate is subjected to uniaxial tensial force (σ). This causes the stress concentration to be on the boundary along the X-axis (major axis). It can be seen that, on increasing the a/b ratio, the stress concentration factor also increases implying the higher concentration of stress as the radius decreases. This is shown graphically in Figure 2.9b, where we see that the stress at the tip of a circular hole is three times the far field (in-situ) stress while for an ellipse, it is seven times the original stress.

The same can be seen from Figure 2.10 (Schijve, 2009) where the comparison has been made for a curve of larger radius and for an almost 90^o curve. The shown section is of a fillet where a plate of large thickness (T) is reduced to a lower thickness (t) through a transition radius (r). The horizontal axis in the figure shows the ratio of the radius of the curve and the smaller thickness of the fillet. It can be seen that for a constant thickness t, as the radius of the curve increases, the value of K_t decreases. Thus for the perpendicular fillet, the stress concentration is maximum in the curve while it is lower for the smooth curve. This highlights the importance of larger radius in reducing the concentration of stress in the curve and thus reduce the amount of bending moment failure of liners in case of tunnel openings.Pop, Pop, and Cosobea (2013) also found similar results while studying the concentration of

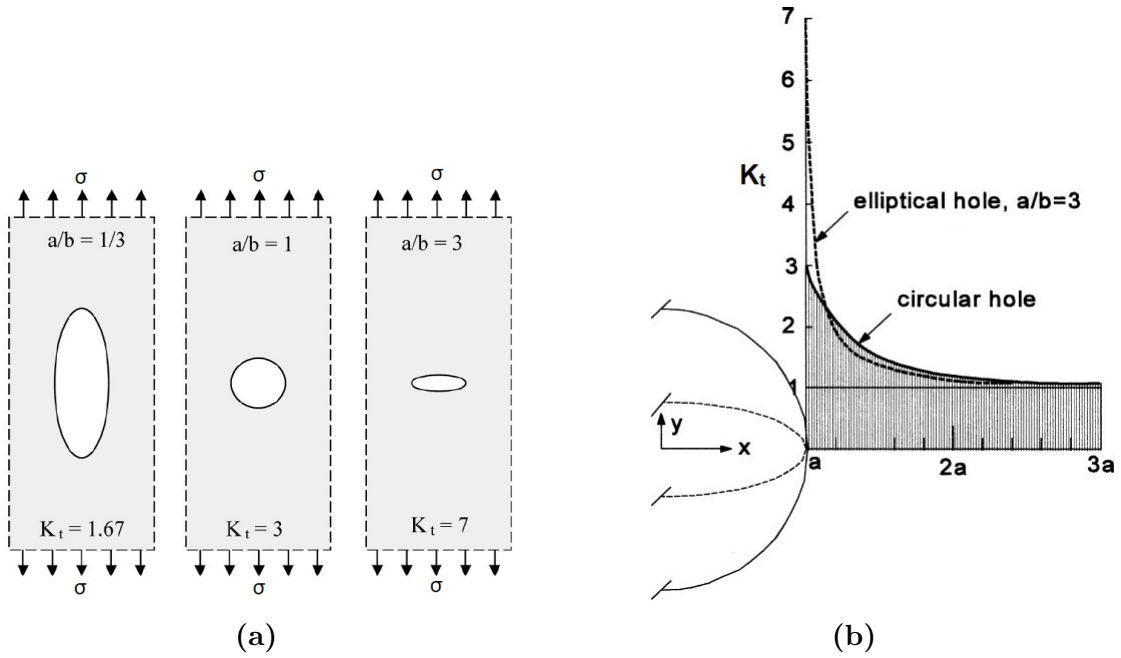

Figure 2.9: (a) Effect of radius of opening on K_t for an infinite sheet under tension and (b) Graphical representation of stress concentration on the tip of openings (Schijve, 2009)

stress around a rectangular opening with different radius of joints in an elastic tape subjected to stretching (tensile load). The finite element results showed that the stress concentration increased with reducing angle of joints thus creating maximum stress at perpendicular joints.

Case 5: Effect of non-homogeneous layer

So far the distribution of stress in a homogeneous layer has been studies which is an ideal condition, however in practical scenario the rock mass is layered and a uniform, homogeneous layer is seldom found. This layered property of rock causes variation of stress around the opening and it is important to know this distribution of stresses for design of support for the openings. Agarwal and Boshkov (1968) studied the distribution of stress around a circular tunnel in a soft medium bounded by hard medium using FEM for different values of ratio of thickness of layer to diameter of tunnel. The material was subjected to three types of loading: (i) vertical loading, (ii) horizontal loading on outer hard medium and (iii) horizontal loading on soft central medium. The loading was done by varying the H/D (central layer thickness/excavation diameter) ratio where $H/D = 0$ signifies homogeneous material around the excavation.

The effect of the different loads on the concentration of stress on the opening contour was studied by the authors. As shown in Figure 2.11a, for the case of vertical loading (overburden pressure), the stress concentration of vertical normal stress (σ_y)

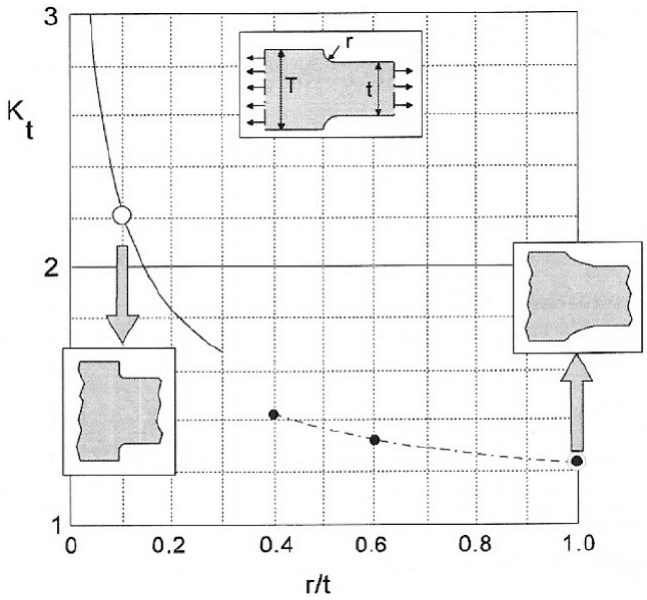

Figure 2.10: Variation of K_t with radius of curvature in a fillet (Schijve, 2009)

along the Y-axis is zero at the opening's contour which gradually increases until it becomes equal to the loading stress. The concentration of horizontal normal stress (σ_x) along the Y-axis, due to the vertical loading is shown by the red lines in the figure. For homogeneous section (represented by the red solid line) the nature of the stress is tensile, which increases to zero as the distance from the boundary increases. This can lead to tensile failure in the crown of opening (G. L. Shrestha, 2005). Similarly, for the layered materials, the stress first increases until the boundary of transition of the layers where the stress rapidly drops and then starts increasing in the new layer towards zero. The solid line shown in Figure 2.11a (Agarwal & Boshkov, 1968) is for homogeneous material (H/D = 0 to 1) while the dotted line is for layered material ($H/D > 1$). The authors also state that for overburden pressure alone of hydrostatic stress state, the maximum value of vertical normal stress (σ_y) along the X-axis decreases as the ration of H/D decreases and for a constant value of H/D, the stress value decreases with increasing distance from the excavation boundary until it becomes equal to the vertical stress far from the boundary.

Similarly, Barla (1970) by the use of a finite element technique studied the stress distribution in a three layered medium where the central layer has different properties than the bounding medium. According to the author, the distribution of stress around the opening in the layer is a function of the geometry (opening shape and thickness of the layer) and the contrast of material properties. The Poisson's ratio is set same for all the layers in this study while the rock cover (h) is set ten times the opening radius (a). The stress distribution is studied in relation to the dimensionless quantity t/a and E_2/E_2 where t is the thickness of the middle layer, a is the radius of the opening, E_1 and E_2 is the elastic modulus of the middle layer and the surrounding

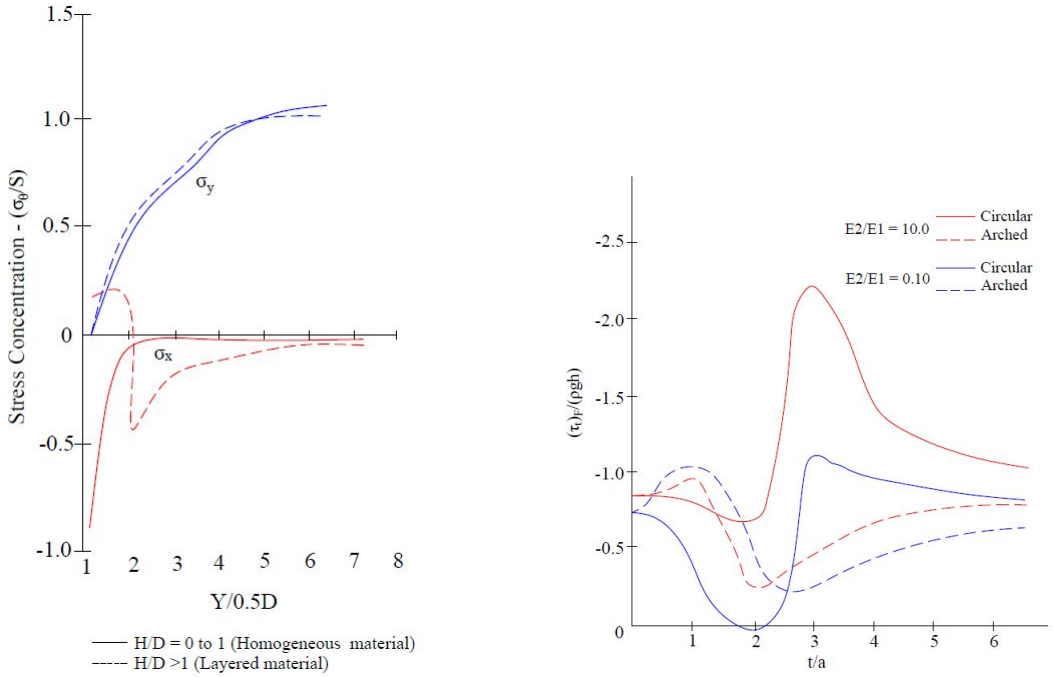

(a) **(b)**

Figure 2.11: (a) Distribution of normal stress around the opening in three layered medium (Agarwal & Boshkov, 1968) and (b) Variation of floor stress of openings in a three layered medium of different material properties (Barla, 1970)

layer respectively. Here, $E_2/E_1 \leq 1$ represents soft middle layer while $E_2/E_1 > 1$ represents hard middle layer.

The authors studied the stress distribution around a circle, arched (Inverted D) and square shaped opening in the rim (crown), back (face) and foot (invert) for various values of t/a and E_2/E_1 ratio. The condition for $E_2/E_1 = 1$ is taken as a homogeneous layer since the values obtained in the condition matched to that of the homogeneous layer. In the rim of the opening for all the shapes, it was seen that the stress distribution first decreased in soft central layer ($E_2/E_1 \leq 1$) and reached a minimum value when t/a *=1* followed by a gradual increment while in case of hard central layer ($E_2/E_1 > 1$), the value increases and reached a maximum when (t/a *=2* followed by decreasing stress value. In both the cases, the value increased/decreased until it reached a stable value (almost same as when the material is homogeneous). In the case of foot stress, the stress for hard central layer first decreased to a minimum value and then increased to a maximum. After reaching a maximum value, the value decreased until it reached a stable value almost equal to when the material is homogeneous while for soft central layer, the behavior is opposite as shown in Figure 2.11b (Barla, 1970). It can also be seen in the figure that the stress for circular section is less than that for an arched section which suggests that the stress accumulation increases with the increase in the angle of excavation and is maximum for the case of

180^o. Also the concentration of stress in the corners is much higher than that would be for the case of homogeneous material.

2.4 Design Practice of Hydropower Tunnels

Underground construction has always been a challenge in the Himalayas due to its weak geology, tectonic activities and presence of several discontinuities like faults and folds. Despite these challenges, tunnel construction has been in practice for a very long time. Recently, due to construction of several hydropower projects, the design and construction of tunnels and caverns are increasing. As of 2018 A.D., more than 200 kms of tunnels have already been constructed with more than 400 kms of tunnel under construction *(Source: Department of Electricity Development (DoED))*(Bhattarai, Karki, Karki, & Shrestha, 2018). The current practice of tunnelling in Nepal relies on the empirically established methods such as the Rock Quality Index (Q-system) and the Rock Mass Rating *(RMR)* system (Section 2.2). These practices have, in many instances, proved to be inadequate for the Nepal Himalayas due to its weak rock mass structure and properties. Many instances of failures have been reported over time, despite providing heavy support linings. Some of the prime examples include headrace tunnel of Chameliya Hydropower where squeezing of over 1 m had been reported; Khimti, Kaligandaki A, Middle Bhotekoshi suffered squeezing; Modi suffered groundwater inflow along with squeezing and Sanjen suffered face collapse during the construction of the project (Karki, Chhushyabaga, & Khadka, 2020). The current practice of underground structure design has been summarized by Karki, Chhushyabaga, and Khadka (2020) and is reported below.

2.4.1 Empirical Methods

Empirical methods are developed by researchers from around the world based on case histories and it provides a good starting point for design and construction. Various methods have been developed over time for accessing the ground conditions (Singh et al., 1992), estimating support pressure (Barton et al., 1974; Dwivedi, Singh, Viladkar, & Goel, 2013a; R. Goel & Jethwa, 1991; R. K. Goel, 1994; R. K. Goel et al., 1995a; Singh et al., 1992; B. Singh, Goel, Jethwa, & Dube, 1997) and estimating tunnel strains (Dwivedi, Singh, Viladkar, & Goel, 2013b; R. K. Goel, 1994; Hoek & Marinos, 2000; Panthi & Shrestha, 2018) and further improvements are also being made. For determining the squeezing ground condition, the most popular methods are those given by Singh et al. (1992) (Equation (2.15)) and R. K. Goel et al. (1995a) (Equation (2.16)). More recently, Jimenez and Recio (2011) (Equation (2.17)) have also provided a relation for the squeezing ground which takes more case studies from Himalayan region. All these relations provide a critical value of overburden based on

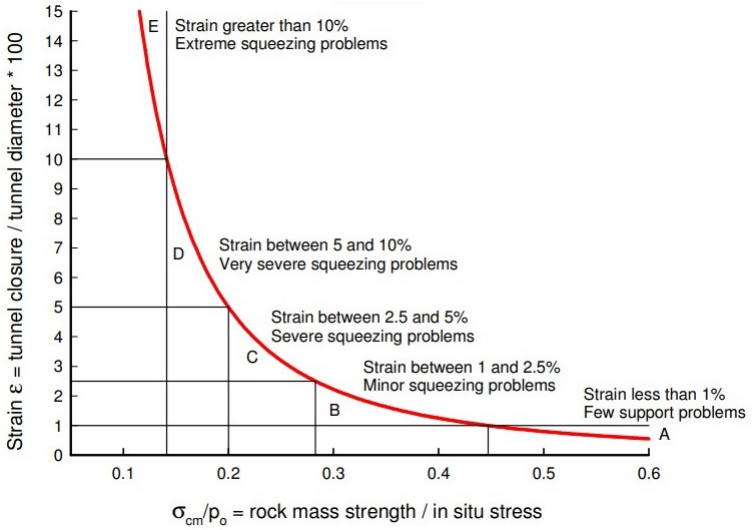

Figure 2.12: Semi-empirical method for classifying rocks based on strain values (Hoek & Marinos, 2000)

the rock mass quality which helps to determine squeezing from non-squeezing ground. The details of all the methods have been provided in Appendix A.

$$H = 350 * Q^{0.33} \tag{2.15}$$

$$H = (275 * N^{0.33}) * B^{-0.1} \tag{2.16}$$

$$H = 424.4 * Q^{0.32} \tag{2.17}$$

Similarly, Hoek and Marinos (2000) established a semi-empirical approach to differentiate the squeezing ground based on curve-fitting technique. This method assumes a circular tunnel geometry in hydrostatic stress field and the analysis is based on the simple closed-form solution. The support is considered to act uniformly over the entire boundary of the underground opening. This method gives a good first estimate of potential tunneling problems due to squeezing conditions in weak rock at significant depth below surface. Based on the chart given in Figure 2.12 (Hoek & Marinos, 2000), the rock mass is grouped into five different categories on the basis of the tunnel closure values.

Differentiating squeezing ground allows designer and engineer to make necessary preparations for proper support of the sections. The support is designed according to the Q and RMR systems in the manner as stated in Section 2.2.

2.4.2 Analytical Method

The analytical approach addresses the nature of interplay between the rock mass that may vary and the installed support, and the effect of variation in assumed rock properties on the support load. The analytical method uses three distinct curves

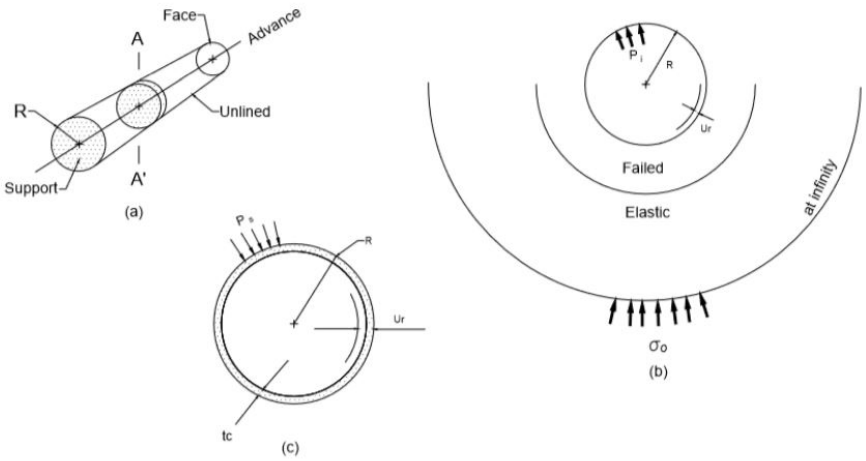

Figure 2.13: (a) Cylindrical tunnel of radius R driven in the rock mass, (b) Cross-section of the rock mass at the section A-A' and (c) Cross-Section of the circular support installed at section A-A' (Carranza-Torres & Fairhurst, 2000)

to study the interplay between the ground and support system. The Convergence-Confinement Method (CCM) is the most widely used method for analytical analysis of underground excavation (Carranza-Torres & Fairhurst, 2000). The CCM comprises of three curves: Ground Reaction Curve (GRC), Longitudinal Displacement Profile (LDP) and the Support Characteristic Curve (SCC). It can be drawn by assuming the tunnel is circular with radius R through a rock mass that is to be subject initially to a uniform far field stress σ_0 as shown in Figure 2.13(b). For the simplicity, it is assumed that all the deformation occurs in a plane perpendicular to the axis of tunnel. Radial displacement u_r and internal pressure$_p$i i.e. the reaction of support on the walls of the tunnel are uniform at the section. Figure 2.13(c) shows that the circular annular support of thickness t_c and external radius R is installed at the section A-A'. The pressure P_s represents uniform load transmitted by rock-mass to the support.

This method assumes a circular tunnel of radius R subjected to a uniform isotropic field stress σ_o. Carranza-Torres and Fairhurst (2000) have explained the effect of tunnel face for the stability of section as the support does not carry the full load of the earth pressure where it is installed. Some part of the load is carried by the face of the tunnel and as the face moves farther from the section under consideration, the load on the support increases. When a tunnel face is about twice the tunnel diameter far from the section considered, only then the maximum deformation occurs in the section. Similarly, the deformation is zero not on the face of the tunnel but about twice the tunnel diameter ahead of the face. This is represented by LDP. GRC shows the nature of the ground as the tunnel is excavated. Initially the ground is in elastic state and as the tunnel is excavated, its nature changes to plastic. The SCC on the

other hand defines the capacity of the support installed in the section. The interaction of the *GRC* and the *SCC* gives the amount of pressure that the support must bear and the deformation that occurs during the installation and after the support has taken the full load imposed over it.

CCM is originally developed for a circular tunnel subjected to hydrostatic stress, the method only gives a preliminary idea about the excavation behavior and must not be fully relied upon for the final design of the tunnel. Vlachopoulos and Diederichs (2009) have provided an improved method for the calculation of the *LDP* which relates the displacement to the normalized plastic radius of the tunnel (plastic radius/tunnel radius). This improved *LDP* which was also initially proposed for circular excavation, can be well used for non-circular case provided the aspect ratio of the tunnel is small (Vlachopoulos & Diederichs, 2014).

2.4.3 Numerical Modeling

The use of numerical modeling technique has recently been put into practice for construction tunnels and caverns in context of Nepalese Himalayas. Numerical modeling utilizes computing power and, using various modeling techniques, can be a precise way of solving very complex problems. Due to the dependency on empirical, analytic methods and experiences, heavy support is provided in the tunnels of Himalayas. This has a negative effect of the cost and time consumption of the project (Karki, Chhushyabaga, & Khadka, 2020). The precision of numerical modeling lies in the accuracy of the input parameters used to produce the model. So, it is very important to obtain precise data on the properties of the rock mass during preliminary investigation. With the help of modeling, we can obtain a safe and optimum support for every support class. The rock failure mechanism also plays an important role during modeling of underground spaces. Hence, it is important to identify whether the rock fails by Elastic Plastic or by Strain softening method. The failure mechanism has an effect on the residual values of the rock and will be discussed later in the following chapters. Numerical modeling must be implemented from the investigation stage of the project to obtain an accurate image of the ground behavior and the support requirement. The results must also be checked against the results of empirical method to confirm the accuracy of the generated models.

2.4.4 Construction Practice

The entire sequence of tunneling in the Himalayas involves sequentially the steps of fixing alignment, drilling, charging, blasting, mucking/hauling, rock bolting and shotcreting and finally providing final support in the form of concrete lining and steel ribs for very weak sections. Drill and blast method is the most common method of

excavation in the region. Due to limited practices of controlled blasting and presence of hard rocks, the rock mass around the excavation boundary also gets disturbed which decreases the strength of the rock mass (Karki, Chhushyabaga, & Khadka, 2020). In addition to the damaged rock mass, high rock cover exerts high pressure in the excavation of the boundary exceeding the strength of the rock mass, causing failure. The support is then designed commonly based on the Q-system. Although the support is designed based on the Q-system, as the rock mass gets weaker, engineers make use of steel sets and concrete lining contrary to the standard Q guidelines. During the final design of the tunnel supports, supports are designed for each class of rocks. Firstly, the results of pre-investigation are used to identify the range of expected rock conditions along the tunnel alignment and based on its results, the ground is classified into a number of classes. Then a support is designed for each class such that it can withstand the extreme condition in the specified class. This process of designing tunnel supports is more or less the same for all the tunnels excavated with drill and blast methods (NTS, 2017). The entire method of tunnel designing in the Himalayas has been summarized by Khakda (2019) and is shown in the Figure 2.14 (Khakda, 2019).

From the past experiences from the tunneling in the Himalayas, it is clear that the empirically established Rock Mass Classification technique for support estimation is insufficient for the region (Karki, Karki, et al., 2020; Khadka et al., 2019). Only relaying on these methods can cause huge loss for the project. It is thus important to realize the importance of geotechnical studies and proper analysis must be done before the execution of project. Geological considerations, hydrological conditions, in-situ stress, tunnel dimension, support elements and construction methodology are the prerequisites for successful tunnel design and these parameters must be carefully measured during the investigation stage so as to obtain more precise estimate of the support system. Since experiences have a lot of positive impacts on facing uncertainties, it is important for engineers and contractors to realize the value of recording the problems and its associated remedies undertaken.

2.5 Conclusion

The weak geology of Nepal along with the presence of major faults has always created a challenge for underground construction. The major geological risks associated with tunneling in the Himalayas include weak rock conditions, rock bursting, heavy water ingress and geothermic heat which are aggravated by the heavy rock cover and tectonic activities. The construction process in the Nepal Himalayas relies on the Rock Mass Classification approaches. These approaches have in many instances failed to address the weak nature of the rock mass resulting in insufficient support

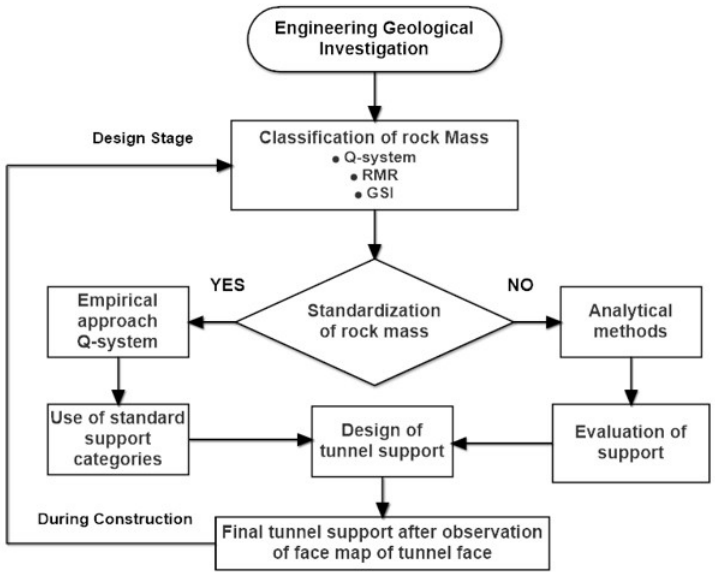

Figure 2.14: Design process for estimation of tunnel support (Khakda, 2019)

recommendation and thus the failure of sections.

Among the various Rock Mass Classification techniques, the Rock Quality Index (Q) is widely adopted for the construction. Although, the Q system is used, engineers and designers tend to provide supports, different from the original recommendation, to excavation in weak rocks based on their self experience. This can result in under or oversupport of tunnel excavations and thus numerical modeling must be used for proper design and analysis of underground structures. Current construction practice adopted in the country has been summarized in Figure 2.14 which shows that numerical modeling is seldom used for the process. The construction process relies on the empirical and analytical methods. The empirical method for squeezing classification, support pressure estimation and convergence estimation can provide valuable insights during the preliminary design but care should be taken since very few relations have developed considering the Himalayan geology. The analytical method also provides insight to the amount of deformation prior to support installation (i.e. the support installation location) and the amount of support necessary for stabilizing the ground but the method should be relied upon for the final design of the tunnel support.

It is also necessary to understand the stress distribution mechanism for proper design of the support systems as the supports are designed for addressing the problems caused by excessive stress accumulation. The corners of excavation in inverted D and horse shoe excavation is critical point of failure as the stress tends to accumulate in the region of sharp angular change. A circular excavation provides uniform stress distribution compared to the horse-shoe or inverted D excavation.

Chapter III
Analysis and Modeling of Supports

3.1 General

The design of tunnel supports, in the Himalayas is generally done on the basis of the Rock Quality Index (Q-system). However, the method is only used as a basis for characterizing the rock mass and the support is changed according to the need and the experience of the designer. Due to this reason, the Reinforced Ribs of Shotcrete *(RRS)* is seldom used for tunnel support in the region. Instead, steel ribs is extensively used and concrete is placed as a final lining in weak section. This section, thus, studies the differences in the performance of *RRS* and steel ribs, composite with shotcrete, in terms of their mechanical behavior. Capacity diagrams, an established technique of structural analysis and concrete design, has been used to study the difference in their behavior. Two composite sections: Steel sets and Shotcrete (S&S) and Reinforced Ribs and Shotcrete (R&S) have been studied according to the equivalent section method. According to the equivalent section method, a single homogeneous section is assumed which has equivalent properties as that of the composite section. The study and analysis of S&S composite has been carried out in the similar way as done by Carranza-Torres and Diederichs (2009) with similar results in their performance. This has then been further extended to the R&S composite and the comparison of the two support combinations has been studied.

In order to carry out the analysis of the composite sections, it is necessary to obtain the load transferred to the liners by the ground. As summarized by Carranza-Torres and Diederichs (2009), three different methods are available for the purpose

1. *Distributed ground pressure approach*: In this approach, the mechanical effect of the ground on the support is regarded as 'dead' load acting on the support.

2. *Subgrade reaction approach*: This approach is similar to the 'distributed ground pressure approach', except that the support is mechanically fixed in the space through elastic (or elasto-plastic) springs that represent the ground.

3. *Ground-support interaction approach*: This approach accounts for the actual mechanical interaction of ground and support. The convergence-confinement method of tunnel design can be regarded as a particular case of this approach.

Among the methods, the ground support approach gives the most realistic behavior of the interaction of the support and the ground and thus this method has been

Table 3.1: Ground parameters used for modelling

Parameters	Units	Values
Unconfined Compressive Strength (UCS)	MPa	50
Intact Rock Modulus (E_i)	MPa	30000
Poisson's Ratio (ν)	-	0.2
Geological Strength Index (GSI)	-	50/25*
Material Constant (m_i)	-	10
Disturbance Factor (D)	-	0.5& 0

**Peak value/Residual value*

implemented to obtain the loads on the support. This is achieved by the use of numerical software *RS2* (Rocscience).

3.1.1 Development of model

While modelling in *RS2*, the external boundary has been taken as 10 times the diameter of the excavation such that the plastic radius formed during the excavation process is well within this defined boundary. In case the plastic radius exceeded the boundary, the boundary could be easily expanded as required. The model has been created in three stages, each representing the in-situ condition, relaxation condition and excavated condition respectively. Relaxation stage has been developed with 50% reduction in the rock mass modulus value where the required lining has been installed. The relaxation stage has been created to represent the effect of the receding face support and also because the 50% reduction in modulus is sufficient enough to replicate practical scenario, where some deformation occurs immediately after the excavation of the section (Hoek, 2001). The failure criteria has been set to Generalized Hoek-Brown Criteria with the disturbance factor (D) set to 0.5 and 0. All the other parameters used in the input for modeling has been given in Table 3.1.

A circular section of radius 3 m has been taken for study. Circular section has been chosen due to its symmetric nature. The section is then subjected to a vertical stress (σ_v) of 12 MPa, which equivalents to a rock cover of around 430 meters. This gives a horizontal stress (σ_h) of 5.62 MPa according to the Equation (2.9). The tectonic stress (σ_{tec}) is taken as 3.5 MPa.

The liners in the *RS2* are done as beam elements with the required input of depth and the modulus of the beam. The support has been provided with an assumption of completely dry condition where no water pressure builds upon the support and the entire stress imposed is due to the gravity effect of the earth load. Only the loads imposed on upper half section has been analyzed since similar behavior will be seen on the lower half section. Figure 3.1 shows the excavation section and associated parameters.

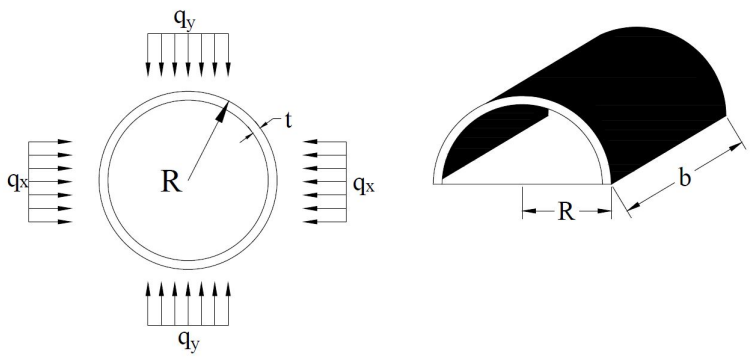

Figure 3.1: Ground loading of circular excavation according to ground support interaction approach.

The parameters q_x, q_y refers to the load transferred over the liner by the ground in MPa, R is the radius of the excavation in meters, b is the longitudinal length in meters and t is the thickness of the liner in meters. After applying the loads, the values of Moment *(M)*, Thrust *(N)* and Shear *(Q)* can be obtained which will be used as input for further analysis.

3.1.2 Development of equivalent section

The thickness (t_{eq}) and Modulus (E_{eq}) of the equivalent section is obtained from Equation (3.1) and (3.2) respectively (Carranza-Torres & Diederichs, 2009). Figure 3.2 shows the schematic diagram of the composite of steel sets and shotcrete along with its equivalent section.

$$t_{eq} = \sqrt{12\frac{D_1 + D_2}{K_1 + K_2}} \tag{3.1}$$

$$E_{eq} = \frac{n(D_1 + D_2)}{t_{eq}} \tag{3.2}$$

The parameters D_1, D_2, K_1 and K_2 are the compressibility and flexibility coefficient of individual support and will be discussed later.

3.1.3 Equivalent section and Capacity Curve

Equivalent section

As shown in Figure 3.2, consider a section of composite liner of width b comprising n units of Material 1 (Shotcrete) and n units of Material 2 (Steel set/RRS) such that each material exist along the width b at regularly spaced interval $s = b/n$. Each of the units '1' and '2' will be assumed to be characterized by compressibility coefficients D_1 and D_2 and by flexibility coefficients K_1 and K_2 respectively. The

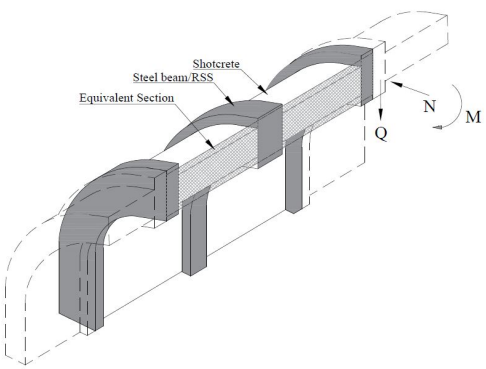

Figure 3.2: Schematic diagram of composite support along with equivalent support.

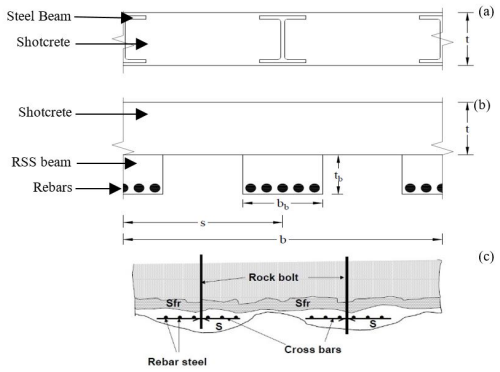

Figure 3.3: Sectional view of (a) S&S beam, (b) R&S beam and (c) RRS Support.

values of compressibility and flexibility coefficient is obtained from Equation (3.3) and (3.4) respectively. Also, these units will be assumed to be symmetrical respect to a common horizontal axis (the neutral axis of the section).

$$\begin{aligned} D &= EA \qquad \text{for plane-stress condition} \\ D &= \frac{EA}{1-\nu^2} \qquad \text{for plane-strain condition} \end{aligned} \tag{3.3}$$

$$\begin{aligned} K &= EI \qquad \text{for plane-stress condition} \\ K &= \frac{EI}{1-\nu^2} \qquad \text{for plane-strain condition} \end{aligned} \tag{3.4}$$

The parameters E is the modulus of the element, A is the cross sectional area of the element and I is the Moment of Inertial of the element.

Figure 3.3 (a) and (c) shows the section of composite liner of shotcrete with steel sets and *RRS* respectively. For calculating the equivalent section of the *RRS*, it is assumed to be a rectangular beam (Figure 3.3(b)) of width defined by the number and spacing of the rebars in the beam (for single layer *RRS* with 6 rebars at 50 mm c/c, the width will be 300 mm). The depth of the beam has been taken equal to the thickness of the reinforced ribs, obtain from the Q chart. The effect of the bolts used to place in the *RRS* in position has been avoided for simplification. The overall moment imposed over the liner, obtained from numerical analysis, is then distributed to individual element according to the thick and thin shell formulations. According to Carranza-Torres and Diederichs (2009), the thick shell formulation better approximate the results for a section with high curvature (circular and semi circular excavations) and so the relation for moment, shear and thrust distribution according to the theory of thick shell has been used and is given Equation (3.5), (3.6) and (3.7) respectively. In the equation, the subscripts '1' and '2' refer to the material 1 (Shotcrete) and

material 2 (Steel sets/RRS).

$$\begin{aligned} M_1 &= \frac{MK_1}{n(K_1+K_2)} \\ M_2 &= \frac{MK_2}{n(K_1+K_2)} \end{aligned} \tag{3.5}$$

$$\begin{aligned} Q_1 &= \frac{QK_1}{n(K_1+K_2)} \\ Q_2 &= \frac{QK_2}{n(K_1+K_2} \end{aligned} \tag{3.6}$$

$$\begin{aligned} N_1 &= \frac{N}{n}\frac{D_1}{(D_1+D_2)} + \frac{M}{nR}\frac{D_2K_1 - D_1K_2}{(D_1+D_2)+(K_1+K_2)} \\ N_2 &= \frac{N}{n}\frac{D_2}{(D_1+D_2)} - \frac{M}{nR}\frac{D_2K_1 - D_1K_2}{(D_1+D_2)+(K_1+K_2)} \end{aligned} \tag{3.7}$$

A demonstration of obtaining the above mentioned relations is provided by Carranza-Torres and Diederichs (2009) and is given in Appendix D.

Capacity diagrams

The graphical representation of induced axial thrust and bending moment on a liner plotted together with the corresponding 'envelop of failure' is referred to as thrust-bending moment interaction diagram. Similarly, the representation of axial thrust and shear force on a liner, together with the corresponding failure envelope is referred to as thrust-shear force interaction diagram. Both graphical representation is commonly referred to as support capacity diagram in structural engineering and concrete design (Carranza-Torres & Diederichs, 2009).

For a given Factor of Safety *(FOS)*, the limiting value of axial thrust associated with failure in compression and tension are given by Equation (3.8) and (3.9) while the critical values of bending moment (M_{cr}) associated to particular values of *FOS* in compression and tension at the same time is given by Equation (3.10).

$$N = -\frac{|M|At}{2I} + \frac{\sigma_c A}{FS} \tag{3.8}$$

$$N = \frac{|M|At}{2I} + \frac{\sigma_t A}{FS} \tag{3.9}$$

$$M_{cr} = \pm\frac{I}{t}\frac{\sigma_c - \sigma_t}{FS} \tag{3.10}$$

The set of Equations (3.8), (3.9) and (3.10) when plotted against each other, with moment on the horizontal axis and thrust on the vertical axis, give the thrust-bending moment interaction curve for the given Factor of Safety. This curve allow us to study the performance of the support, i.e. it allows us to study whether the forces are

Table 3.2: Properties of elements in a composite section.

Steel Beam		**RRS**	
Weight of beam	24.2 kg/m	No. of Rebars	6 (single layer)
Cross sectional area	3080 mm^2	Diameter of rebar	16 mm
Depth of beam	200 mm	Spacing of rebars	75 mm
Moment of Inertia	$21.2 * 10^6 mm^4$		
Compressive Strength	400 MPa		
Tensile Strength	400 MPa	**Equivalent rectangular beam**	
Young's Modulus	200 GPa	Depth of beam	350 mm
Poisson's Ratio	0.27	Width of beam	450 mm

Table 3.3: Thickness and modulus of equivalent section for different composites.

	S&S composite			**R&S composite**		
Spacing of liners (b/s) [m]	0.3	0.5	1	0.3	0.5	1
Thickness (t_{eq}) [m]	0.22	0.22	0.21	0.69	0.62	0.51
Modulus (E_{eq}) [MPa]	35921.86	33688.58	32118.56	20083.53	17532.13	16727.84

below or above the limits of the material. Whenever a point lies on the outside the upper boundary, it indicated failure in compression and when it lies outside the lower boundary, it indicates failure of the material in tension.

3.1.4 Analysis

The properties of steel beam (ISMB 200x100) and *RRS* beam used for the analysis is given in Table 3.2 and the obtained value of thickness and modulus of the equivalent section is given in Table 3.3. The shotcrete is provided of 200 mm thickness and 40 MPa strength.

After assigning the liner of properties given in Table 3.3, the bending moment has been obtained from *RS2* and shown in Figure 3.4. The total moment over composite liners have also been compared to the moment imposed when only shotcrete of thickness of 200 mm has been used (solid black line). The plot is shown only for the upper half of the opening with distance along the boundary shown in the same figure, since the behavior on the lower half is similar due to symmetry of the section.

Figure 3.4a shows the total moment over the liners for disturbance factor *(D)* of 0 and Figure 3.4b for D = 0.5. It can be seen that total moment is almost ten times greater in case of D = 0.5 which tells us that the moment over the liner increases as the rock mass gets damaged. Another thing to notice is the variation of moment with the variation of the beam spacing. As the spacing of the beam decreases, the total moment over the composite liner starts to increase for both *RRS* and shotcrete (R&S) and steel and shotcrete (S&S) composite. This can be explained from the structural behavior of the beam (liner), that the moment capacity of a beam increases when the length of the beam decreases. Similarly, when the spacing (length) of the liners decreases, the moment capacity increases and the liner can take up higher bending

moment.

From both the figures (Figure 3.4a and 3.4b), it can be seen that the moment over the S&S composite is less than the moment over the R&S composite. Comparing the moment over the composite liners with the moment induced over 200 mm thick shotcrete lining only, we see that the moment in S&S composite is almost similar to that of the shotcrete while it is far greater for R&S composite. This result when compared to the capacity plot (moment vs thrust) given in Figure 3.5, we see that the shotcrete liner element completely fails whereas in case of S&S and R&S composite, it is safe for 0.3 m (Figure 3.5a) and 0.5 m (Figure 3.5b) of beam spacing. *(Note that the shown curves are for a FOS of 1.5 and in case of S&S in 0.5 m spacing, the shotcrete is completely safe for FOS 1 curve).* From Figure 3.4 and 3.5, we could thus say that the *RRS* element might lead to oversupport of the section as it tends to bear higher moment than S& S composite when both the supports show safe design.

Moment over Individual Support Elements

Upon comparison of the distributed moments over the shotcrete and the beam elements according to Equation (3.5), we see that the shotcrete element takes higher moment in case of S&S composite than the R&S composite (Figure 3.6a). Also, the moment over the shotcrete increases as the spacing of the beam element decreases i.e. the moment is highest for beam spacing of 1 m and lowest for beam spacing of 0.3 m in both the composites. Upon comparing Figure 3.6b and Figure 3.6c we see that the steel beam takes very less moment (almost 10 times less) than the *RRS* beam. From Figure 3.6b and 3.6c, we also see that the moment over the beam is maximum for spacing of 0.3 m and minimum for 1 m spacing. This is consistent with the results of Figure 3.6a since the shotcrete takes maximum load, the beam element takes the minimum load and vice-versa. This is also shown by the percent graph in Figure 3.7. From Figure 3.7 we see that the shotcrete element takes higher moment in case of S&S composite and correspondingly the beam elements take lesser moment. The opposite is also true for the R&S composite. This shows that the load sharing between individual elements is more uniform in case of R&S composite. The steel beams only takes minimum amount of the bending moment and this result is consistent with the findings of Carranza-Torres and Diederichs (2009). It was also seen that the percentage of load taken up by the individual element in the composite structure is independent of the amount of disturbance to the rock mass i.e. the percentage of load acting on an element is same for a given loading configuration and not affected by the D value. The maximum value of moment, although, increases as the ground disturbance increases (for higher value of D).

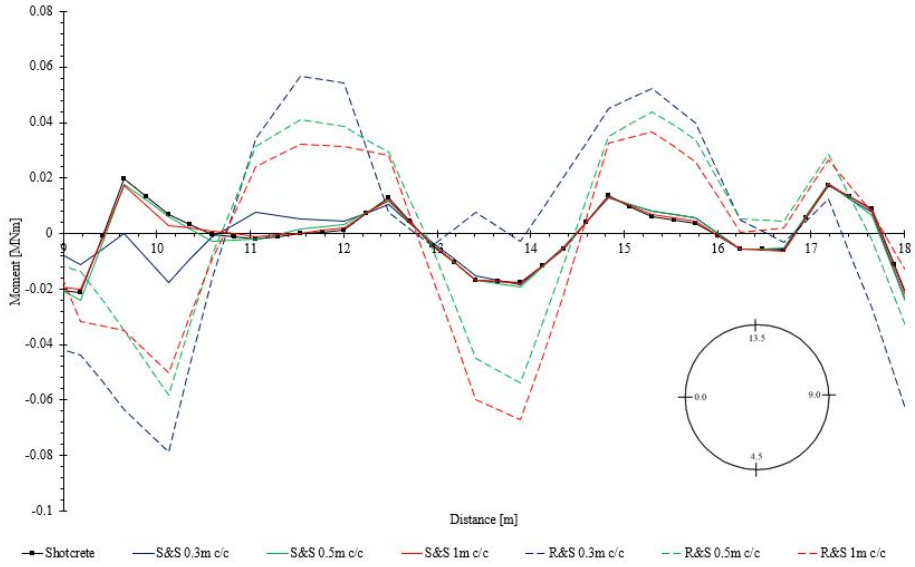

(a) D = 0

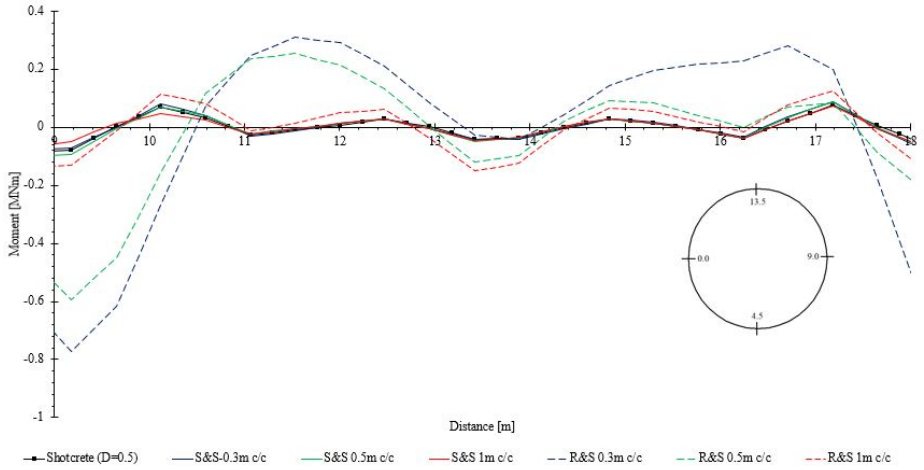

(b) D = 0.5

Figure 3.4: Distribution of total moment in various liners.

3.2 Modeling in Weak Rocks

Due to the geological setting of the Himalayas, underground construction faces many challenges most of which is excessive deformation due to rock squeezing. Rock squeezing is mainly seen in weak rocks which occurs due to the failure of rock masses around the excavation under the influence of high rock cover and tectonic stress. This problem is aggravated by the presence of joints and faults in the region. It is thus necessary to know the behavior of the rock mass and its strength, including their peak and residual strengths for proper design and analysis of the structures. Although the rock mass fails after the surrounding stress exceeds its peak strength, collapse of the structure does not occur immediately as the nature and properties of the rocks allows it sustain stress until its residual strength. The residual strength can be described as the reduced capacity of the rocks, or the rock mass in general, to sustain the stress

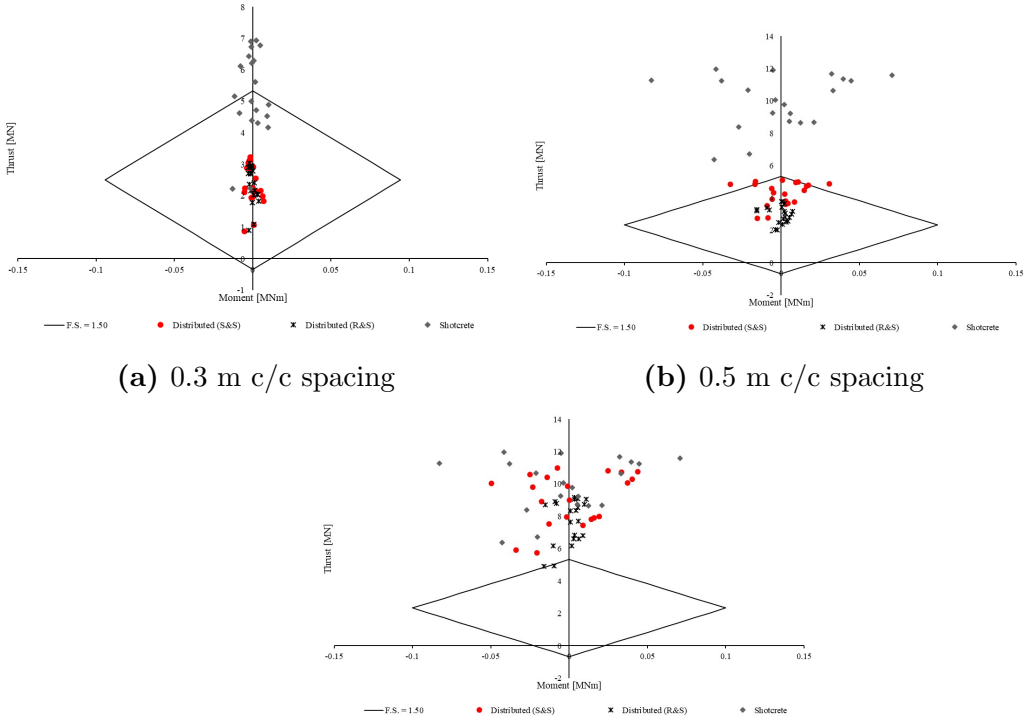

(a) 0.3 m c/c spacing

(b) 0.5 m c/c spacing

(c) 1 m c/c spacing

Figure 3.5: Thrust-Moment interaction diagram for shotcrete element in composite section.

after initial failure occurs on reaching its peak strength.

Various researches have been carried our for the studying the failure characteristics of the rocks. Traditional methods included laboratory tests which was expensive and the major shotcoming of lab tests were that sufficient information would still be unavailable for the preliminary design of the structures. Hoek, Kaiser, and Bawden (1995) developed the Geological Strength Index (GSI) (Section 2.2.5) to estimate the peak strength of jointed rock mass based on the geological conditions of the rock mass. This allowed designers to access the characteristics of the rock mass without direct access from the tunnels. This system provided complete set of mechanical properties for both Hoek-Brown and equivalent Mohr-Columb failure criteria but was not able to give information for estimation of the residual strength.

3.2.1 Rock Failure Models

Cai, Kaiser, Tasaka, and Minami (2007), suggested that understanding of the rock mass strength behavior, including the peak and residual strength, will facilitate the cost-effective design of tunnel support. Hoek (2007) had suggested post failure characteristics for different quality of rock masses which states that the elastic-brittle, strain-softening, and elastic-plastic failures are characteristics for very good quality

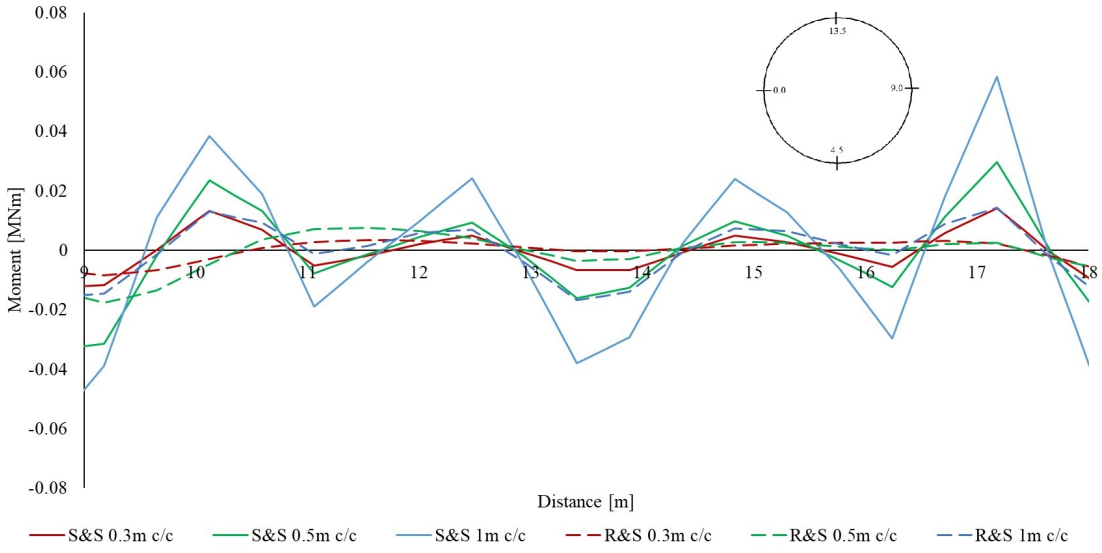

(a) Moment acting in shotcrete element

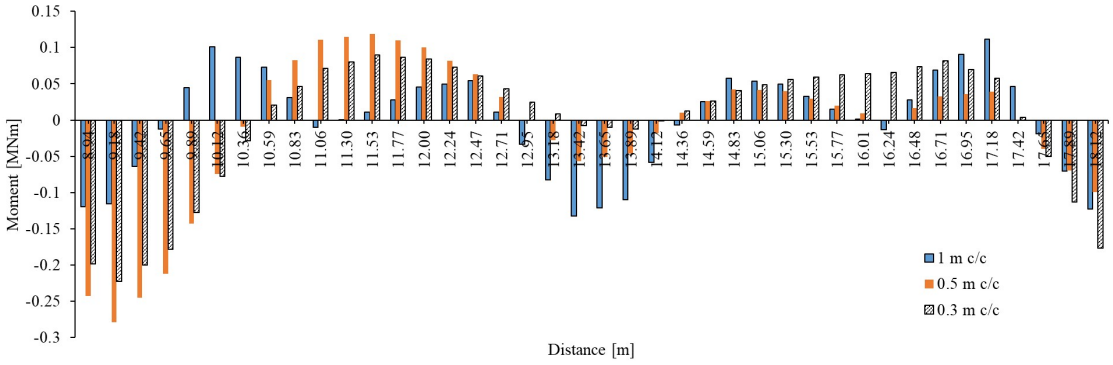

(b) Moment acting in RRS beam element

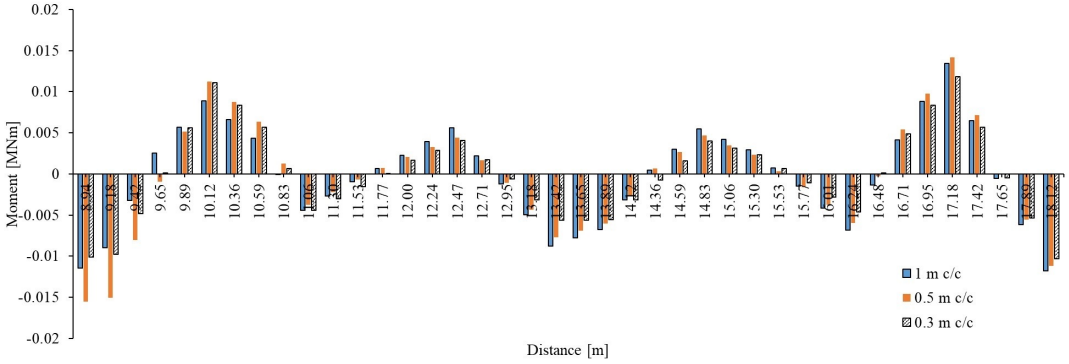

(c) Moment acting in Steel beam element

Figure 3.6: Bending moment acting over the individual element in the composite sections.

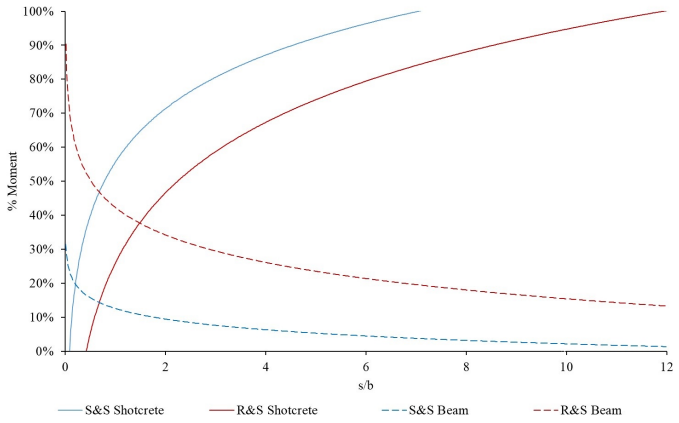

Figure 3.7: Percent distribution of moment in individual elements of the composite supports.

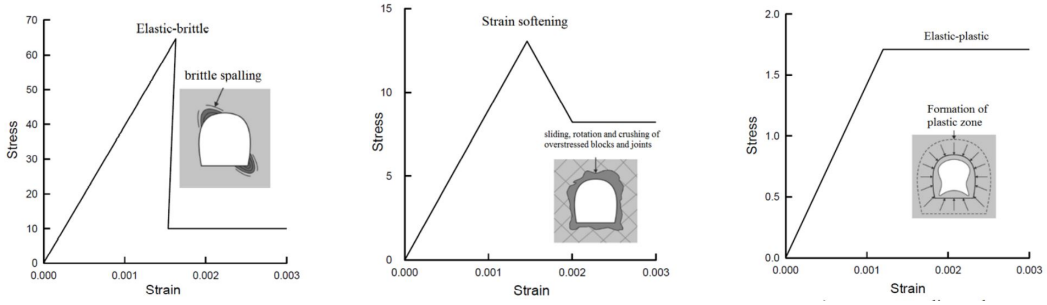

(a) Very good quality hard rock mass.

(b) Average quality mass.

(c) Very poor quality rock mass.

Figure 3.8: Post failure characteristics of different quality of rock mass. (Khakda, 2019; Lorig & Varona, 2013)

hard rock mass, average quality rock mass and very poor-quality rock mass respectively. Figure 3.8 (Khakda, 2019; Lorig & Varona, 2013) shows the three different post failure modes of the rock.

Among these failure behavior, the rock masses in general exhibit strain-softening behavior, except when highly disturbed, so that the residual strength parameters are lower than peak parameters (Cai et al., 2007). Strain-softening behavior describes the gradual loss of load bearing capacity of a material. Peak strength is the maximum shear strength or shear stress at yield point given by a curve obtained by plotting shear displacement against shear stress at constant normal stress. Residual strength is the shear strength that levels out at a constant value with increasing shear displacement in a shear test at a constant normal stress (Goodman, 1989). Similarly, according to Hoek (2007), in case of elastic-perfectly- plastic behavior of rock, the residual strength of rock mass parameter is considered as equal to the peak strength of rock mass parameters as can be seen in Figure 3.8c.

Cai et al. (2007) also discussed on the importance and necessity for estimating the residual strength fo the rocks on design of support for the underground excavation

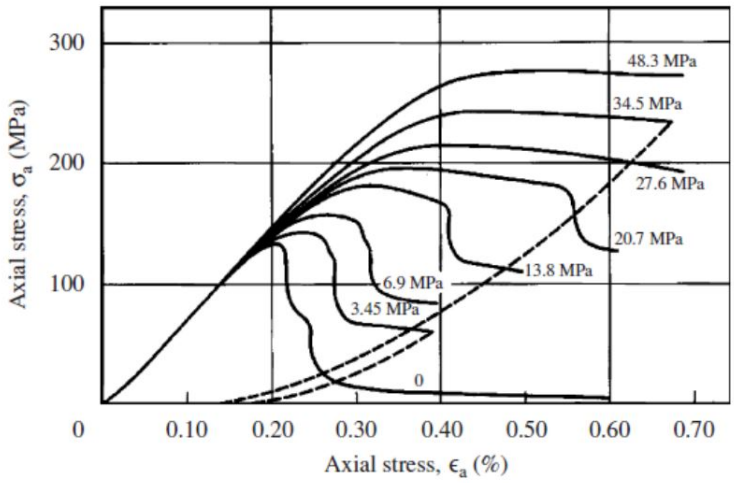

Figure 3.9: Stress – strain curves for Tennessee Marble at different confining stresses. (Wawersik & Fairhurst, 1970)

which has been summarized by Khakda (2019) and given below:

Influence of residual strength of rock mass to design underground structure:

- The post – peak behavior of rock is important in the design of underground excavation because it has significant influence upon the stability of the excavation.
- The rocks retain some strength even when their maximum load-carrying capacity has been exceeded.
- The peak and residual strength of rocks increase with increasing confining pressure as shown in Figure 3.9, triaxial test on marble (Wawersik & Fairhurst, 1970). At low confinement stresses, the loss of cohesive strength component around peak load leads to strain localization with significant stress drop, which is traditionally called strain-softening behavior.

Need of accurate determination of the residual strength of rock mass:

- The post-peak strength depends on the resistance developed on the failure plane against further straining. Initially, the fracture orientation, degree of interlocking, surface irregularity or roughness will affect the level of resistance. However, as strain increases, the residual strength will be less.
- In the field, the post-peak strength will be influenced by the boundary conditions as well. If further straining is constrained, then, the residual strength level cannot be reached and the rock mass can thus support a higher load than the residual strength would suggest.
- It is very challenging and difficult task to correctly represent the strain-softening behavior of rock masses due to a lack of large scale test data.

- Most numerical tools designed for the rock engineering application, however, provide strain-softening constitutive models of varying sophistication to describe the behavior of jointed rock masses.
- In these models, the residual strength of rock mass and the rate of the post-peak strength degradation play an important role in the determination of the size of the plastic zone and the associated rock mass deformation, affecting the final rock support system design.
- If the residual strength is not determined appropriately, an optimal rock support design can never be achieved. Therefore, the basic guidelines are that the residual strength of rock masses has to be properly determined in order to design the appropriate rock support system.

3.2.2 Selection of Residual Parameters

Several researchers have determined different methods for determining the residual parameters for rock mass. As reported by Cai et al. (2007), Russo, Kalamaras, and Grasso (1998) suggested to set the residual *GSI* value at 36% of the peak *GSI* value, which according to Cai et al. (2007) underestimates the residual *GSI* values for poor quality rocks and overestimates for good quality rocks. Similarly, Ribacchi (2000) suggested to use the relations given in Equation (3.11) to estimate the strength of jointed rock masses.

$$\left.\begin{aligned} m_b &= 0.65 m_r \\ s_r &= 0.04 s \\ or,\ (\sigma_c)_r &= 0.2\sigma_c \end{aligned}\right\} \tag{3.11}$$

where, m_b and s are the Hoek-Brown peak strength parameters, the subscript 'r' indicates residual values and σ_c is the uniaxial compressive strength of the intact rock. According to Cai et al. (2007), these relations may only be valid for rock masses in which the joints are characterized by a thin infilling or slightly weathered to unweathered joint walls. The corresponding *GSI* reduction that would fir such parameters is approximately $GSI_r = 0.7GSI$.

Similarly, Cai et al. (2007) analyzed the residual strength by studying the effect of Block Size (V_b) and Joint Surface Condition (J_c). The residual *GSI* (GSI_r) is thus a function of residual J_c^r and V_b^r and is given by Equation (3.12).

$$GSI_r(V_b^r, J_c^r) = \frac{26.5 + 8.79 ln J_c^r + 0.9 ln V_b^r}{1 + 0.0151 ln J_c^r - 0.0253 ln V_b^r} \tag{3.12}$$

Similarly, the author suggests that since fracturing and shearing do not affect the

Table 3.4: Reduction in peak GSI for determining the residual GSI value. (Khakda, 2019)

GSI	Rock Model	Residual GSI
$20 < GSI < 30$	Elastic-Plastic	No reduction in peak *GSI*
$30 < GSI < 50$	Strain softening	Reduce between 60–70% of peak GSI
$50 < GSI < 65$		Reduce between 40–50% of peak *GSI*

intact rock properties, the mechanical parameters σ_c and m_i should be unchanged for residual strength calculation. Other Hoek-Brown parameters are obtained by the same equation as for peak strength only by replacing the peak *GSI* by residual *GSI*. It was seen that for $GSI < 40$, s, the cohesive strength component, becomes very small and can be ignored in defining the residual strength. For $GSI > 40$, a is approximately 0.5, whereas a is slightly larger than 0.5 for $20 < GSI < 40$ Cai et al. (2007). Also the authors suggests that the disturbance factor for the residual is 0 since the rock masses are in a damaged and residual state.

Khakda (2019) performed analysis on case histories from the Himalayan region, especially the Lesser Himalayas. Two-dimensional and three-dimensional study were carried out to determine the amount of reduction in the peak *GSI* value for different rock mass. Consistent with the results of Cai et al. (2007), Khakda (2019) suggested the reduction in the peak value for determining the residual *GSI* value as given in Table 3.4. The results were in good aggreement with the findings from Cai et al. (2007).

3.2.3 Two-Dimensional modeling of face support

For support of weak rock mass, it is essential to provide face support or to stabilize the rock mass before the excavation. Pre-support is commonly adopted since in such cases and is acheived by use of spiling bolts or forepoles. Figure 3.10 shows the use of spiling bolts to overcome the problem of squeezing in very weak rock mass in Super Madi Hydroelectric project and Super Dordi Hydroelectric project in Nepal. The tunnel excavation was done in weak rock mass in case of Figure 3.10a while a section in the tunnel failed due to excessive water pressure in Figure 3.10b which was later overcome by use of closely spaced spiling bolts of 32 mm diameter and the water was also allowed to be released to prevent the additional pressure on the supports. Modeling of such supports comes as a challenge in modeling since such supports required three-dimensional rock models. The condition of rock mass ahead and behind of the face requires a 3D model. Although, axissymetric modeling can be developed in 2D model

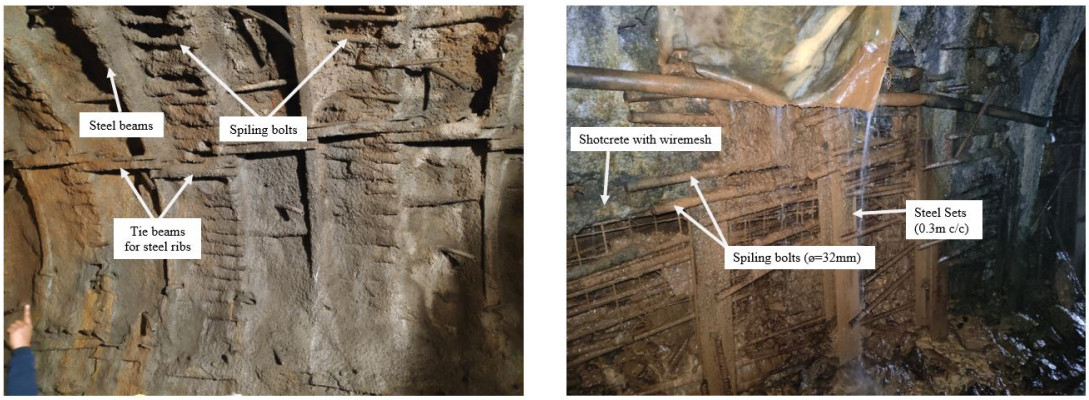

(a) Super Madi HEP **(b)** Super Dordi HEP

Figure 3.10: Use of spiling bolt support in tunnels from Lesser Himalayas region of Nepal.

which allows to study the behavior of the rock mass ahead of face and the results of the axissymetric model can be used in a 3D model, it is difficult to represent the rock mass ahead of a face in a simple two dimensional model. Performing three dimensional modeling is time consuming and requires high computational power, due to which is it rarely adopted during the design of underground structures. In contrast, two dimensional methods allows a designer to study several sections since it is simpler to use and the computational time is very less. In order to overcome this problem of modeling, Hoek (2001, 2004) proposed a solution to model the effects of forepole in a 2D model allowing a designer to effectively design and model a weak rock mass excavation.

In the absence of a general rule to model the forepole, Hoek (2001, 2004) developed an equivalent model of the forepole by taking weighted average of the strength of the forepole elements. Thus by providing an improved rock mass above the excavation allows to simulate the forepole arch in a two-dimensional model. This method as suggested by Hoek (2001), although does not correctly represent the three-dimensional bending strength of the umbrella, it permits the construction of a 2D model that behaves numerical well. Also, the performance of tunnels supported with forepole umbrellas designed in this manner confirms that the improved strength estimates appear to be reasonable as found by Hoek (2001). This assumption has also been utilized successfully by Karki, Karki, et al. (2020) for modeling a squeezing ground of a hydropower tunnel in the Lesser Himalayas. This methodology, as shown in Figure 3.11, has thus been adopted to model the weak rock mass in this study.

Figure 3.11 shows that first the support is designed according to the rock mass classification and is checked for its sufficiency for the ground condition through numerical modeling. If the support proves to be sufficient, the design is adopted as the final design and in case of failure of the support, assessment of the rock quality

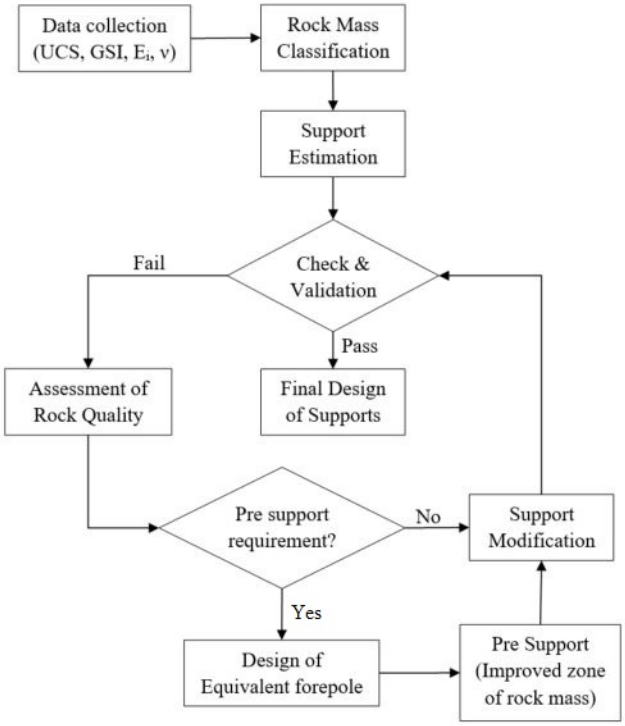

Figure 3.11: Methodology for pre-support of excavation in weak rock mass.

is done. This assessment allows the designer to determine whether pre support is required and in case where it is required, the forepole is modeled with appropriate parameters estimated by weight average and use of RocLab software. Pre-support is provided in the model through improved rock mass above the excavation and other support modification such as installation of steel sets is done contrary to the empirical support estimation. This modified support is again checked for failure and the process is repeated unless the design is found to be safe.

The properties of the improved rock mass equivalent to the forepole umbrella is calculated by multiplying the strength of each component: rock, steel pipe and cement grout, by the cross sectional area of each component and then dividing the sum of these products by the total area. By assuming that the steps in the tunnel roof required to install the forepoles are approximately 0.6 m deep, a rock beam of dimension 0.6 m deep and 1 m wide will be taken for the calculation of the strength parameters. The forepole is assumed to have an outer diameter of 114 mm and inner diameter of 100 mm and are spaced at regular interval of 0.5 m. As an example, a section of Chameliya hydropower project (Ch. 3+190) is shown whose rock mass properties is detailed in Table 5.2. The quantities of the section with the forepole thus are as follows:

The resulting rock mass strength for this composite beam is thus 2.136/0.62 = 3.45 MPa. This rock mass strength is used as input in the RocLab to find the corresponding properties of the equivalent rock material. Figure 3.12 shows the result

Component	Area (m^2)	Strength (MPa)	Product
Rock	0.6	0.727	0.4362
Forepole	0.005	250	1.25
Grout	0.015	30	0.45
Sum	0.62		2.1362

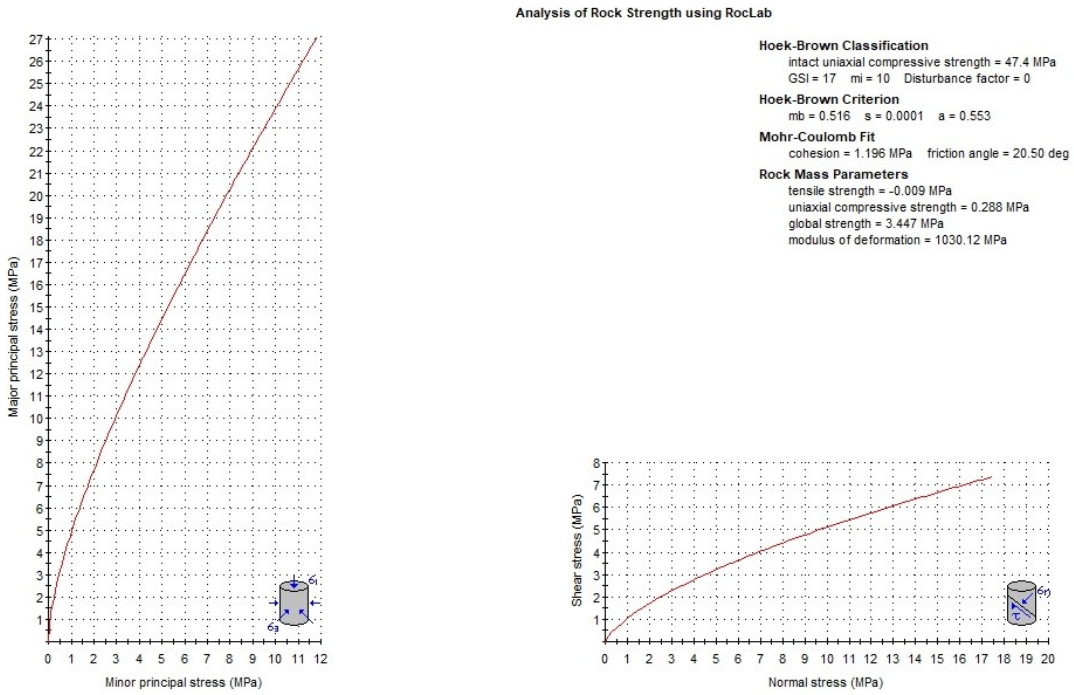

Figure 3.12: Results from RocLab for Chainage 3+190 m of Chameliya headrace tunnel.

from RocLab for the improved rock mass. The *GSI*- and the intact rock constant m_i are unchanged for the improved rock mass since the effect of forepole is to improve the overall strength of the rock mass and not to change the characteristics of the rock. This results in the following properties of the material:

Geological Strength Index (GSI)	17
Hoek-Brown Constant m_i	10
Intact Rock Strength σ_{ci}	47.4 MPa
Rock Mass Strength $\sigma_r m$	3.45 MPa
Material constant m_b	0.516
Material constant s	0.0001
Material constant a	0.553
Deformation Modulus E	1030.12 MPa

3.3 Conclusion

The major difference in performance between the two composites of steel and shotcrete (S&S) and *RRS* and shotcrete (R&S) is seen in taking up the bending moment load.

The R&S composite takes higher value of moment suggesting its better capacity in taking moment compared to the S&S composite. Also in case of S&S composite, majority of the moment is taken up by the shotcrete element in contrast to the R&S composite where the moment is almost uniformly distributed among the support elements (shotcrete and *RRS* beam).

The spacing of liners has significant contribution in distributing the moment in individual element, i.e. the moment over the shotcrete decreases with decreased spacing while the moment over the beam element (steel and *RRS*) increases with decreased spacing. Although the capacity of the R&S composite in taking bending moment is higher than S&S composite, both the composite shows similar and safe behavior for a given (weak) ground condition. This could imply that R&S support could lead to oversupport of the ground as can be seen in Figure 3.5 where both the support is safe for 0.3 and 0.5 m spacing while both fails for 1 m spacing supported by Figure 3.4 which shows higher capacity in bending for R&S composite. It is seen that the shotcrete element takes higher moment in S&S composite and the reason could lie in the load sharing mechanism among the elements. In case of the S&S composite, the load could be taken up only the shotcrete element first until its elastic limit is reached and then transfer the remaining load to the steel beam. While in R&S composite, the load sharing between the two element might start from an early stage leading to more or less uniform distribution of moment among the elements. Through the analysis we can say that the *RRS* shows better performance in bending than the steel beam due to which it can take more load compared to the steel beam resulting in lesser load to the shotcrete. However, the general practice in the tunneling in Nepal Himalayas is to use steel ribs and through this study it can be concluded that although *RRS* shows better performance in bending, the use of steel ribs is also suitable since it also provides sufficient support for the excavation.

Also while modeling in weak rock mass, it is essential to determine the rock model to be used. Among the three models, the strain-softening and the elastic-plastic model is better suited for the Himalayan geology. As shown by Khakda (2019), the selection of the residual parameters while modeling can be done based on the *GSI* values for which Khakda (2019) has provided a guideline (Table 3.4). While constructing tunnels and caverns in the weak geology of the Himalayas, designers tend to use heavy support through closely space steel ribs and use of forepoles, however, it is not done in numerical modeling. Since modeling of support ahead of the face required three-dimensional model, it is seldom done during the designing phase. This could lead to insufficient support design and thus a methodology has been proposed to model the pre-supports like spiling bolts and forepole in two-dimensional model. The modeling can be achieved by providing improved rock mass parameters above (or around) the crown of the excavation. The improved rock mass is determined by

weighted average method as suggested by Hoek (2001). The method leads to reduced amount of support required for the excavation and could be practically used during the design phase. However, it should be kept in mind that the accuracy of the model always depends on the accuracy of the input parameters and thus should be used with care.

Chapter IV
Description of Case Studies

4.1 General

Since the study focuses on the modelling of rock mass in weak geology, tunnel sections from three hydropower tunnels in the Lesser Himalayan region has been selected. The sections have been selected based on the availability of data of rock mass properties, support design and measured deformations. The data and the required information has been extracted from published reports, research articles and laboratory test reports. Selective sections from each of the tunnel has been modelled using the commercially available finite element modelling software *RS2* developed by RocScience. The study sections have been selected such that it represents rock mass from poor to extremely poor condition.

4.2 Chameliya Hydropower Tunnel

4.2.1 Introduction

Chameliya Hydropower Project is located in *Darchula* district, about 270 km North-West of *Dhangadi* in *Sudurpaschim* province, Nepal. The project lies in the Lesser Himalayan region in the catchment of Chameliya river. The project completed in 2074 B.S. with an installed capacity of 30 MW. The project is a run-off-river project with a design discharge of 36 m^3/s and a gross head of 103.7 m. The project is currently owned and operated by the Nepal Electricity Authority (NEA). The project incorporates a headrace tunnel of length 4067 m with a horse-shoe excavation of diameter 5.1/4.2 m depending upon the rock mass quality encountered.

4.2.2 Geology of Area

The project lies in the western part of the Lesser Himalayan Region. The project area is located in the west-central part of the Lesser Himalayan Zone and is 60 km north of the Main Boundary Thrust (MBT) and close to the Main Central Thrust (MCT). The main rock types along the alignment of headrace tunnel are dolomite, sandstone, slate, dolomite interbedded with phyllite (Basnet, 2013). The rocks are highly jointed, weathered with number of shear bands and crushed zone as shown in Figure 4.1 obtained from Khakda (2019). As seen in the figure, the major rock type until Adit 2 is slate and dolomite and the Q-value encountered in the section is between the range of 1 and 2. The rock mass is classified as poor based on the rock

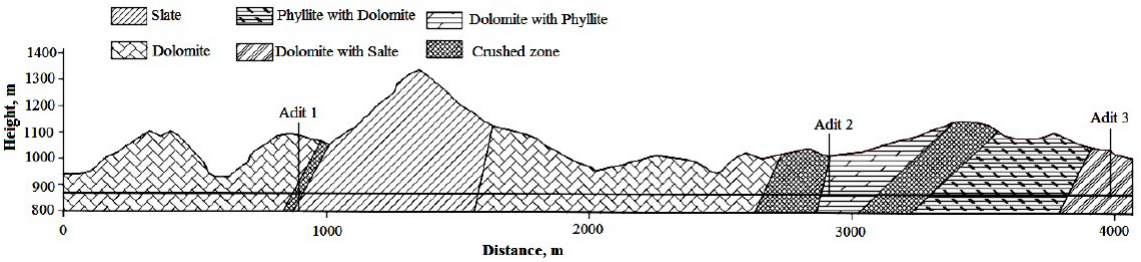

Figure 4.1: Longitudinal geological map of Chameliya hydropower tunnel along the alignment (Khakda, 2019)

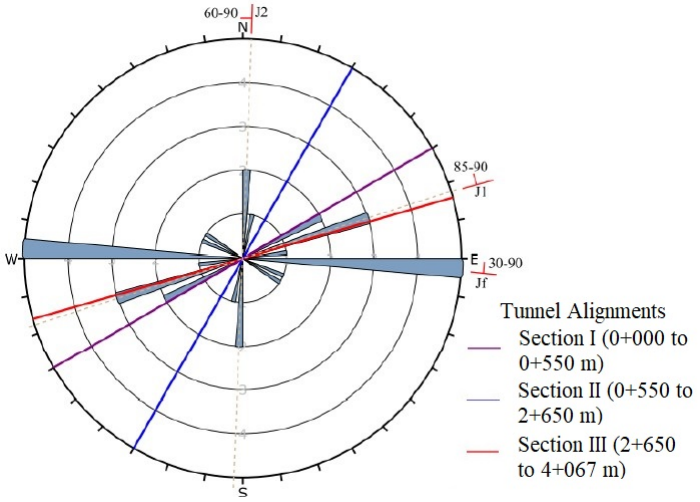

Figure 4.2: Orientation of major joint sets and headrace tunnel alignment of Chameliya HEP (NEA, 1997)

mass quality and no severe problems were encountered in the region. However, from Adit 2 to Adit 3, the rock mass is classified as extremely poor with Q values less than 1. Major stability problems were encountered in the region with squeezing upto 2.39 m *(chainage 3+398 m.* The maximum rock cover above the tunnel is nearly 470 m between Adit 1 and 2 while it is around 275 m between Adit 2 and 3.

Figure 4.2 shows the orientation of Chameliya headrace tunnel along with the major joint sets in the area obtained from NEA (1997). It can be seen from the figure that there are three sections of the headrace tunnel with the first section aligned favorably with respect to foliation joint (J_f) but is parallel to a random joint which can cause some minor instability problem. The second section, which covers most of the tunnel, is aligned most favorably to the joint sets. The last section is parallel to joint set J_1 which could cause some instability problems. There are three joint sets with random joints as seen from the figure.

Table 4.1: Details of squeezing section from chainage 3+172 to 3+820 m in Chameliya headrace tunnel (Basnet, 2013; Khakda, 2019)

S.N.	Chainage (m)	Rock Type	Rock Cover (m)	Q value	Support Category	Measured Convergence (m)
1	3+172	Highly fractured and heavily jointed Dolomite	199.7	0.02	R5	0.238
2	3+190	Dolomite, Fractured, Shear band	203.9	0.031	R5	1.326
3	3+253		220.1	0.01		0.104
4	3+275		230.7			0.822
5	3+296	Thinly foliated phyllite within very thin band of dolomite	239.5	0.01	R6	0.650
6	3+305		243.2			1.117
7	3+314	Very weak thinly foliated Phyllite with some bands of dolomite	246.3			0.198
8	3+398		274.4			2.319
9	3+404	Very thinly foliated, highly jointed or fractured and crushed Talcosic Phyllite with few dolomite and several shear/talc bands, few bands of dolomite	275.2	0.008	R6	2.142
10	3+420		277.1			1.570
11	3+439		275.5			1.752
12	3+454		274.4			1.420
13	3+499		268.0			0.801
14	3+543		249.9			2.090
15	3+681		210.8			0.952
16	3+709		212.5			2.038
17	3+733	Highly jointed or fractured, thinly foliated talcosic phyllite	219.1	0.01	R6	0.630
18	3+764	Jointed or fractured, thinly foliated phyllite. At right wall dolomite and phyllite present	230.0	0.015	R5	0.510
19	3+795		222.6			0.062
20	3+820		211.4			0.941

4.2.3 Design of Tunnel Support

The design of tunnel support in the region is done based on the Q-system proposed by Barton et al. (1974). Based on the encountered rock mass quality, the Q-value along with the support provided in the site is summarized in Table 4.1 (Basnet, 2013; Khakda, 2019) (The support empirically defined according to the Q value can be obtained from Chart B.3). The support provided in the site is categorized into 6 classes from *R1* to *R6* whose details is provided in Table 4.2 (Khakda, 2019). Tunnel section from chainages 0+000 to 3+100 m was excavated by adopting the conventional drill and blast methodology. But for the sections with severe squeezing problems, different methods were attempted such as over excavation but unsuccessful, fore-poling, sequential excavation (top heading and benching), excavation through light controlled blasting and manual excavations etc. The support system provided in the site according to the rock mass class is shown in Figure 4.3 (Shah, 2016).

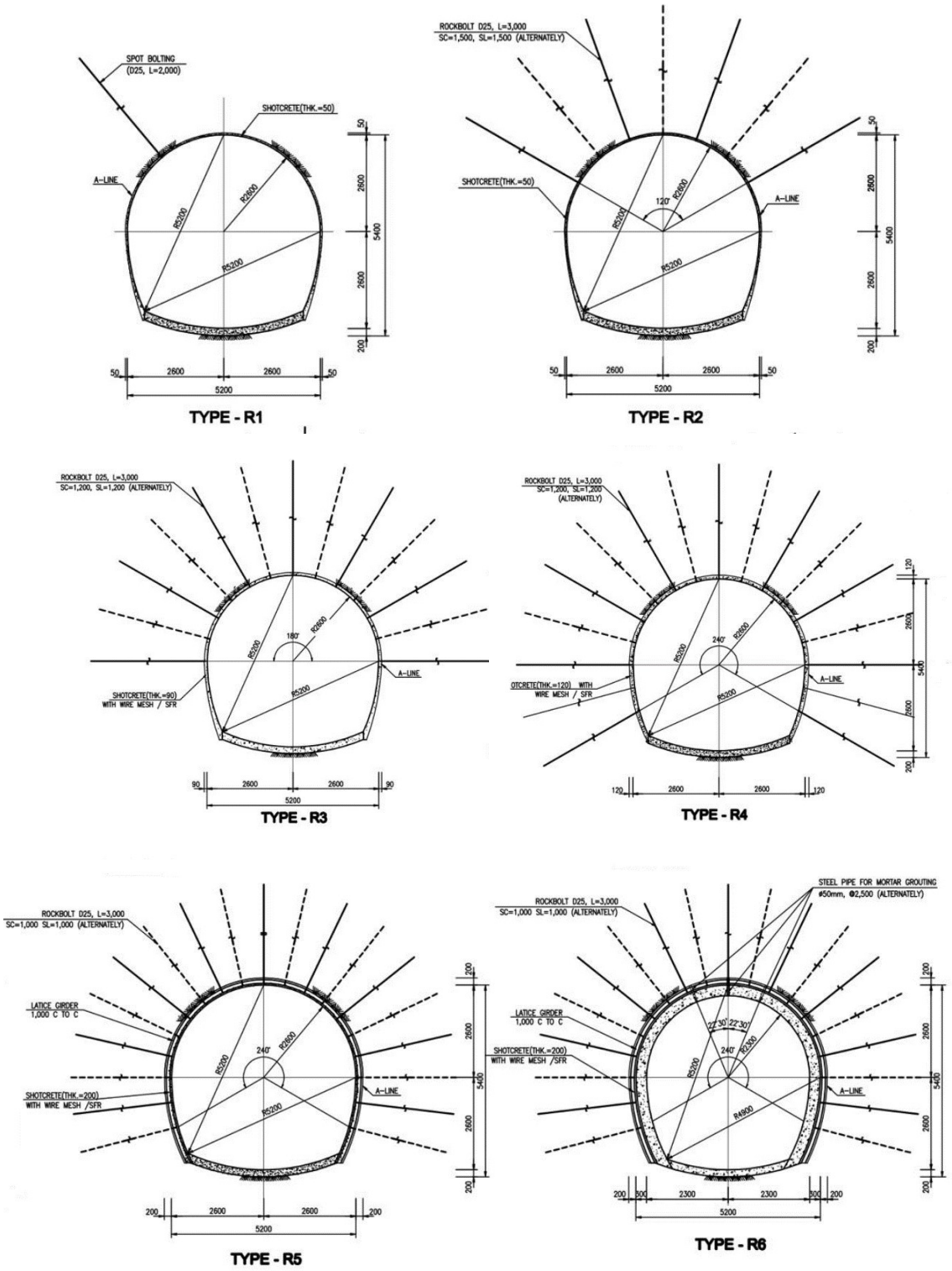

Figure 4.3: Tunnel support used in Chameliya headrace tunnel (Shah, 2016)

Table 4.2: Rock mass classification and support pattern for Chameliya hydropower tunnel based on the Q-system (Khakda, 2019)

Rock Class	Q-value	Support Category	Rock Support Details
Strong	$10 < Q$	R1	25 mm dia. 3 m rockbolts in distribution 2.0x2.5 m^2. 50 mm SFRS in walls and crown , 200 mm thick concrete lining is applied in invert without steel support
Very Good	$4 < Q < 10$	R2	25 mm dia. 3 m rockbolts in distribution 1.5x1.5 m^2. 50 mm SFRS in wall and crown, 200 mm thick concrete lining is applied in invert without steel support
Good	$1 < Q < 4$	R3	25 mm dia. 3 m rockbolts in distribution 1.2x1.2 m^2. 90 mm SFRS in wall and crown, 200 mm thick concrete lining is applied in invert without steel support
Fair	$0.1 < Q < 1$	R4	25 mm dia. 3 m rockbolts in distribution 1.2x1.2 m^2, upper 240^0. 120 mm SFRS in wall and crown, 200 mm thick concrete lining is applied in invert without steel support
Poor	$0.01 < Q < 0.1$	R5	25 mm dia. 3 m rockbolts in distribution 1.0x1.0 m^2, upper 240^0. 200 mm SFRS in wall and crown, 200 mm thick concrete lining is applied in invert without steel support, 4 bar lattice girder bar size 18, 26 mm is provided at 1.0 m c/c
Very Poor	$Q < 0.01$	R6	25 mm dia. 3 m rockbolts in distribution 1.0x1.0 m^2, upper 240^0. 200 mm SFRS in wall and crown, 200 mm thick concrete lining is applied in invert without steel

4.2.4 Instability Problems

The major problem of instability was encountered in the section between chainage 3+100 to 3+900 m. Due to presence of weak rock mass which was highly weathered and the geology being significantly different from the initially predicted properties during pre-feasibility stage, the tunnel suffered heavy squeezing. Talcosic phyllite of extremely poor quality along with major crushed zone was encountered in the region which caused several instances of several mud flows and floor heaving along with wall and crown closure. Figure 4.4 (Shah, 2016) shows the problem of squeezing and mud flow encountered in the project. The provided support failed with cracking of shotcrete and buckling of steel ribs in the region and the excavation work had been delayed for a long time. A maximum closure of 2.39 m was recorded in the area and the sections had to be re-excavated with new lining installation. Table 4.1 gives the details of the squeezing sections in the project. Apart from this weak section of about 550 m length, other sections encountered minor stability problems of rock spalling, minor instances of mud flow, etc. which was addressed with wire mesh shotcrete and rock bolts.

(a) **(b)**

Figure 4.4: (a) Squeezing and (b) Mud flow in sections of Chameliya headrace tunnel (Shah, 2016)

4.3 Kaligandaki 'A' Hydropower Tunnel

4.3.1 Introduction

The Kaligandaki 'A' Hydroelectric project is located in the Lesser Himalayan region of Nepal about 200 km west of Kathmandu. The construction of the project, owned by Nepal Electricity Authority (NEA), began in 1997 A.D. and was completed in 2002 A.D. The project has an installed capacity of 144 MW with generation capacity of 842 GWh electricity annually. The project has a tunnel of length 5950 m of horse-shoe shape with a cross-sectional area of around 60 m^2 and a excavation diameter of 8.4 m. The final diameter of the concrete lined tunnel is 7.4 m with a circular profile. The project has a net head of 115 m with a design discharge of 141 m^3/s (NEA, 2004).

4.3.2 Geology of Area

Geologically the project lies in the Lesser Himalayan highly deformed rock formations and is relatively close to the Main Boundary Thrust *(MBT)* in the south and the Main Central Thrust *(MCT)* in the north (P. K. Shrestha & Panthi, 2014a). Figure 4.5 (Khakda, 2019) shows the geological profile of the headrace tunnel which shows that the tunnel mostly passes through highly deformed graphitic phyllite, siliceous phyllite and phyllitic slate intercalation. The first few hundred meters upstream section of the headrace tunnel consists of highly fractured and weathered siliceous dolomite in intercalation with graphitic phyllite.

The project area lies very close to several local faults, namely *Badighat*, *Andhikhola* and *Kaligandaki* faults. A branch of the *Andhikhola* fault, *Andhi Fault*, crosses the headrace tunnel at about 700 m from the intake (Figure 4.5). The rock

mass along the tunnel alignment varies from extremely poor to fair quality with Q values ranging from 0.01 to 3.62. As can be seen from the Figure 4.5, the rock cover over the tunnel is more than 600 m with more than 80% of the tunnel subjected to overburden exceeding 200 m.

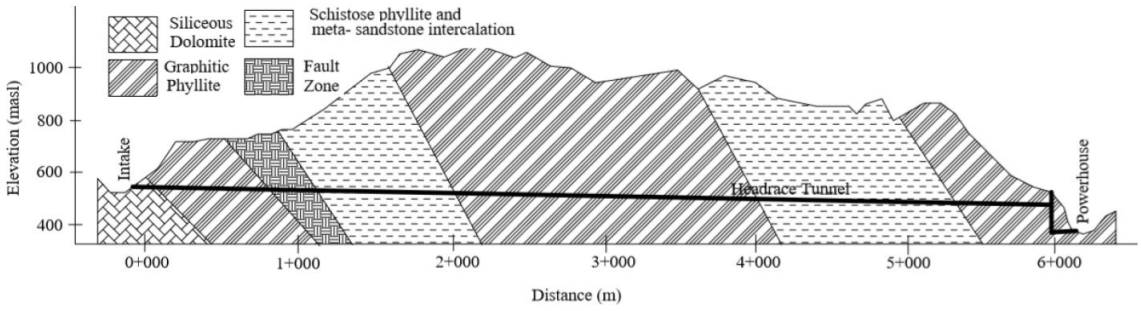

Figure 4.5: Geological Profile of Kaligandaki 'A' headrace tunnel (Khakda, 2019)

Figure 4.6a (Panthi, 2006) shows the major joint sets and the tunnel orientation. As can be seen from the figure, the orientation and dip of the joints are highly scattered giving no distinct joint system except for foliation joints. The foliation joint has an strike orientation between $N85^0$ to 140^0E with dip angle between $25 - 55^0$ towards South-West. The alteration and weathering of discontinuity surface are considerable and the joints are filled with highly sheared clay, quartz and calcite veins.

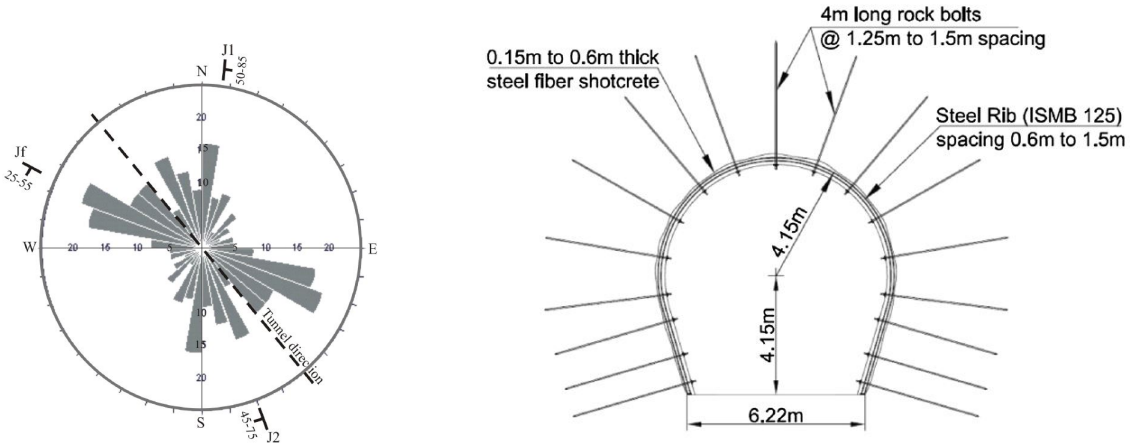

(a) **(b)**

Figure 4.6: (a) Orientation of main joint sets and Kaligandaki 'A' headrace tunnel (Panthi, 2006) and (b) Typical tunnel section with applied supports (P. K. Shrestha & Panthi, 2014a)

4.3.3 Design of Tunnel Support

The headrace tunnel was excavated using heading and benching in the weak rock mass and full face excavation in the relatively good rock mass. Use of heavy tunnel linings were done to address the squeezing problem in weak rock mass. The preliminary rock support that was commonly applied consisted of steel ribs of *ISMB125* spaced 0.6–1.5 m apart, steel-fiber-reinforced shotcrete of thickness 0.15–0.6 m, and grouted rock bolts 4 m long and 25 mm in diameter. Spiling bars 25 mm in diameter were also used in limited stretches of the tunnel when the rock mass was of exceptionally poor quality. After the tunnel had been fully excavated it was supported by a full concrete lining (Panthi & Shrestha, 2018; P. K. Shrestha & Panthi, 2014a). Figure 4.6b from P. K. Shrestha and Panthi (2014a) shows a typical section with applied supports. It should be noted that Figure 4.6b is only a representative figure showing the support elements and the actual supports provided in the tunnel varies according to the encountered rock mass conditions.

4.3.4 Instability Problems

Based on the pre-construction results, it was estimated that the tunnel might be subjected to heavy squeezing in the upstream section. The rest of the tunnel alignment was assumed to have fair to good quality rock mass except for some sections with highly sheared and deformed rock mass. Accordingly, the estimated temporary tunnel support was also small. However, large variations were observed in the results obtained during the excavation.

The rock was found to be very weak, highly sheared thinly foliated and intensely folded during the excavation. This resulted in severe failure of the tunnel sections with tunnel collapse and moderate to high squeezing of the excavation contours. Presence of weak and thinly foliated phyllite with high degree of strength anisotropy resulted in the reduction of self supporting capacity of the rock mass causing the collapse of sections. While, presence of weak phyllitic rock with low strength along with the presence of high overburden stress resulted in squeezing of the sections (Panthi & Nilsen, 2007). With overburden ranging from 425 m to 620 m, the section passed through highly schistose graphitic phyllite. A maximum of 76 cm of convergence was recorded in the tunnel (Panthi, 2006). Severe squeezing was encountered in about 2 km of the section of tunnel between chainage 1+964 to 4+032 m. Highest convergence was recorded in the spring line of the section. Figure 4.7 (Panthi, 2006) shows the stability issue encountered in the Kaligandaki 'A' headrace tunnel. Figure 4.7a shows the face collapse in chainage 1220 m while Figure 4.7b shows the failure (cracking on the right wall) of concrete lining due to high squeezing pressure.

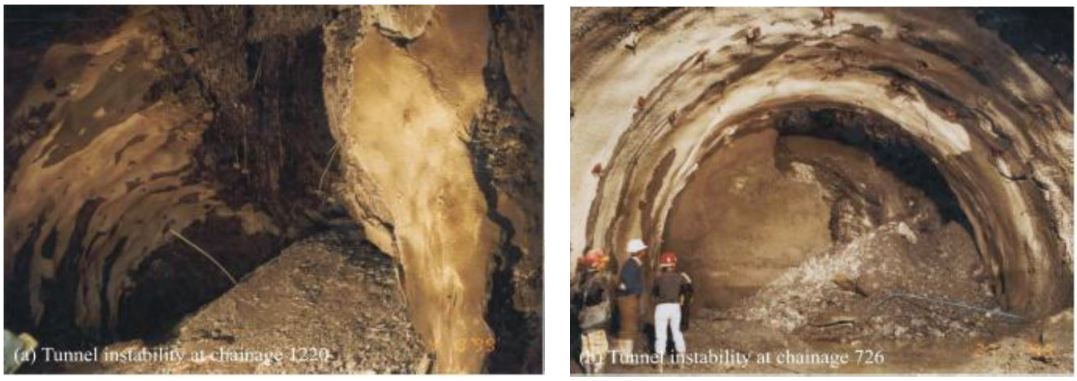

(a) **(b)**

Figure 4.7: (a) Collapse due to strength and stress anisotropy and (b) Cracks formed in the lining due to high squeezing pressure (Panthi, 2006)

4.4 Khimti Hydropower Tunnel

4.4.1 Introduction

Khimti I hydropower is located in the Lesser Himalayan region in *Bagmati* province about 100 km east of Kathmandu. The construction of the project was completed in 2000 A.D. and since then the project has been in commercial operation. The project has an installed capacity of 60 MW and generates approximately 350 GWh electrical energy annually. The project is a high head scheme with design discharge of 10.75 m^3/s and a gross head of 684 m. The total length of waterways is approximately 10 km with 7,888 m long inverted D-shaped headrace tunnel. The cross sectional area of the headrace tunnel varies from 11–14 square meters with the excavation diameter ranging from 4–4.3 m, according to the construction methodology applied (CCC, 2002; G. L. Shrestha, 2005; P. K. Shrestha & Panthi, 2013). The tunnel is 7620 m long and ends in a surge chamber, from where an 898 m long, 45 degree inclined penstock shaft, with steel lining embedded in concrete, leads to the powerhouse. Except the first downstream end of 418 m with full reinforced concrete lining, the tunnel is built on Norwegian tunneling principles and is unlined or shotcrete supported. Modern support means such as pre and post grouting, steel fibre shotcrete, spiling and rock-bolts have been used as temporary and final rock support (Panthi, 2006).

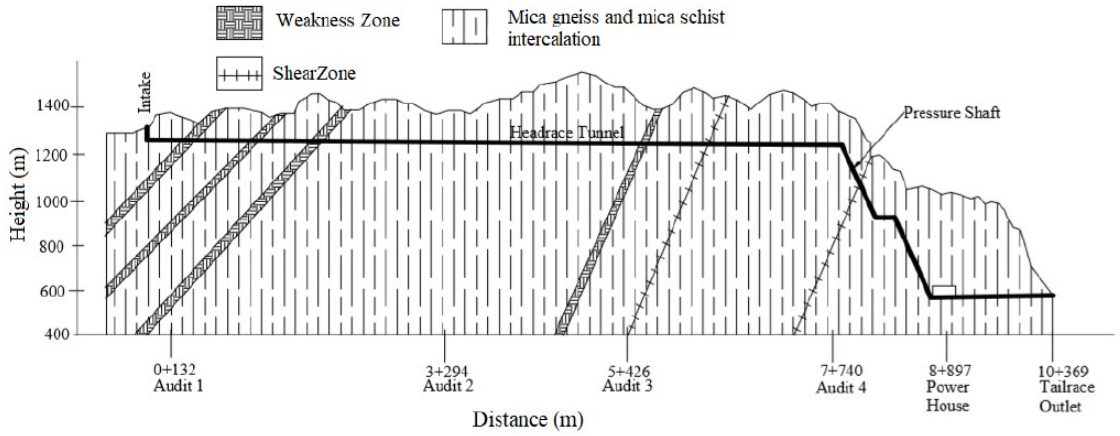

Figure 4.8: Geological profile of Khimti I hydropower project (Panthi, 2006)

4.4.2 Geology of Area

The project area lies in the Midland Schuppen zones of the Melung Augen Gneiss. The rocks in this zone are represented mainly by grey, coarse-to very coarse-grained, porphyroblastic augen gneiss, banded gneiss, and granitic gneiss with bands of very weak, green chlorite and bright grey talcose schist. Structurally the zone is bounded by two major faults: the Midland Thrust and the Jiri Thrust to the south and north, respectively (G. L. Shrestha, 2005). Since the project area is bounded by the Main Central Thrust (MCT), the rock mass along the headrace tunnel is highly jointed, sheared, deeply weathered and deformed. Figure 4.8 (Panthi, 2006) shows the geological profile along the headrace tunnel of the project. With respect to joint filling and alteration, most of the discontinuities at the Southern section of the headrace tunnel (downstream from Adit 3) are filled with clay and bands of chlorite and talcose schist and have been characterized as impermeable with respect to water leakage. In contrast, the discontinuities present at the Northern section of the headrace tunnel are either open or filled with coarse grained permeable silt materials. The intercalation effect of mica schist is also present there, but at greater intervals. In this northern section several open joints with aperture up to 10 cm have been observed during tunnelling. The degree of weathering along the tunnel alignment also varies greatly and is classified as medium to highly weathered according to ISRM (1978). In some sections the degree of weathering was so deep that decomposed and highly sheared organic clay was found in the tunnel. Especially the tunnel section 500 meters downstream from Adit 2 (between chainage 3450 – 3900) was deeply weathered (CCC, 2002). The valley side slope in this stretch of the tunnel is flatter (about 25 degrees) and the rock cover is slightly more than 100 meters (Panthi, 2006).

Figure 4.9, from Panthi (2006), shows the orientation of major joints in the loca-

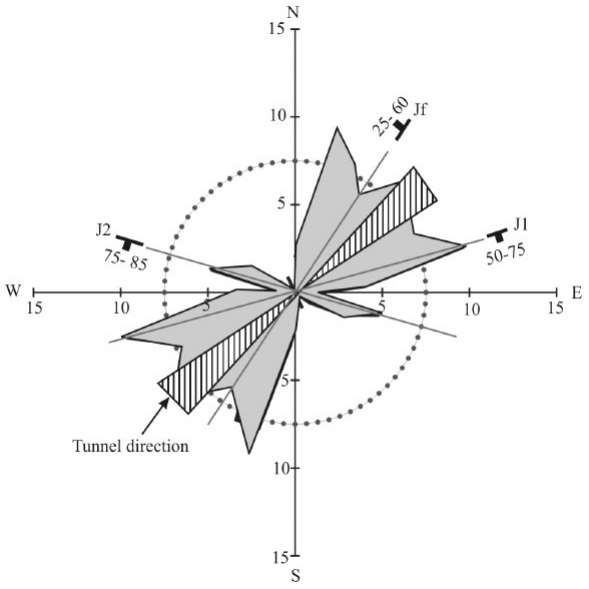

Figure 4.9: Orientation of main joint sets and headrace tunnel of Khimti I hydropower (Panthi, 2006)

tion. From the figure, it can be seen that there exists three major joint sets along the tunnel alignment. The general strikes of the main foliation joints (J_f) were found varying from $N15^0$ to 60^0E. As can be seen in the Figure, this is not very favorable relatively to the headrace tunnel alignment, which also is oriented in Northeast / Southwest direction. The foliation joints are mostly dipping towards Northwest with a varying dip angle of 50 to 60 degrees at the Southern part of the tunnel (adit 4 area), and this trend changes gradually making the dip angle more flat with almost 25 degrees at its Northern part (adit 1). The joint set number one (J_1) is oriented with almost the same strike direction as the foliation joints and is very close to parallel to the tunnel alignment but dipping opposite to the foliation joints (dip angle 50 to 75 degrees towards Southeast). Joint set number two (J_2) is oriented in Northwest Southeast direction with very steep dip angle (70 to 85 degrees) towards Southwest.

4.4.3 Design of Tunnel Support

The tunnel support design was done according to the Q-system of classification. The rock class of the tunnel were divided into five categories according to the Q value and the support design was done according to the need of the rock mass quality. The rock quality found in the tunnel alignment, reported by G. L. Shrestha (2005), consists mostly of weak rock (i.e. $Q < 1$) *(about 72%)*. The distribution of the rock mass consisted of: 7 to 8 percent of exceptionally poor rock mass, 21 to 22 percent of extremely poor rock mass, 43 to 44 percent of very poor rock mass and 27 to 28 percent of fair to poor rock mass. This classification is based on the Q chart (Figure B.3) and the support details for the different class has been given in Table 4.3 (G. L. Shrestha,

Table 4.3: Recommended tunnel support for Khimti hydropower project (for tunnel width of 4 m and ESR of 1.6) (G. L. Shrestha, 2005)

Class	**Q value (RMR value)**	**Support**	**Description**
I	> 4	Spot bolting or unsupported	Mainly competant and stable rock
Fair and Good Rock	> 56		
II Poor rock	1–4 44–56	Bolts in pattern of 1.5x1.5 m In fractured rock area, and mostly at crown 5 cm fibre shotcrete shall be applied	Jointed and fractured strong rock with limited clay and water
III Very Poor Rock	0.1–1 23–44	Bolts in pattern of 1.0x1.5 m Fiber shotcrete: crown 10 cm and wall 5 cm Spiling c/c 0.5 m in crown for $Q < 0.4$. Spiling length 4 m, or pull + 1.5 m at $10 - 15^0$ & end fixed	Heavily jointed/fractured medium strong to weak rock. Support to be applied not more than 1 pull behind face. Reduced pull normally not needed
IV Extremely Poor Rock	0.01–0.1 3–23	Bolts in pattern of 1.0x1.2 m Fiber shotcrete: crown 15 cm and wall 10 cm Spiling c/c 0.4 m in crown & 1 m in walls. Spiling length 4 m, or pull + 1.5 m at $10 - 15^0$ & end fixed with bolts or straps	Weathered/weak rock, may be peeled with pocket knife. Support to be applied immediately. Reduced pull be utilized. Max pull length of 2.5 m id water-in-leakage
V Exceptionally Poor Rock	< 0.01 < 3	Bolts in pattern of 1.0x1.0 m Fiber shotcrete: 20 cm thick Spiling c/c 0.3 m in crown & 0.7 m in walls. Spiling length 3 m, or pull + 1.5 m. If needed 2 layers one at $10 - 15^0$ & second at $30 - 45^0$ & end fixed with bolts or straps	Very weak normally containing $> 60\%$ clay, easily separated by fingers. Schist with water. Support to be applied immediately. Reduced pull be utilized. Max pull length 2.0 m if water-in-leakage

2005). In cases where stability problems were encountered in the initially adopted system (Table 4.3), the support system was supplemented by adopting adjustments based on the site-specific experiences. Those adopted adjustments are summarized by G. L. Shrestha (2005) and given in Table 4.4 which was found to be practical and effective. Overall the design of the tunnel supports can be summarized as:

- Preparation of tunnel log and estimation of Q values
- Design of tunnel support based on the Q-chart (Figure B.3)
- Observation, monitoring in problematic sections and providing additional supports where required

Table 4.4: Supplementary design principles for squeezing ground in Khimti I HEP(G. L. Shrestha, 2005)

1	Concrete invert for the rock class V
2	Concrete invert for the rock class IV also if the deformation measurement do not clearly indicate stable condition
3	If the shotcrete in the squeezing areas is highly cracked and deformed, scaling and replacing with the steel fiber reinforced shotcrete. If just minor cracks exist, add a layer (30 mm) of shotcrete

4.4.4 Instability Problems

According to Panthi (2006), two major stability problems were encountered in the headrace tunnel of Khimti I hydropower. The first one was related to tunnel collapse caused by the presence of thick bands of highly weathered and sheared chlorite and talcose mica schist intercalated between realtively strong but fractured gneiss that allowed ground water to move into such bands (Figure 10a). The second was related to large leakage through open and permeable joints present in the gneisses and loss of valuable water from the tunnel during operation as shown in Figure 10b. Apart from these, squeezing was also reported to occur in the tunnel sections through weak sheared schist and schistose mica schist (Dwivedi et al., 2013b; G. L. Shrestha, 2005). The maximum convergence recorded was 160.2 mm in Adit 1 at chainage 500 m (G. L. Shrestha, 2005). Panthi (2006) reports that the problem of squeezing was mostly observed at relatively high overburden (above 200 meters) areas upstream and downstream of adit 3 and at the weakness zones downstream of adit 1 with relatively low overburden (approximately 100 meters).

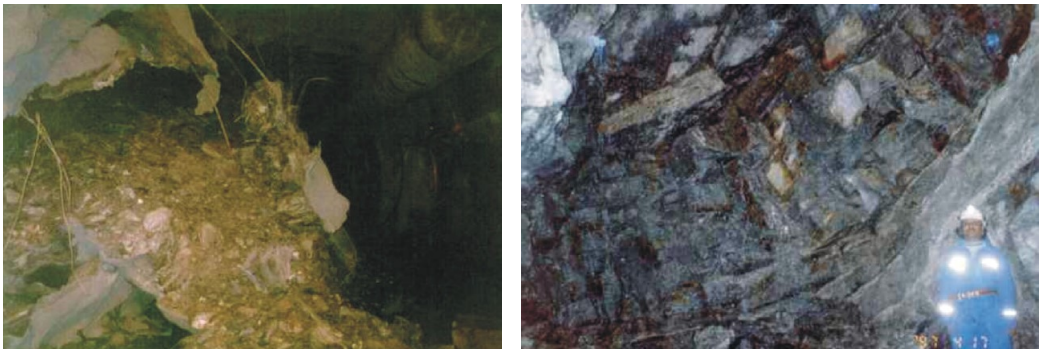

(a) **(b)**

Figure 4.10: Tunnel instability (a) collapse after application of support and (b) open and permeable joints within gneiss (Panthi, 2006)

Chapter V
Numerical Modelling

5.1 General

There is a common practice of designing the support linings based on the empirical approaches in Nepal Himalayas. This practice has led to insufficient design of supports resulting in the failure of the supports and thus the excavation. In order to provide sufficient support systems in weak grounds, changes to the empirical support recommendations are made based on the experience of engineers and geologist. Heavy supports are provided around the excavation contour, which in many cases could be avoided if proper study and analysis of the rock mass in the section were made. Tunnel excavations in general have been either under or over supported in the Nepal Himalayas, especially in the weak sections. The empirically established methods do not account for the complex behavior of the stress distribution around the rock mass and cannot assess the risk associated with the excavation process. This shortcoming can be addressed by Numerical modeling and design which allows analyzing the stress distribution during a continuous construction/excavation process. Numerical methods utilizes the computational powers to study and analyze various parameters that affect the excavation and modeling process. These models are formulation of real time problems using mathematical relations that help provide insight into the interaction of different entity and their holistic behavior. However, the cost of precise results is parameter calibration, model setup, computational time and post-processing time (Mendive, Sterin, Rellan, Sfriso, & Fuentealba, 2016).

In order to represent the complex behavior of the rock mass, three-dimensional modeling is required. However, the time and computational power required for the 3D analysis has limited its utilization and two-dimensional modeling approach is still the most common tool in current practice of tunnel projects' design (Janin et al., 2015). Janin et al. (2015) investigated and compared the ability of the 2D and 3D numerical approaches to reproduce the real behavior of tunnel based on in-situ measurements and found that the 2D solution produced numerical results that reproduced the in-situ ground deformations globally. However, the 2D simulation cannot represent the complex behavior of support loading, particularly near the tunnel face. Thus, 3D modeling is necessary, especially for weak ground where the rock mass behavior ahead of the tunnel face plays an important role in the stability of the excavation.

There exist various choice of numerical modeling software for the analysis of rock mass behavior which can be categorized, based on their modeling technique, into two

types:

1. **Continuous models**: Here, the rock mass is modeled as a continuous medium. Only a limited number of discontinuities (joints, faults, etc.) may be included in this model. This approach is most widespread approach to model the tunneling problems which simulates the rock mass interaction towards opening by taking equivalent continuum. Finite Element Method *(FEM)*, Finite Difference Method *(FDM)* and Boundary Element Method *(BEM)* utilizes continuous model.

2. **Discontinuous models**: Here the rock mass is modeled as a system of individual blocks interacting along their boundaries and encompasses the discontinuities like block joints and their structural arrangements. These models represent the nature of rock mass more close to the reality and provide a clear picture of potential local failure around the underground openings. Distinct Element Method *(DEM)* and Discontinuous Displacement Analysis *(DDA)* utilizes discontinuous model.

5.2 Finite Element Model

Finite Element Modeling *(FEM)* is most widely used software for solving the rock engineering problems. The idea of finite element method is to break up the continuum into discrete number of smaller elements i.e. it divides a region into finite numbers (finite elements) which are connected between them by nodes (vertices). The elements can be in one, two or three-dimensional space. Discretization plays an important factor, which has a great impact on the result. Finer the mesh, the more accurate the result, but more time consuming. Modeling can be done as two-dimensional or three-dimensional and the result of 3D analysis are more accurate compared to the 2D analysis. The 2D analyses can be modeled as plain stress, plain strain and axisymmetric approaches (Figure 5.1) (Moldovan & Popa, 2012). In plain stress the normal and shear stress in the direction, perpendicular to the X-Y plane (out-of-plane) is taken zero. In this case, it is considered that the solid has uniform thickness, which is less than the other two dimensions. The plain strain approach is used when the strain is zero in the direction not being modeled. Here the dimension is very large in the third plane, due to which it cannot deform in the plane, compared to other two dimensions. This approach is commonly used in the analysis of tunnels, dams and other geological works. Additionally, the plain strain analysis can be used when traverse sections of multiple tunnels are modeled. The axisymmetric allows to analyze a 3D model, which is rationally symmetric about an axis. Although the input is 2D, the analysis results apply to the 3D problem.

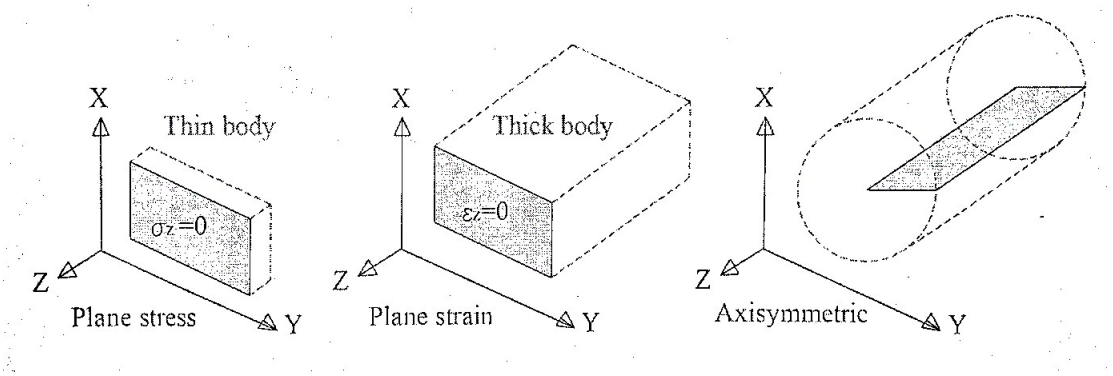

Figure 5.1: Two-dimensional modeling approaches (Moldovan & Popa, 2012)

Moldovan and Popa (2012) states that during analysis by numerical modeling, the initial ground conditions are of major importance. They can be inputted into the modeling as effective stress. The vertical and horizontal stress of the ground are specified in terms of material unit weight, pore water pressure, and the coefficient of Earth pressure K_0. The effect of support can also be studied through Numerical Modeling. In Finite Element analysis, the linear elements are usually modeled as beam elements and applied to model rock support, i.e. steel sets, shotcrete and concrete (Hussain et al., 2018). Assessment of these supports can be done and their failure can also be studied through modeling technique. This allows to identify the sufficiency of the support to the induced pressure which helps to identify the optimum support requirement.

FEM is a powerful technique and is extensively used for solving problems rock engineering problems such as characterization, design support assessment, and back analysis of tunnel. This method resolves complex engineering problem utilizing plane strain 2D analysis, axismmetric 2D analysis, and 3D analysis. However, Hussain et al. (2018) states that despite numerical modeling being an exact calculation method, due to the errors that can emerge from *FEM*, it should be considered as a tool to investigate the mechanism of behavior rather than obtaining precise predictions about tunnel performance. The errors that can emerge are due to the lack of data during initial stages of excavation and are derived from empirical relations.

Analysis software (RS2)

RS2 (formerly RS^2 or $Phase^2$) is a two-dimensional finite element program for soil and rock applications. *RS2* can be used for a wide range of engineering projects including excavation design, slope stability, groundwater seepage, probabilistic analysis, consolidation, and dynamic analysis capabilities. The software, developed by RocScience, is commercially available and allows to model rock mass in plain strain and axisymmetric approaches. Support modeling can also be achieved through the

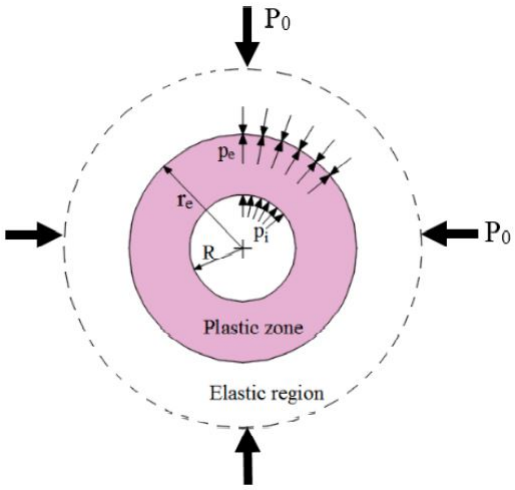

Figure 5.2: Circular tunnel in an elasto-plastic rock mass subjected to hydrostatic initial stress field (Sofiano & Nomikos, 2006)

software which allows to study the interaction of the support linings with the stress distribution around the excavation. The software allows staged excavation and support of the the underground structures which replicates the real scenario of excavation procedure.

2D model

Consider a circular excavation of radius R, excavated in an elasto-plastic rock mass subjected to a hydrostatic initial stress of initial stress of P_0 as shown in Figure 5.2. If the support pressure (p_i) is less than a critical pressure (p_c), then a plastic zone of radius r_c is formed around the opening. For such a tunnel, the lower value of the minor principal stress in the yielded zone occurs at the tunnel boundary and is equal to the support pressure p_i. The upper value of the minor principal stress, when a plastic zone is formed around the opening, occurs on the elastic-plastic zone interface (Sofiano & Nomikos, 2006).

The model developed in this study considers the non-hydrostatic stress field where the principal major and minor stress are taken as the gravity induced vertical stress and its equivalent horizontal stress obtained according to the Equations (5.13) and (5.14) respectively. The rock mass is modeled as elastic perfectly plastic and strain softening material based on the *GSI* value of the rock mass (Table 3.4). The excavation has been modeled as horse-shoe or inverted D as constructed in the selected case studies ans the dimension of the model is taken as 12 to 15 times the diameter of the excavation. This has been done to cover the plastic radius within the limits of the model since for very weak rock mass, large plastic radius are obtained which might exceed the boundary limits if set very low. Since the excavation has significant rock

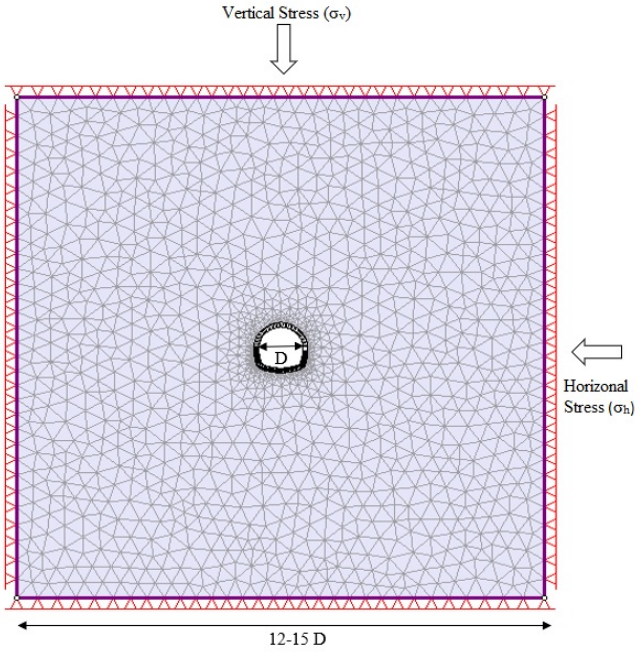

Figure 5.3: 2D model developed for the analysis of sections *This is a representative model for section at Ch. 3+190 m of Chameliya HRT).*

cover above it, the boundary are set to be rigid in both X and Y direction. Figure 5.3 shows the model generated for one of the selected sections of Chameliya headrace tunnel.

5.3 Numerical Steps

The following steps are used for modeling and analysis in this study:

i Full face excavation has been considered by drill and blast method since the tunnels are relatively smaller in cross section.

ii A plane-strain model has been developed as shown in Figure 5.3 whose core modulus, within the excavation boundary, is reduced in every stage to represent the receding tunnel face from the section at study.

iii The final deformation at the final stage (where core modulus = 0) is used to determine the amount of deformation prior to support installation by the relation proposed by Vlachopoulos and Diederichs (2009).

iv The tunnel closure is determined by knowing the maximum displacement of tunnel and the radius of plastic zone.

v Support are provided as liner beams around the excavation which provides additional internal pressure in the excavation.

Table 5.1: Properties of support elements used for the analysis of study sections.

Rock Bolts		**Shotcrete**		**Steel Ribs**			
Bolt Type	Fully Grouted	*Modulus (MPa)*	31622.78	*Steel beam*	ISMB 200	*Modulus (MPa)*	200000
Diameter (mm)	25	*Poisson's Ratio*	0.2	*Area (mm^2)*	3080	*Comp. Strength (MPa)*	400
Modulus (MPa)	210000	*Comp. Strength (MPa)*	40	*Depth (mm)*	200	*Tensile Strength (MPa)*	400
Tensile Capacity (MN)	0.254	*Tensile Strength (MPa)*	5	*Moment (mm^4)*	$21.2 * 10^6$	*Poisson's Ratio*	0.27

5.4 Analyzed Tunnel Sections

Eight different tunnel sections have been studied from three different hydropower tunnels in the Lesser Himalayan Region of Nepal. The tunnel sections are selected with rock mass from poor to exceptionally poor quality (according to the Q-system of classification, Figure B.3) and various supports combinations has been checked against its stability. All the study sections have been provided with liner of the same properties given in Table 5.1.

Table 5.2 gives the rock mass properties for the selected study sections. Generalized Hoek-Brown failure criterion is used for the estimation of the rock mass properties and for numerical modeling. The disturbance factor *(D)* has been considered based upon the degree of disturbance due to blast damage and stress relaxation. The value has been selected from the guideline provided by Hoek (2007) (Figure C.1) which has been chosen from 0.2-0.5 for the different rock classes.

Table 5.2: Rock Mass Parameters for study sections from selected case studies.

Case Study	**Chameliya HRT**				**Kaligandaki A HRT**		**Khimti I HRT**	
Chainage (m)	**0+310**	**3+103**	**3+190**	**3+404**	**0+763**	**2+167**	**0+607**	**5+191**
Q-value	0.08	1.25	0.013	0.008	0.02	0.008	0.005	0.02
Overburden (m)	220.7	181.2	217.5	283.9	246	620	97.04	281.5
Vertical Stress (MPa)	6.22	5.11	6.13	7.89	6.64	17.27	2.62	7.6
Horizontal Stress (MPa)	4.6	4.4	4.58	4.38	2.5	7.04	3.01	2.11
Poisson's Ratio	0.15	0.15	0.15	0.1	0.15	0.15	0.1	0.1
UCS (MPa)	60	60	12	12	40	40	15	24
σ_{cm} *(MPa)*	5.49	8.46	0.72	0.56	2.24	2.57	0.93	2.74
GSI	29	46	17	14	20	20	10	20
*Residual GSI**	–	16.1	–	–	–	–	–	–
E_i *(GPa)*	26	10	10	7	27	27	8.58	13.7
m_i	10	10	10	8	7	9	19	26
Source	(Basnet, 2013; Khakda, 2019)				(Dwivedi et al., 2013b) (Khakda, 2019; Panthi, 2006) (P. K. Shrestha & Panthi, 2014a)		(Panthi & Shrestha, 2018) (P. K. Shrestha & Panthi, 2013)	

*Residual values have been taken from Khakda (2019) as described in Section 3.2

Here, *UCS* is the Uniaxial Compressive Strength, σ_{cm} is the Rock Mass Strength, *GSI* is the Geological Strength Index, E_i is the Intact Rock Modulus and m_i is the rock constant from Hoek et al. (2002).

5.5 Estimation of Rock Parameters

Generalized Hoek-Brown failure criteria has been used for the analysis of the selected sections from the case study. The Hoek-Brown criteria developed by Hoek and Brown (1980) was introduced to provide input data for analysis required for the design of underground excavations in hard rock. This criterion was later redefined to account for the wide range of the practical problems in rock mechanics. The Generalized Hoek Brown criteria (Equation (5.1)) was introduced by Hoek et al. (2002) which included improvements in the correlation between the model parameters and the geological strength Index *(GSI)*.

$$\sigma_1 = \sigma_3 + \sigma_{ci}\left(m_b\frac{\sigma_3}{\sigma_{ci}} + s\right)^a \tag{5.1}$$

where m_b is a reduced value of the material constant m_i, s and a are constants for the rock mass and is given by Equation (5.2), (5.3) and (5.4) respectively.

$$m_b = m_i exp\left(\frac{GSI - 100}{28 - 14D}\right) \tag{5.2}$$

$$s = exp\left(\frac{GSI - 100}{9 - 3D}\right) \tag{5.3}$$

$$a = \frac{1}{2} + \frac{1}{6}\left(e^{GSI/15} - e^{20/3}\right) \tag{5.4}$$

Here D is the disturbance factor which depends upon the degree of disturbance to which the rock mass has been subjected by blast damage and stress relaxation. It varies from 0 for undisturbed mass to 1 for very disturbed mass and guidelines for preliminary estimate for its value has been given by Hoek et al. (2002) and is provided in Appendix C (Figure C.1).

The value of of rock constant m_i is an important parameter during the estimate of the rock mass properties for which Hoek (2007) have provided a chart for its estimation, given in Appendix C (Table C.3).

Similarly, the relation for obtaining the value of rock mass modulus given by Hoek et al. (2002) is given by Equation (5.5)

$$\left.\begin{aligned} &E_m(GPa) && = \left(1 - \frac{D}{2}\right)\sqrt{\frac{\sigma_{ci}}{100}}10^{\frac{GSI-10}{40}} \\ &\text{for } \sigma_{ci} \leq 100 \text{ MPa} && \\ &E_M(GPa) && = \left(1 - \frac{D}{2}\right)10^{\frac{GSI-10}{40}} \\ &\text{for } \sigma_{ci} \geq 100 \text{ MPa} && \end{aligned}\right\} \tag{5.5}$$

The rock mass strength can be calculated by Equation (5.6) as given by Hoek et al.

(2002).

$$\sigma_{cm} = \sigma_{ci} \frac{(m_b + 4s - a(m_b - 8s)) \left(\frac{m_b}{4} + s\right)^{a-1}}{2(1+a)(2+a)} \tag{5.6}$$

where the parameters are as defined above.

Hoek (2006), based on measured data of rock modulus derived Equation (5.7) which is best suited when reliable intact rock properties are not available. When intact rock properties are available, the authors suggested to use Equation 8 for obtaining the modulus value. Also, the rock modulus value is highly sensitive specimen damage unlike the strength value. So, in order to used Equation (5.8), Hoek (2006) proposed Equation (5.9) to obtain the intact modulus value based on the intact strength and modulus reduction *(MR)* value. The selection guideline for *MR* value as proposed by Deere (1968) is provided in the Appendix C (Table C.4).

$$E_{rm}(MPa) = 100,000 \left(\frac{1 - D/2}{1 + exp((75 + 25D - GSI)/11)} \right) \tag{5.7}$$

$$E_{rm}(MPa) = E_i \left(0.02 + \frac{1 - D/2}{1 + exp((60 + 15D - GSI)/11)} \right) \tag{5.8}$$

$$E_i = MR\sigma_{ci} \tag{5.9}$$

Other rock properties essential for two-dimensional numerical modeling and their estimation have been summarized below:

Geological Strength Index (GSI): The *GSI* value are obtained in the field through visual inspection of the rock mass condition with the aid of the chart provided in Figure B.1. During numerical analysis, in situations where the field inspection or face map of the study sections are not available, the *GSI* value can be empirically estimated from the relation provided by Hoek (2006) (Equation (5.10)).

$$GSI = RMR_{89} - 5 \tag{5.10}$$

The RMR_{89} value is obtained from the field during rock mass classification, however, where Q system has been adopted, the *RMR* value can be obtained empirically by Equation (5.11) provided by (Barton, 1995).

$$RMR = 15logQ + 50 \tag{5.11}$$

Among the different types of rock models available as described in Chapter III, the choice of the model is done based on the *GSI* value. In case of strain-softening model, the residual parameter of *GSI* have been selected based on Table 3.4 (Section 3.2.2).

Disturbance Factor (D): The selection of *D* value is done according to Figure C.1. It should be noted that the choice of the *D* value from the table only provides

a starting point for estimate and should be changed according to the rock mass condition (Hoek et al., 2002).

Poisson's Ratio (ν): The Poisson's ratio value should be lab tested but in case of unavailability of lab tested value, the relation provided by Hoek et al. (1995) (Equation (5.12)) can serve as a good estimate.

$$\nu_{rm} = 0.32 - 0.0015 * GSI \tag{5.12}$$

Unconfined Compressive Strength (UCS): The UCS value of intact rock in one of the most important parameters in numerical analysis. Laboratory tested value must be utilized for proper results and analysis. Hoek (2007) have provided a chart for the estimate of the UCS value in situation where the value lab tested value cannot be obtained and is provided in Appendix C (Table C.1).

Vertical Stress (σ_v): The vertical stress is obtained as the gravity loading induced by the rock mass over the crown of the tunnel section. This is thus a function of the overburden and the unit weight of the rock and is obtained from Equation (5.13).

$$\sigma_v = \gamma H \tag{5.13}$$

Here γ is the unit weight of the rock material which is generally taken as 0.027 MN/m^3 (Carranza-Torres & Fairhurst, 2000) and H is the overburden in meters.

Horizontal Stress (σ_h): The horizontal stress is obtained as a sum of tectonic stress and the horizontal component of the vertical stress. The tectonic stress is included in order to account for the loading caused by the seismic movement and is given by Equation (5.14) (P. K. Shrestha & Panthi, 2014a, 2014b). In the Lesser Himalayas of Nepal, the major stress is oriented horizontally with Northeast-Southwest trend (Panthi, 2006) which can also be seen on the World Stress Map (Heidbach, Rajabi, Reiter, Ziegler, & Team, 2016).

$$\sigma_h = \frac{\nu}{1-\nu}\sigma_v + \sigma_{tec} \tag{5.14}$$

Dilation Parameter: The dilatancy of the material is a measure of how much volume increase occurs when the material is sheared. For a Mohr-Coulomb material, dilatancy is an angle that generally varies between zero (non-associative flow rule) and the friction angle (ϕ) (associative flow rule). For Hoek-Brown materials, dilatancy is defined using a dimensionless parameter that generally varies between zero and m. Low dilation angles/parameters are generally associated with soft rocks while high dilation angles/parameters are associated with hard brittle rock masses. The value of the dilation parameter is suggested to start from $0.333 * m$ or $0.333 * \phi$ for soft

rocks and $0.666 * m$ or $0.666 * \phi$ for hard rocks RocScience (n.d.). However, for very weak rock mass Lorig and Varona (2013) suggests to take a value of 1^0 or 2^0 and not zero since taking zero would result in excessive displacement and extent of yielding.

5.6 Procedure of Modeling

For the selected sections, the numerical modeling has been done by plain-strain, two-dimensional modeling through *RS2*. All the essential parameters have been referred from published reports and articles and in case of unavailability of certain parameters, empirical estimation has been done as described in Section 5.5.

Step 1: Development of rock model

The rock model in *RS2* has been developed by generating stages within the model to represent the effect of receding face for tunnel support. Vlachopoulos and Diederichs (2014) state that in order to accurately simulate the loading of the support or the effects of sequential excavation, the 2D model must capture the pre-face conditions, the state of displacement and plasticity at the face and the subsequent development of deformation and yielding. By creating a staged model where an internal pressure is applied to represent the in-situ condition (before tunnel excavation) and by gradually reducing the internal pressure over a number of stages until the internal pressure is zero (excavated condition), the effects of 3D excavation can be studied by 2D analysis. As the internal pressure is reduced, the rockmass surrounding the excavation yields and a plastic zone develops around the tunnel causing the rock mass to deform gradually over the various stages.

Methodologies commonly employed to represent the 3D effects of tunneling by 2D modeling are by straight excavation, average pressure reduction, excavation of concentric rings and face de-stressing (with or without softening) (Vlachopoulos & Diederichs, 2014). In this paper, the face replacement technique with material softening (reduction of modulus of the surrounding materials) has been used. In face replacement, the tunnel core is replaced with an unstressed, elastic material in each stage and the tunnel boundary is allowed to converge until a temporary equilibrium is reached. This face replacement can be made more efficient by softening of each core replacement which results in an efficient excavation sequence (Vlachopoulos & Diederichs, 2014). The softening of the core has been done over 20 stages to achieve higher accuracy over the amount of boundary deformation in the excavation. For extremely weak sections, much of the deformation have been set to occur during the initial stages so that greater control can be achieved for support installment during the subsequent stages.

Step 2: Rock Support Characteristic Curve

The Longitudinal Deformation Profile *(LDP)*, a part of the Convergence Confinement Method *(CCM)* by Carranza-Torres and Fairhurst (2000), allows designer to estimate the amount of deformation behind and ahead of the face of tunnel before support installation. Along with *LDP*, Ground Reaction Curve *(GRC)* and Support Characteristic Curve *(SCC)* together forms the *CCM*, which is one of a popular method for analytical support design of tunnels. Since, the tunnel face contributes to the stability of the section by carrying some amount of load, the deformation is not zero on or ahead the face of tunnel. According to Carranza-Torres and Fairhurst (2000), when the tunnel face is about two diameters away from a section, only then the section undergoes maximum deformation. Similarly, the deformation is zero two diameters ahead of the face. Thus, the *LDP* is used to relate the deformation perpendicular to the tunnel axis with the position along the axial direction (i.e. it is used to predict the amount of radial deformation at various position along the axis of the tunnel).

Vlachopoulos and Diederichs (2009) proposed an improved version of *LDP*, for circular excavation under isotropic stress, by relating it to the normalized plastic radius of the tunnel *(plastic radius/tunnel radius)*. Since the development of plastic zone around the tunnel affects its stability, it becomes very important to identify the location for support installation. For inverted D and horse-shoe shaped excavation under anisotropic stress, Vlachopoulos and Diederichs (2014) proposed that the *LDP* for circular excavation can be used for non-circular provided that the aspect ratio of the opening is small. Similarly, for anisotropic condition, the authors on their preliminary analysis, state that the *LDP* based on K=1 can be used to calibrate the 2D models using the direction of maximum yield i.e. the direction of minimum stress.

In this study, deformation values at various location from the face of tunnel is determined for an unsupported opening is determined using *LDP*. For weak sections, the deformation value very close to the face has also been determined to allow support installation close to the face of tunnel. For the development of the *LDP*, two input parameters: radius of plastic zone and the maximum deformation of an opening has been obtained from preliminary rock model modeled in Step 1. This rock model is later optimized to allow relaxation equal to the obtained deformation values and the support installation is done in the subsequent stage.

Step 3: Model Calibration

After developing the rock model in *RS2*, the model has been calibrated according to the deformation values obtained from the *LDP* to determine the appropriate stage for support installation. By knowing the amount of deformation prior to support

installation, the modulus value which yields the obtained deformation can be found and the support can be installed in that particular stage. For weak sections, it is essential to support the rock mass ahead of the face as well as provide support close to the face. Supports should be provided in weak grounds such that it allows ground deformation while providing sufficient support. By use of the *LDP*, the amount of closure near to the face is obtained and the rock model is calibrated for core modulus such that the required closure value is achieved. The model is run several times in unsupported condition to achieve the desired result.

Step 4: Support Design and Installation

After calibration of the model, with the rock modulus set to obtain the required deformation values, the support is provided to the excavation. Instead of providing the supports in a single stage, the supports are provided individually in different stages in order to match the practical approach of support lining installation. The supports are provided such that it allows the ground relaxation equal to the allowed deformation obtained from the analytical method (*LDP* chart). Various combinations of support are provided to study its behavior in the excavation. Q recommended support is first compared with the designed/site provided support (based on the support diagrams) and their results analyzed for their performance with respect to the stress distribution. In situation where the provided support and the Q recommended supports fails in the ground condition, necessary changes are made in the support definition to allow safe bearing capacity of the supports.

Support Modification

When the Q recommended support and the site provided supports fails for the ground load acting over them, changes are made in the design of the support system. The failure of the supports mainly occur in the weak ground sections and the changes in the support are made incorporating the practical support elements used in the Himalayas. This includes heavy steel ribs lining with forepole installation, concrete lining, thick shotcrete lining, etc. Finally, more optimized support is recommended by providing yielding supports and introducing necessary changes in the excavation profile.

The flowchart shown in Figure 5.4 summarizes the modeling procedure applied for the analysis of the sections in the study. The flowchart has been categorized into two sections: Rock Model Design and Support Design. The model design basically comprises of Step 1 and 2 briefed above where the numerical model is developed and calibrated according the deformation values obtained from the analytical method. The support design covers Step 3 and 4 described above where, after the calibration of

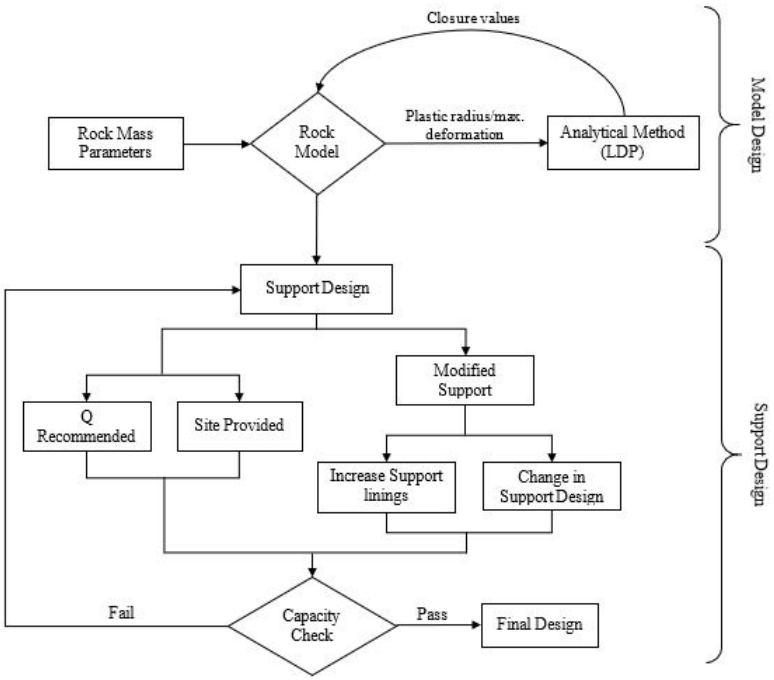

Figure 5.4: Methodology adopted for numerical modeling in *RS2*.

the model, the support is provided according to the Q recommended and designed/site provided support and is checked for its capacity. If the support fails, the support is modified by increasing the linings which is again checked for its overall capacity. Then the final design is recommended. As an alternate, yielding support is also tested with different excavation profile to optimize the support requirement.

5.7 Results

Four different sections from Chameliya headrace tunnel and two sections each from Kaligandaki 'A' and Khimti I headrace tunnel has been taken for this study. The details of the sections have been tabulated in Table 5.2.

5.7.1 Case Study: Chameliya Headrace Tunnel

The Chameliya headrace tunnel is a horse-shoe shaped tunnel with a diameter of 5.2/4.2 m based on the rock mass condition of the area. The tunnel faced severe squeezing in the faulted zone with complete failure of the installed supports. The failed section had to be re-excavated with new support installation. Since much of the relaxation of the stress had already occurred during the time between failure and re-excavation, the newly designed support was able to withstand the stress with safe construction of the tunnel. Through this study, the support design has been done considering the initial ground and stress condition, prior to failure, by the use of the numerical modeling. Four different sections with poor to extremely poor rock mass

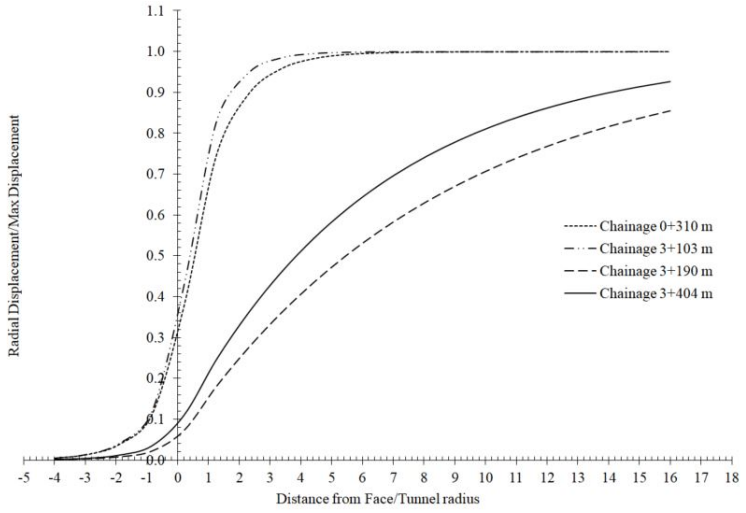

Figure 5.5: Longitudinal Deformation Profile for selected sections of Chameliya headrace tunnel.

(classification according to the Q-system, Figure B.3) have been studied with their rock mass properties tabulated in Table 5.2.

Figure 5.5 shows the Longitudinal Deformation Profile *(LDP)* for the four sections from which the amount of deformation that occurs during support installation (i.e. amount of ground relaxation) is determined. Looking at the curve for the section 3+190 m, we obtain the allowable closure to be 0.41 m when the support is installed 0.5 m from the face. Since, the ground in this section is extremely poor, the support is provided close to the face to allow stability of the opening and provide a safe working environment.

Section at Chainage 3+190 m

First the support provided in the site (designed support) is modeled which shows that maximum bending moment occurs in the invert of the section since the support does not form a continuous close ring, which is essential for weak rock masses. Figure 5.6a shows the bending moment acting over the liners with negative moment in the corners and positive moment in the invert, Figure 5.6b shows the failed element of liners (except invert) which fails in tension (all the elements of the liner fails due to the excessive bending moment). It can be seen that all of the elements has failed showing the insufficiency of the designed support. The site support consists of 100 mm shotcrete with 3 bar lattice girders (18, 26 mm diameter) at 1 m c/c spacing and an invert of 400 mm thickness. Rock bolts of 3 m length and 25 mm diameter is also provided at a spacing of 1 m c/c. This *R5* category of support has been shown in Figure 4.3.

Similarly, the Q recommended support has been modeled which shows that the

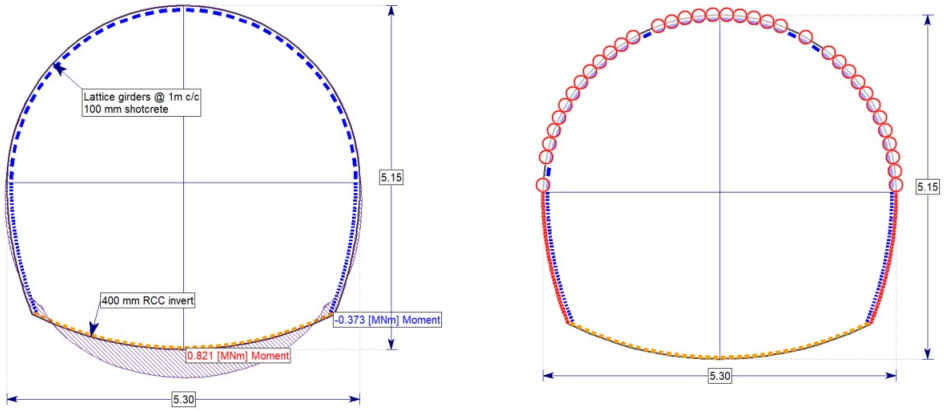

(a) **(b)**

Figure 5.6: (a)Bending moment and (b) Failure region of liners for designed (site provided) support for Ch. 3+190 m of Chameliya HRT.

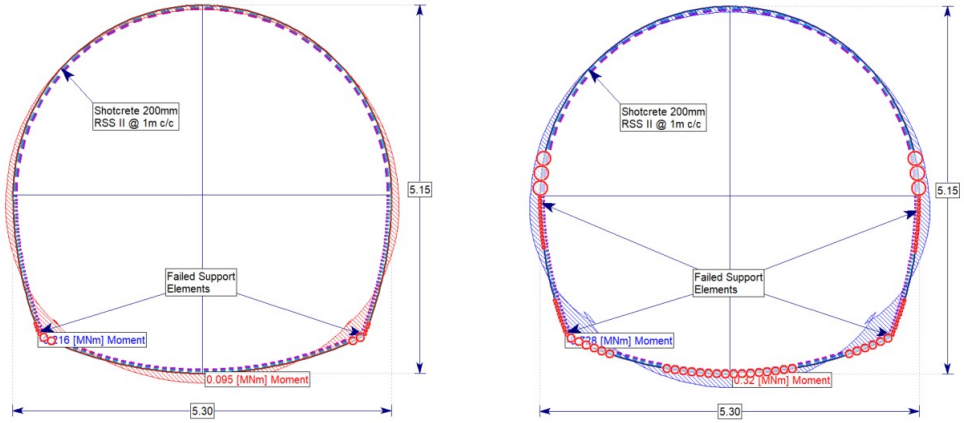

(a) **(b)**

Figure 5.7: Bending moment and failure point for (a) Shotcrete element and (b) RRS element in Q recommended support for Ch. 3+190 m of Chameliya HRT.

Reinforced Ribs *(RRS)* fails in springline, invert and the corners of the excavation (Figure 5.7b). The *RRS* element has been modeled as an equivalent beam element as detailed in Section 3.1.2. There is minimum failure of the shotcrete element (Figure 5.7a) since most of the load is taken up by the *RRS* element, this can also be seen from Figure 3.6a and 3.6b. This shows the inadequacy of the Q recommended support for the weak Himalayan geology. Thus it is necessary for proper design of support linings for safe construction in the Himalayan region. The details of design and Q recommended support is given in Table 5.3.

The general practice in the country is to increase the liner amount until the safe design is achieved. Thus, the support has been modified by providing additional support elements. The additional support has been provided considering the general practice adopted in the region with forepoling, closely spaced steel sets and concrete lining. Thickness and spacing of the additional liners has been gradually increased

until the excavation becomes safe, as shown by the numerical model. Figure 5.8 shows the support elements of modified support *(note that forepole and rock bolts have not been shown in the figure)* along with the points of failure and the bending moment acting over the liners. Here the concrete lining has been provided at a distance of 1 m from the face (calculated from *LDP*, Figure 5.5), prior to the failure of the steel beams. Delaying the installation of the concrete lining could lead to failure of steel sets in the section. Forepoling has been achieved by the same procedure highlighted in Section 3.2.3. The modified support consists of heavy linings with 200 mm fiber reinforced shotcrete, ISMB 200 steel sets at 0.5 m c/c spacing and a final concrete lining of 500 mm thickness (Figure 5.11a). All the supports have been provided in different stages in the numerical model. First the forepole is provided to stabilize the rockmass ahead and above the crown then a layer of shotcrete with steel ribs is provided as close to the face as possible. The shotcrete & steel sets are provided after allowing a relaxation of 0.41 m which when back calculated from the *LDP* is located about 0.5 m from the tunnel face. This support acts as a temporary support and allows reduced rate of radial deformation. Some minor failures around the corners, invert and nearby the spring line can be seen for the shotcrete element while for the steel element, failure can be seen around the corner of the excavation. Both the failure of the shotcrete and the steel elements occurs in compression and are safe in shear. The concrete lining is then installed at around a distance of 1 m from the face of the tunnel prior to complete failure of the shotcrete.

Also in order to overcome the extreme moment in the invert of the section, the lining has been provided continuously forming a close ring. This has resulted in lesser moment in the invert but the tension moment created at the corners is large which resulted in the failure of the corners. This can be avoided by providing additional concrete lining at the corners as suggested by Khadka et al. (2019).

Figure 5.9 shows the moment distribution along the excavation contour for shotcrete element *(concrete in case of modified support)*. The distance along the contour has been shown in the top right of the figure. From the figure, we can see that the moment over the shotcrete element in the Q support is very low while the moment acting over the *RRS* element is nearly the same as the moment acting over the concrete element in modified support. However, the *RRS* elements fails severely compared to the modified support (Figure 5.7 and 5.8), showing the inadequacy of the Q support guideline in the region. Also, the support installation location has an important role in the stability of underground excavation, since installing concrete lining too late can lead to failure of the modified support too. Thus, proper support design and analysis must be done for safe construction of the structure.

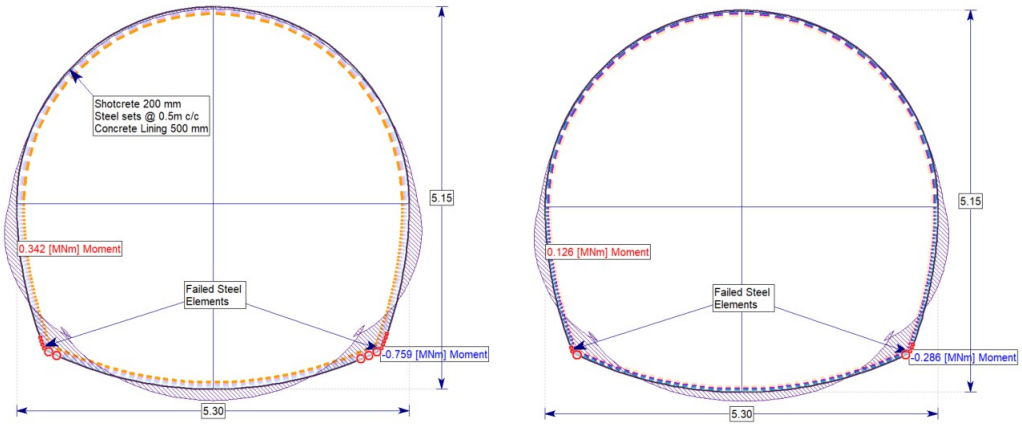

(a) **(b)**

Figure 5.8: Bending moment and failure point for (a) concrete and (b) steel beam element in modified support for Ch. 3+190 m of Chameliya HRT.

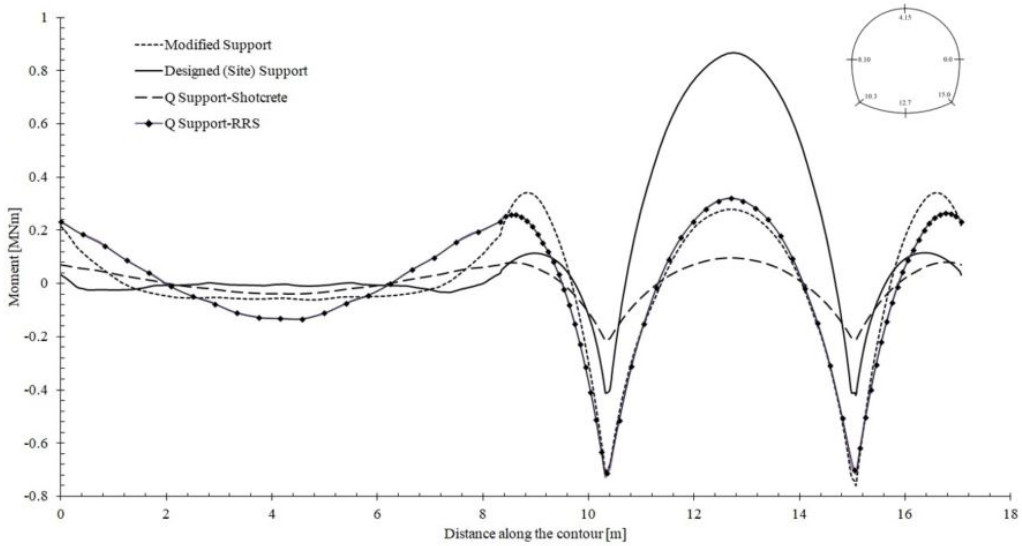

Figure 5.9: Bending moment around the liner for different support systems for Ch. 3+190 m of Chameliya HRT.

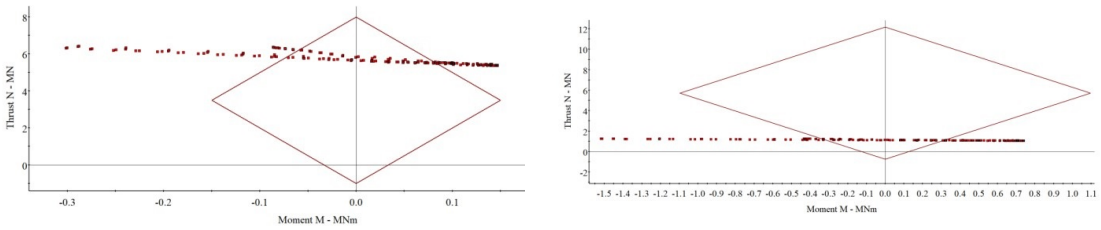

(a) **(b)**

Figure 5.10: Capacity Plot for (a) shotcrete element and (b) RRS element for Q recommended support for Ch. 3+404 m of Chameliya HRT.

Section at Chainage 3+404 m

Similar results were seen from the analysis of supports at chainage 3+404 m. The section, with a Q value of 0.008, falls in the 'Extremely Poor' category according to the Q system of classification (Figure B.3). The designed (site) support in this region failed completely in walls and invert and the support recommended by the Q chart also prove to be inadequate. The Q recommended support: 200 mm shotcrete with RRS beam of category III provided at a spacing of 1 m c/c, failed in the crown, in the walls and springline, the bottom corners and the invert. Uniform support was provided throughout the excavation forming a ring like support to avoid the excessive built up of moment in any region. This extremely poor rock mass should be well supported in advance (ahead of face) by use of face supporting techniques, which the Q-chart lacks. Figure 5.10 shows the capacity plot (moment vs thrust) for the shotcrete element and RRS element for a Factor of Safety of 1.5. It can be seen from the figure that the shotcrete element fails in compression while the RRS element fails in tension.

The support was thus changed with addition of support elements of increased thickness and number. It was found that the excavation became stable for a support combination of 200 mm fiber reinforced shotcrete, ISMB 200 at 0.3 m c/c spacing and forepoling was installed to stabilize the rock mass above the crown. Rock bolts of 3 m length and 25 mm diameter at 1 m c/c spacing was also kept in place. This combination of support was installed 0.5 m from the face of the tunnel. The installation of support was in the model was achieved in different stages. A final concrete lining was also provided with a thickness of 400 mm at the crown and 600 mm at the walls and invert, which was installed at a distance of 1 m from the face of tunnel (Figure 5.11b). The support installation was in different stages allowing a relaxation of 0.4 m for the initial support (shotcrete + steel sets) and 0.5 m for the final concrete installation. This support combination allowed a final deformation of 0.41 m in the section.

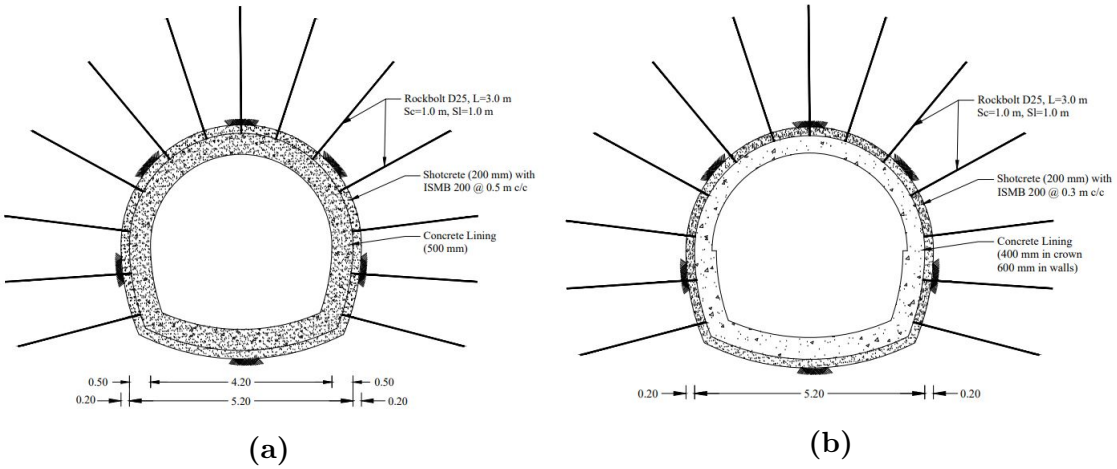

Figure 5.11: Modified support in Section (a) 3+190 m and (b) 3+404 m. *(All dimensions are in meters unless specified and forepole support has not been shown in the figure but applied in the model)*

Section at Chainage 0+310 m and 3+103 m

The sections at chainage 0+310 m falls in 'Extremely Poor' rock mass while that of 3+103 m falls in 'Very Poor' rock mass category according to the Q system of classification with their Q values as 0.08 and 1.25 respectively. However their rocks are relatively stronger in comparison to the other studied sections with compressive strength of 60 MPa. Similar approach of support analysis, as before, was adopted in these sections and it was found that for the section at 3+103 m, the rock support recommended by the Q system is sufficient while for 0+310 m, increasing the lining thickness was enough for the stability of the excavation with no additional support. Increasing the thickness of the shotcrete to 150 mm was sufficient for the section 0+310 m. Comparing the designed support and the Q recommended support for the two sections (Table 5.3), there is not much difference in the amount of the support. This shows that the Q recommended support proves to be insufficient only for extremely and exceptionally poor rock masses of the Himalayas. However, as with other sections, the bottom corner of the excavation fails due to the high concentration of stress around the region which can be mitigated by providing additional shotcrete/concrete in the area.

Circular Excavation

The practice of providing heavy support linings to stabilize weak rock mass has been the common approach in the Nepal Himalayas. This leads to large amount of support like in the case for the section at chainage 3+190 and 3+404 m where the overall linings thickness is 700 mm and 800 mm respectively in addition to the rock bolts and forepole support. This results in reduction of tunnel section which can

Table 5.3: Q Recommended and Designed Support for selected sections of Chameliya headrace tunnel.

Chainage (m)	Q-Value	Q Recommended	Designed Support
0+310	0.08	S(fr) 12–15 cm + RRS I @ 2.9–4.0 m c/c + Bolting @ 1.3 m	Pattern bolting (ϕ=25 mm, L=3 m) @ 1 m c/c, invert=300 mm, shotcrete = 100 mm
3+103	1.25	S(fr) 6–9 cm and Bolting @ 1.7–2 m	Pattern bolting (ϕ=25 mm, L=3 m) @ 1.5 m c/c, invert=200 mm, shotcrete = 75 mm
3+190	0.013	S(fr) > 15 cm + RRS II @ 2.3 m c/c and bolting @ 1 m c/c	Pattern bolting (ϕ=25 mm, L=3 m), invert=400 mm, lattice girder (3 bar, bar size–18,26 mm) @ 1 m c/c, shotcrete = 100 mm
3+404	0.008	S(fr) > 15 cm + RRS II @ 1.7–2.3 m c/c and bolting	Pattern bolting (ϕ=25 mm, L=3 m), invert=400 mm, Steel ribs @ 0.5 m c/c, shotcrete = 100 mm

S(fr) is fiber reinforced shotcrete; RRS is Reinforced Ribs of Shotcrete; ϕ, L is the diameter and length of rock bolts.

have negative effects on the overall performance of the structure. So, in order to account for the increased thickness, over excavation of the section must be done and this comes with additional expense of stability issues. Since, a circular excavation provides an effective path for stress distribution, without its concentration at any particular region (Figure 2.5a); this alternative has been studied for its effectiveness in weak rock masses.

Figure 5.12 shows the stress distribution (stress concentration) around the opening of horse-shoe (Figure 5.12a) and circular (Figure 5.12b) excavation for chainage of 3+190 m. The red crosses shows the direction of major and minor stresses and as the stress concentrates in a region, the density of the markers also increase. This signifies the high concentration of stress near the bottom region of the horse-shoe excavation while it is more or less uniform in case of circular excavation. Thus the amount of support requirement also significantly decreases in a circular section. Upon analysis of various support combinations of Chainage 3+190 m of Chameliya HRT for a circular excavation, it was found that the designed support (refer Table 5.3) was sufficient for the ground condition when the thickness of shotcrete was increased to 200 mm. Further the Q recommended support was also seen safe with RRS II at 2.3 m c/c spacing, shotcrete of 200 mm and rock bolts at 1 m c/c spacing. This shows the advantage of circular excavation over other shapes in weak rock masses.

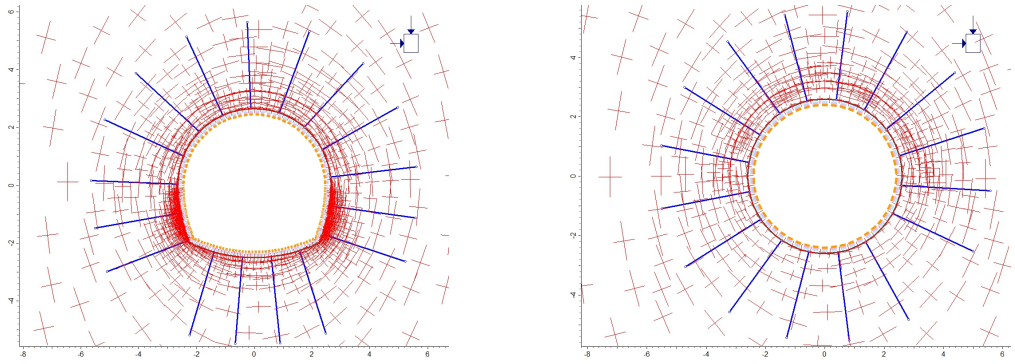

(a) **(b)**

Figure 5.12: Stress distribution around (a) Horse-shoe and (b) Circular excavation for section at chainge 3+190 m of Chameliya headrace tunnel.

(a) **(b)**

Figure 5.13: (a) Schematic diagram showing yielding liner and (b) Sliding gap in steel sets (Hoek & Briceno, 2009)

Yielding Support

Yielding support provides support to the ground while also allowing it to deform to a certain limit. Yielding support becomes beneficial in squeezing ground where the rock mass should be allowed to deform to provide long term stability for the structure. Yielding support was first implemented in Yacambu-Quibot tunnel in Venezuela. The project, which took 32 years for completion, consists of 5 m diameter, 23.3 km long water tunnel excavated in silicified and graphitic phyllite with overburden of upto 1270 m. The tunnel faced severe squeezing problem which was overcome by use of circular section with yielding supports (Hoek & Briceno, 2009). Figure 5.13a and 5.13b (Hoek & Briceno, 2009) shows a schematic diagram of the liner with sliding gap and sliding gap placed between steel sets. In order to optimize the tunnel supports in squeezing sections of the Chameliya headrace tunnel, modeling was also done by introducing sliding gaps in the liners. This was achieved by providing locking strain in the liner. Enabling locking strain meant that no axial force would act over the liner until the locking strain value is attained thus allowing the ground to converge further even after installation of the liner. The locking strain is provided as a percent

calculated as:

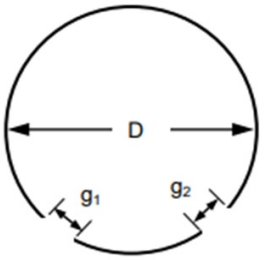

$$\frac{\Delta L}{L} = \frac{\Sigma(\text{gap lengths})}{\text{Initial circumference}} = \frac{g_1 + g_2}{\pi D} * 100\% \qquad (5.15)$$

where D is the diameter and g_1 and g_2 are gap length as shown in the figure alongside.

It should be noted that in an *RS2* model, there is no physical location of the sliding gap in the liners and the locking occurs when the total average strain along the liner is equal to the locking strain. For the analysis of the sections, after determining the relaxation stage at a fixed distance from the face of the tunnel, initial support is provided with sliding gap in the model. After the liner starts taking load (i.e. when the strain locking starts), final liner is installed for the stability of the excavation.

Section at Chainage 3+190 m

For the section, a strain locking value of about 2% has been provided i.e. a total closure of 0.3 m has been allowed for the section and the support is installed 0.5 m from the face of tunnel which allows stress relaxation upto 0.3 m, prior to the support installation. With the installation of the yielding liner, the support closes when the deformation of the excavation reaches a value of about 0.7 m at which the support starts taking the load of the rock mass. This has been shown in Figure 5.14a where the ground deformation is shown by the Ground Reaction Curve *(GRC)* curve. The Support Characteristic Curve *(SCC)* shows the maximum pressure bearing capacity of the support system. The provided support consists of 200 mm thick shotcrete and ISMB 200 spaced at 0.5 m c/c, effects of rock bolt has not been considered in the *SCC*. From the figure it is clear that the support combination is not able to withstand the ground pressure in normal condition (dotted line), however by providing yielding supports, the support system safely supports the rock mass while allowing it to deform (solid line). At a closure of 0.67 m, the liners locks in place and starts taking load as shown by the solid line in the figure. This support however is just sufficient to withstand the load and thus final concrete lining of 400 mm is provided after the initial support locks in place and starts to take ground load. Figure 5.15a shows the bending moment over the initial liner (with sliding gap) when it takes maximum load and Figure 5.15b shows the capacity plot of final concrete lining. In Figure 5.15b, it can be seen that some of the points lie outside the FOS 1.5 curve, these points belong to the bottom corners where the stress concentration. The high stress concentration

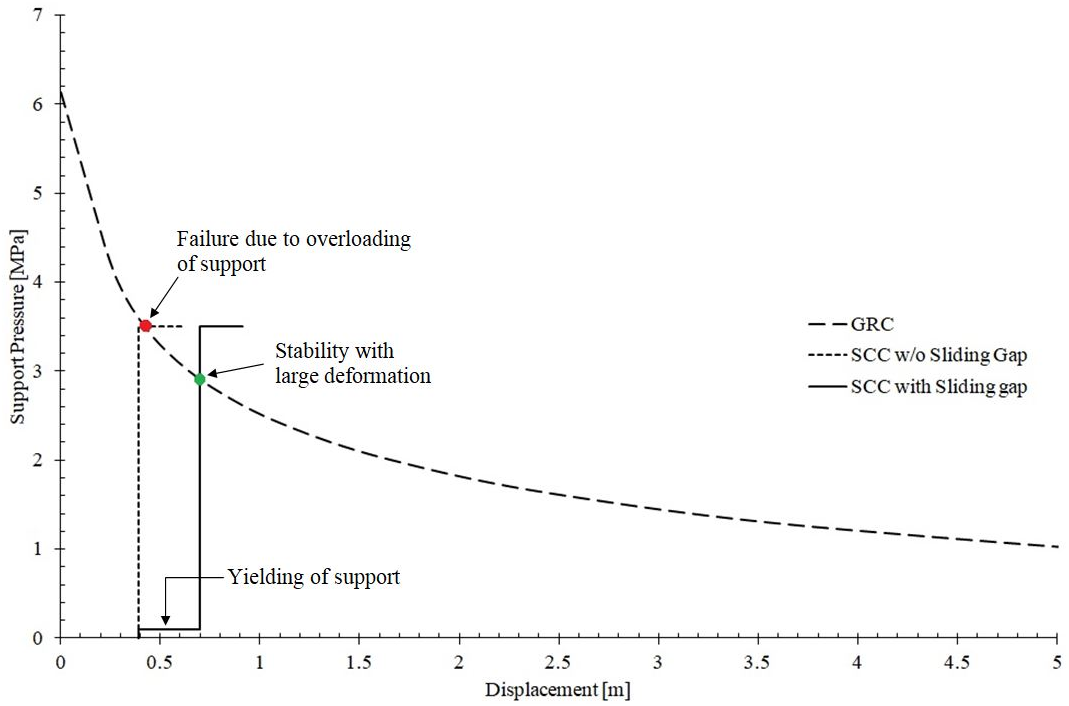

(a) Ch. 3+190 m

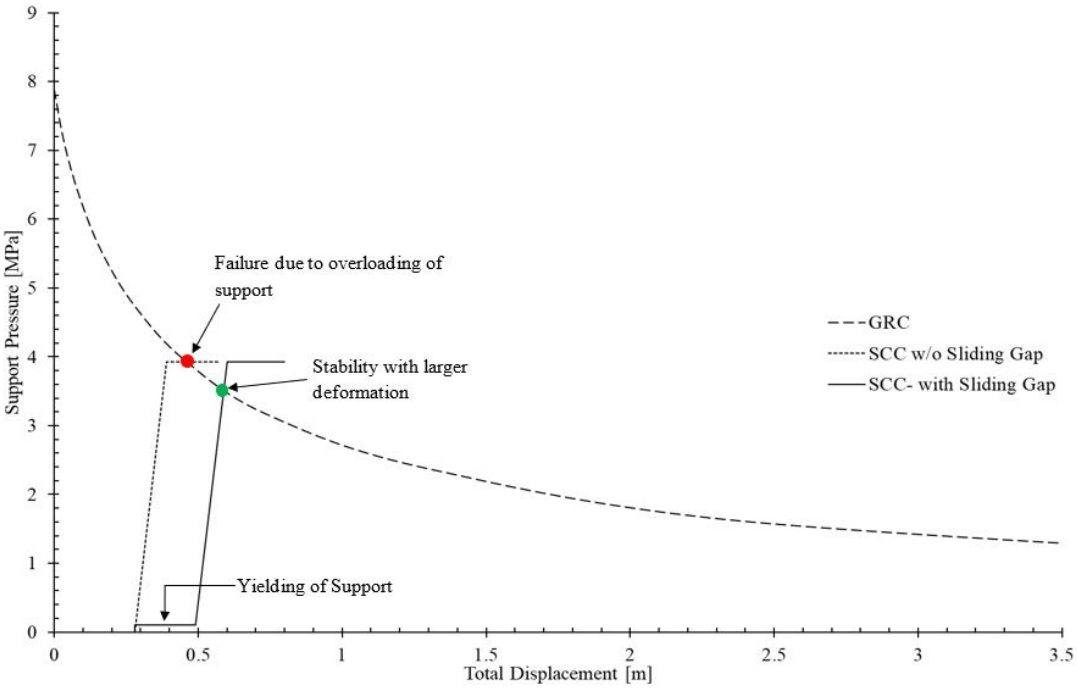

(b) Ch. 3+404 m

Figure 5.14: Effect of support with and without sliding gap in ground deformation in sections from Chameliya HRT.

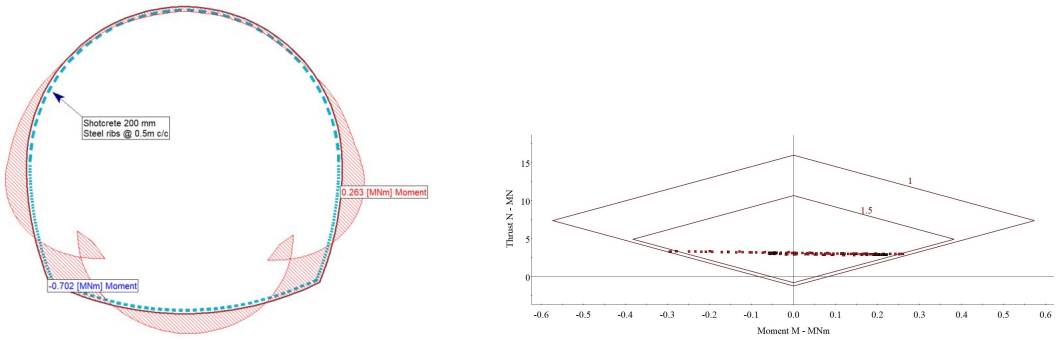

(a) **(b)**

Figure 5.15: (a) Bending moment and (b) Capacity Plot for liner with sliding gaps for Ch. 3+190 m of Chameliya HRT.

can also be seen through the large bending moment in the region in Figure 5.15a, as mentioned earlier, this can be solved by increasing the thickness of concrete in the region.

Section at Chainage 3+404 m

Yielding support was also checked for the chainage 3+404 m allowing 0.4 m of closure of the section, equivalent to 3% strain locking. It was seen for the section that although the section became more stable, the amount of lining requirement was still high. Thus only providing yielding liner did not result in any reduction of support liner and a combination of circular section with sliding gap in the support was studied.

By providing a circular section, the stress concentration becomes more uniform without high concentration in any particular region around the opening due to which the support requirement also decreases as seen in Section 5.7.1 above. In addition to providing the circular section, inclusion of yielding support in weak rock masses allows more safe and economic construction of the structure. By allowing a closure of upto 0.4 m after the installation of support in the section at chainage 3+404 m (Figure 5.14b, the amount of support requirement was reduced to 600 mm total thickness of the lining. An initial support of shotcrete of 300 mm thickness and steel ribs at 0.5 m c/c spacing was provided with strain locking at 3% after allowing a stress relaxation of upto 0.30 m as obtained from the *LDP* (Figure 5.5). After the initial support locks in place and starts to take the ground load, the final support of 300 mm thick concrete lining was provided to complete the support installation. Along with this, pre-support was also achieved with installation of forepole along with rock bolts at 1 m c/c spacing. With the installation of the forepoles, the final concrete lining of 200 mm is sufficient in the crown of the section. The final deformation of the section was achieved as 0.78 m. Figure 5.16 shows the capacity plot for Factor of Safety of 1 and 1.2 for the final concrete lining which shows that the section is completely safe

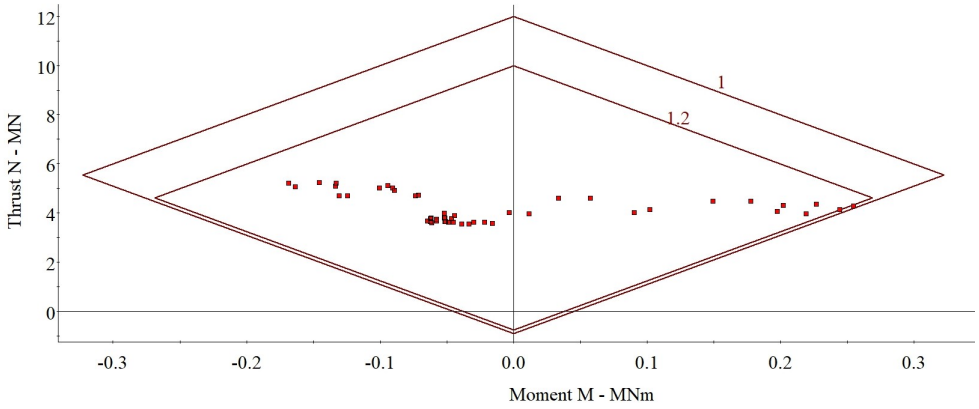

Figure 5.16: Capacity Plot for final concrete lining after installation of yielding support in Ch. 3+404 m of Chameliya HRT.

within FOS of 1 while some failures can be seen for FOS of 1.2 which belongs to the springline region of the section. In overall the section is seen as safe, thickness of lining in the springline region can be increased for additional safety.

Analysis Yielding Liners

The yielding supports used in the section at chainage 3+190 m and 3+404 m resulted in reduced support thickness and safe support of the excavation. However, it was seen that the horse-shoe excavation with yielding support did not have significant impact on the amount of liner for the section at Ch. 3+404 m. This shows that for extremely weak rock mass, circular excavation is required. This result is consistent with the final design in Yacambu-Quibot tunnel of Venezuela. In the tunnel, providing yielding support to in the horse shoe excavation lead to failure of the section due to long term loading i.e. the support started to fail approximately 10 years after the installation of the support as reported by Hoek and Briceno (2009). This was mitigated by rehabilitating the section by re-mining the collapsed section and providing circular excavation with yielding supports which consisted 50 cm thick shotcrete shell in two layers embedded with steel sets with sliding gaps. This shows that providing yielding liner might not always prove to be a safe support and the factor to be considered is the sequence of the installation of the support elements and the activation of those elements.

Similarly, after the failure of supports in Chameliya headrace tunnel, the section was re-excavated and yielding supports were provided in the weak sections. In doing so, most of the ground stress had already been released in the form of closure of the excavation which proved to be beneficial for the project. But this resulted in the increased cost and time of the project. During re-excavation of the failed sections, circular section were adopted with yielding sections as reported by Shah (2016). Figure 5.17 shows the squeezing treatment done in the failed sections of the Chameliya

Table 5.4: Remedy and tunnel supports used for squeezing ground in Chameliya headrace tunnel (Shah, 2016)

Zone	Total Length (m)	Over excavation	Tunnel Support
A: Squeezing extremely severe	418	Upto 6.6 m diameter of circular shape	Steel ribs with yielding support, 60 cm reinforced shotcrete
B: Squeezing extremely severe but stable	226	Upto 6.4 m diameter of circular excavation	40 cm thick shotcrete lining
C: Squeezing very severe but stable	198	Upto 6.3 m diameter of circular excavation	35 cm thick reinforced shotcrete

project and Table 5.4 summarizes the support adopted for the squeezing ground after the failure of initially designed supports.

Since most of the stress had already been released during the failure of the tunnel, the newly provided support was able to successfully support the section. This study, however, is done for initial excavation of the tunnel i.e. considering the situation where the section has not already failed and yielding support has been designed for this situation. A total strain of 2% and 3% has been allowed respectively to section at chainage 3+190 and 3+404 m which is equivalent to additional closure of 0.3 m and 0.4 m for each chainage. The final support lining as highlighted earlier consists of 600 mm of shotcrete and concrete with steel sets. This support closely matches with the remedial measures adopted in reinforcing the section (Table 5.4). This shows that additional closure of 0.2-0.3 m has significant contribution to the stability of the section.

5.7.2 Case Study: Kaligandaki A and Khimti I Headrace Tunnel

The Kaligandaki A headrace tunnel is a horseshoe shaped tunnel with excavated diameter of 8.7 m and cross sectional area of 58 m^2 (P. K. Shrestha & Panthi, 2014a). The 5950 m long tunnel is fully concrete lined as final support with circular section and 7.4 m finished diameter (Panthi, 2006).

Khimti I headrace tunnel is inverted D shaped with a diameter of 4/4.3 m according to the construction methodology applied. The tunnel has a length of 7888 m with a cross sectional area of 14.28 m^2. The tunnel mainly passes through gneiss rock mass with highly jointed, deeply weathered and deformed rock mass. Problems of tunnel collapse and water leakage was encountered during the construction of the project.

The support analysis for these two case studies follows the same approach as

(a) Re-excavation of section

(b) Steel rib installation

(c) Liner with sliding gaps

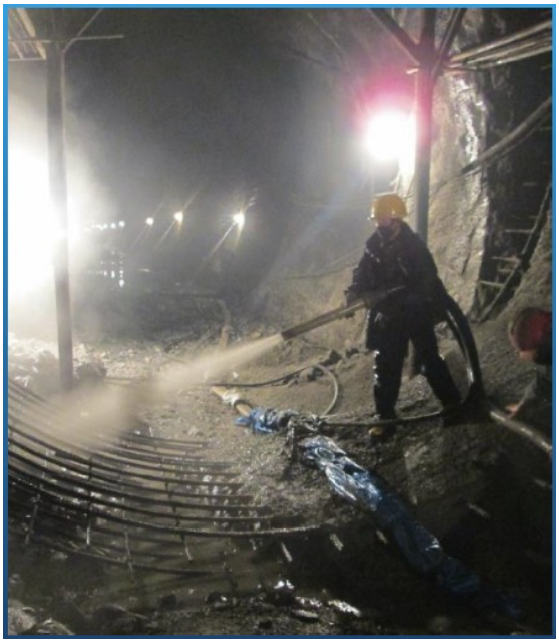

(d) Final concreting

Figure 5.17: Squeezing treatment of failed section in Chameliya headrace tunnel (Shah, 2016)

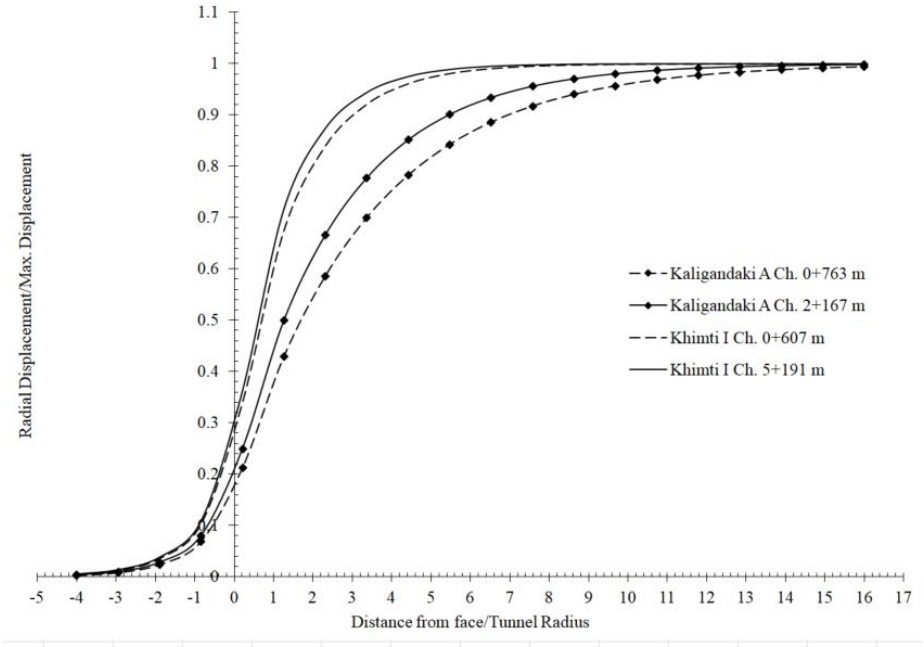

Figure 5.18: LDP for study sections of Kaligandaki A and Khimti I HRT.

described above for the case of Chameliya HRT. Two section from each case study is taken for study. The sections are selected for extremely poor and exceptionally poor rock mass according to the Q system of classification, for each case study. The Longitudinal Deformation Profile *(LDP)* for the selected sections are shown in Figure 5.18 and the rock mass properties of the sections are given in Table 5.2.

Section from Kaligandaki A HRT

From Figure 5.18, the displacement prior to support installation is determined and the support is installed in the model allowing the stress relaxation equal to the obtained deformation from *LDP*. For the section of 0+763 m of Kaligandaki A HRT, providing support 0.5 m ahead of face resulted in a closure value of 0.24 m. The maximum deformation in the section for unsupported condition was obtained as 1.28 m. Although the section belongs to extremely poor category, the maximum deformation is far less than that obtained for Chamleiya section of the same rock category since the rock mass is relatively strong with an intact rock strength of 40 MPa.

For modeling of the support, the results obtained from the analysis of Chameliya headrace tunnel is tested in the region which results in a support combination of fiber reinforced shotcrete of thickness $>$ 20 cm, minimum concrete lining of 300 mm and steel sets spaced at 0.5 m c/c. Forepole and rock bolts are installed for the stability of the rock mass around the excavation. These supports are installed in various stages with shotcrete and steel lining 0.5 m from the face and concrete lining at 1 m from the face of the tunnel. Due to the support of forepole, concrete lining is not necessary

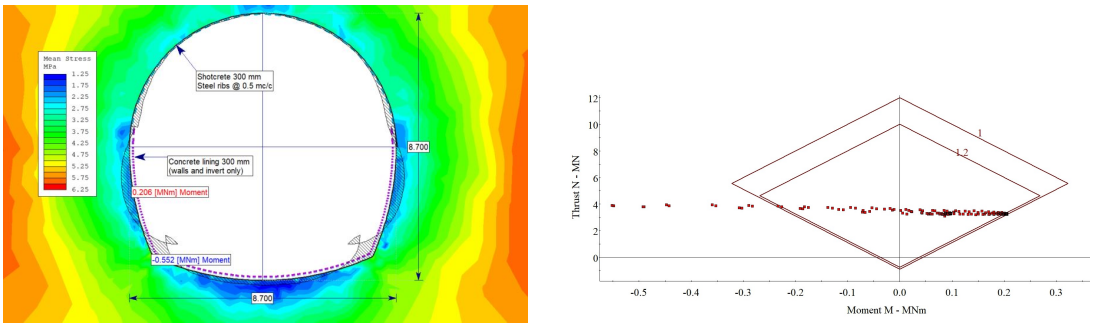

(a) **(b)**

Figure 5.19: (a) Support element with bending moment and (b) Capacity Plot for liners in Ch. 0+763 m of Kaligandaki A HRT.

in the crown and is provided only in walls and invert of the section. Figure 5.19a shows the support elements used in the model along with the bending moment over the supports. It can be seen that negative bending moment of 0.552 MNm occurs in the corners of the section for concrete lining. Comparing this with Figure 5.19b, the moment vs thrust plot, it is clear that the region with the negative moment fails while all other section is safe for a FOS of 1. Some failure can be seen in the walls with maximum positive bending moment (0.206 MNm) for a FOS of 1.2. Although the section is already safe (within FOS 1), this can be compensated by increasing the liner thickness in the failure region. Another thing to notice in Figure 5.19a is the stress contour near and far from the excavation boundary. In the region near the excavation contour, the stress is very less (blue coloured) implying the failure of the rock mass such that it cannot withstand higher stresses. As we move away from the contour, the stress gradually increases with maximum stress far from the contour. This shows that the extent of damage zone, around the excavation, caused by blast damage reduces the rock mass capacity to withstand high stress while far from the contour, the rock mass is not disturbed and thus the stress value is high in this region. Similarly, the stress is relatively higher in the crown region than in the walls and the invert which is caused by strengthening the rock mass in the crown by use of forepole prior to the excavation of the section.

Similarly the results from analysis of Chameliya for exceptionally poor rock mass section were also tested at chainage 2+167 m of Kaligandaki A headrace tunnel with Q value of 0.008. From the *LDP* (Figure 5.18), we get the deformation of 0.78 m at a position of 0.5 m from the tunnel face and a maximum unsupported deformation of 3.37 m upon complete excavation of the section. A support combination of fiber reinforced shotcrete of 300 mm thickness embedding ISMB 200 at 0.3 m c/c was installed as primary support. This was later supported by providing a final concrete lining 1 m from the face of tunnel. Concrete lining of thickness 400 mm in crown, 600 mm in walls and 500 mm in invert was required for the section to be completely safe

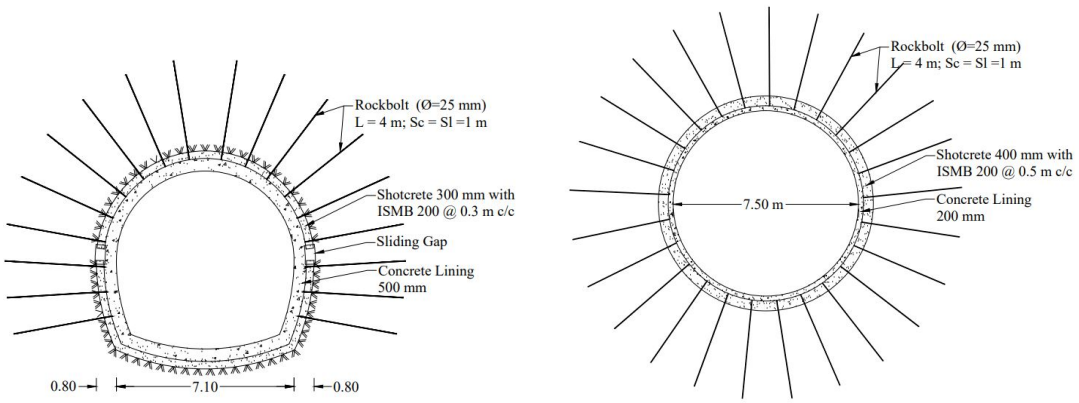

(a) **(b)**

Figure 5.20: Support element for (a) Yielding support in horseshoe excavation and (b) Circular excavation for Ch. 2+167 m of Kaligandaki A HEP.

(additional lining is required in the corners equal to 700 mm thickness). Forepole and rock bolts are also installed in the section. This support agrees with the finding from Chameliya section.

In order to optimize the support required for the section, yielding support is tested for the horse-shoe and circular excavation. The supports were provided allowing a closure of about 0.3 m after its installation. This results in a total deformation of about 1 m after the excavation stabilized. The amount of support required includes forepole umbrella with rock bolts installed at 1 m c/c spacing, 300 mm of fiber reinforced shotcrete, ISMB 200 at 0.3 m c/c spacing and final concrete lining of 500 mm. The concrete lining is installed after the initial support of shotcrete and steel sets locks in place and starts taking the ground load. Figure 5.20a shows the details of the section with yielding support.

Since the total thickness of the yielding support is 800 mm while that for non-yielding is 900 mm, there is not much reduction in the amount of support thickness. However, the advantage of the yielding liner includes in the providing a safe working condition for the workers by providing support against failure while providing closure of the ground to reduce the amount of support. Circular excavation is also tested for the section (Figure 5.20b). For circular opening, as seen in Figure 5.20b, the amount of support required for stabilizing the rock mass includes shotcrete lining of 400 mm thickness with steel ribs at 0.5 m c/c spacing. Forepole and rock bolts are also provided as support and the opening is provided with a final lining of 200 mm thick concrete. This results in total thickness of liner of 600 mm without sliding gaps in the support. This support closely matches the final support used in the site.

Section from Khimiti I HRT

Two sections at Chainage 0+607 m and 5+191 m have been taken for study which falls in the category of exceptionally poor and extremely poor with Q values of 0.005 and 0.02 respectively. The rock mass parameters for the sections have been tabulated in Table 5.2 and Figure 5.18 shows the *LDP* according to Vlachopoulos and Diederichs (2009).

The supports were modeled by providing supports as highlighted in Table 4.3. These supports were provided in the site and the supports are in good agreement with the results of numerical modeling for the selected sections. However, the support provided in Table 4.3 is sufficient only for the walls and crown of the section and it provides no hint on the amount of support to be installed in the invert of the section. The invert lining might have been provided at a later time after the face is significantly away from the section. This allows the invert to converge further allowing the stress to be released which results in lower amount of support requirement for the invert. This practice, although results in lower lining requirement, it might result in failure of the entire section in extreme case as the support is discontinuous. On numerical analysis it was found that by delaying the supporting of the invert, about 400 mm of concrete lining was sufficient while if the support is to be provided while supporting the walls and crown, 700 mm of thick invert lining is required for both the sections.

Table 5.5 provides the final deformation obtained via numerical modeling along with the support provided for all the study sections.

5.8 Analysis and Discussion

From the analysis of the eight sections from three different case studies located in the Lesser Himalayan Region of Nepal, we can see that the support recommendation provided by the Rock Mass Classification approach is insufficient. The Rock Quality Index (Q-system) is the most common approach of support design in the region. However, contrary to the approach, concrete lining and steel ribs are provided for supporting weak sections. These supports are provided based on the experience of the designers and engineers. From the study it is seen that the classification system fails as the rock mass gets weaker, especially in the region of extremely to exceptionally poor rock mass. For rock mass of Q value greater than 0.1 i.e. for very poor rock mass and above, the classification system is sufficient for stabilizing and supporting the sections with minor changes in some situations. Based on the results of study, a support guideline has been prepared for the Himalayan geology considering the commonly used support elements in the country. Since most of the hydropower tunnels have a diameter of less than 10 m in the region, the results of the study is only suitable for span/ESR value less than 10. Table 5.6 provides a

Table 5.5: Deformation values with corresponding support: Results from numerical analysis.

Case Study	Chainage [m]	Excavation/ Support	Support Details	Deformation [m]
Chameliya	0+310	HS/ Design	S(fr): 0.15 m	0.14
	3+103	HS/ Design	S(fr): 0.075 m; Concrete: 0.2 m at invert	0.11
	3+190	HS/ Modified	S(fr): 0.2 m; Steel ribs @ 0.5m c/c; Concrete: 0.5 m	0.45
		Circular/ Q	S(fr): 0.2 m; RRS II @ 2.3m c/c	0.41
		Circular/ Modified	S(fr): 0.2 m; 3 bar lattice @ 1 m c/c	0.41
		HS/ Yielding	S(fr): 0.2 m; Steel @ 0.5m c/c; Concrete: 0.4 m	0.67
	3+404	HS/ Modify	S(fr): 0.2 m; Steel @ 0.3m c/c; Concrete: 0.4 m at crown, 0.6 m at walls and invert	0.41
		HS/ Yielding	S(fr): 0.3 m; Steel @ 0.3 m c/c; Concrete: 0.5 m	0.74
		Circular/ Yielding	S(fr): 0.3 m; Steel @ 0.5 m c/c; Concrete: 0.2 m at crown, 0.3 m at walls	0.78
Kaligandaki A	0+763	HS/ Modified	S(fr): 0.3 m; Steel @ 0.5 m c/c; Concrete: 0.3 m	0.23
	2+167	HS/ Modified	S(fr): 0.3 m; Steel @ 0.3 m c/c; Concrete: 0.4 m crown, 0.6 m walls, 0.5 m invert	0.75
		HS/ Yielding	S(fr): 0.3 m; Steel @ 0.3 m c/c; Concrete: 0.5 m	1.02
		Circular	S(fr): 0.4 m; Steel @ 0.5 m c/c; Concrete: 0.2 m	0.6
Khimti I	0+607	Inverted D/ Design	S(fr): 0.2 m; Concrete: 0.4 m	0.13
	5+191	Inverted D/ Design	S(fr): 0.15 m	0.07

S(fr): Fibre reinforced shotcrete; HS: Horse-shoe excavation

summary of the support system for extremely and exceptionally poor rock masses for the Himalayas which has been graphically plotted based on the original Q chart (Figure B.3) for span/ESR value upto 10 and given in Figure 5.21.

The support recommendation in Table 5.6 and Figure 5.21 has been made based on the Q support guideline (Figure B.3) for span/ESR value less than 10. The notable differences in the original chart and the provided support recommendation are summarized below:

1. Forepole/Spiling bolt (face support) has been introduced for Extremely Poor and Exceptionally poor rock mass.
2. The minimum thickness of fiber reinforced shotcrete for exceptionally poor rock

Table 5.6: Support recommendation for weak rock mass of the Himalayas.

Q-value	Rock Class	Forepole/ Spiling Bolt	Rock Bolts	Spacing of steel ribs	Thickness of initial shotcrete	Thickness of final shotcrete/ concrete
0.1–0.04	Extremely Poor	ϕ = 25/32 mm with cement grouting	$S_l = S_c$ = 1–1.2 m	0.5–1.0 m c/c	9–15 cm	–
0.04–0.01				0.3–0.5 m c/c	15–20 cm	30–60 cm
< 0.01	Exceptionally Poor		$S_l = S_c$ = 1 m	0.3 m c/c	>20 cm	> 60 cm

- Rock bolts are provided of 25 mm diameter.
- Steel sets are provided of ISMB200 section.
- The spacing of steel sets should not be reduced below 0.3 m for convenience of construction.

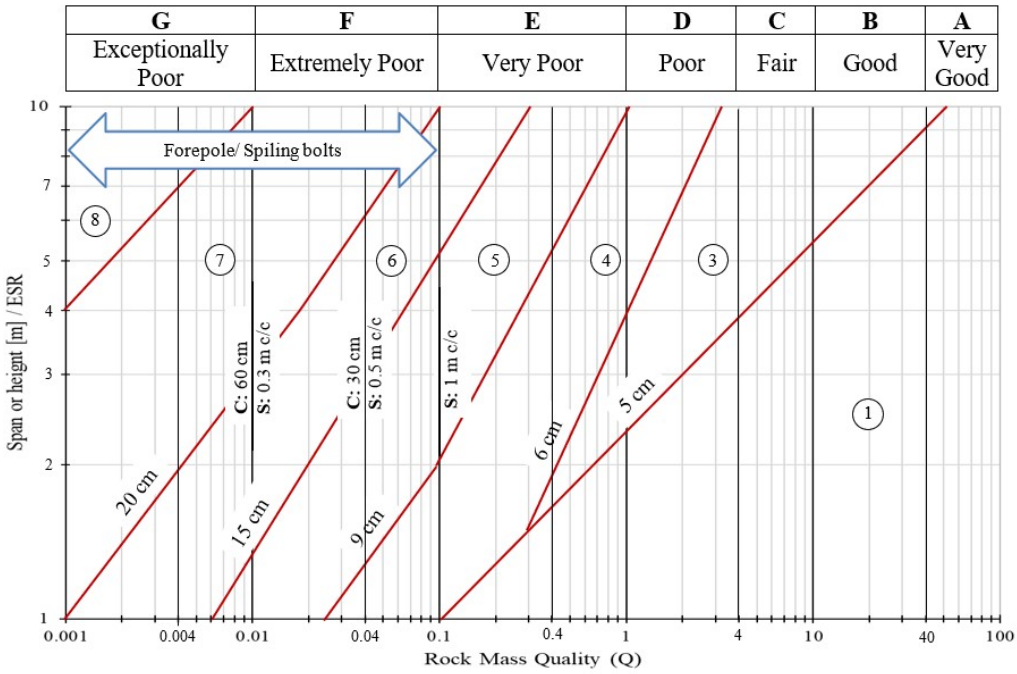

Figure 5.21: Support recommendation for the underground construction in Himalayan rock mass.

class (Support category 7) is set as 200 mm.

3. Reinforced Ribs of Shotcrete have not been included, instead steel ribs and concrete lining are defined.
4. Steel sets have been introduced for Extremely Poor and weaker rock mass class. The minimum spacing of steel ribs is 0.3 m c/c for exceptionally poor rock class, considering the convenience and workability for support installation. Similarly, the spacing must be adjusted between 0.3 m and 1 m for extremely poor rock mass, as per the encountered rock quality. In the graph, the spacing of steel ribs applied to the rock class to the left of where it is defined.
5. Concrete lining has been introduced as final liner for Q value less than 0.04.

The provided thickness is the minimum amount for the rock class and should be increased according to the encountered rock quality. Similar to the steel ribs spacing, the thickness of the concrete lining applied to the rock class left of where it has been defined.

6. Support category 2 has not been included in the chart since it applies to span/ESR value greater than 10.

The above supports are recommended in case of normal support without sliding gaps and horse-shoe excavation. This support can be further decreased by providing circular excavation and yielding supports in case of extremely squeezing ground. The details of the support system provided in the Figure 5.21 is similar to the original support recommendation (Figure B.3) with changes as listed above and is as follows:

(1) Unsupported or spot boltin
(3) Systematic bolting, S(fr), 5-6 cm
(4) S(fr) and bolting, 6-9 cm
(5) S(fr) and bolting, 9-15 cm, Steel ribs 0.5-1 m c/c
(6) S(fr) and bolting, 15-20 cm, Steel ribs 0.3-0.5 m c/c, CL 30-60 cm
(7) S(fr) and bolting, $>$ 20 cm, Steel ribs 0.3 m c/c, CL $>$ 60 cm
(8) Special evaluation

On comparing the results from the analysis with the squeezing criteria defined by Hoek and Marinos (2000), a borderline can be defined for the need of yielding supports. From the analysis of the section at Ch. 3+190 m and 3+404 m of Chameliya and Ch. 2+167 m of Kaligandaki A HEP, it can be seen that all the sections requires yielding supports- for stability of the excavation. In case of Ch. 3+404 m of Chameliya, circular section with yielding liner was required in order to decrease the lining amount. Apart from these three sections, no other section required yielding support and normal support was sufficient to stabilize the excavation. Comparing the need of different supports with the squeezing classification done by Hoek and Marinos (2000), we can see that for sections whose rock mass strength/in-situ stress (σ_{cm}/P_0) ratio is below 0.15, providing yielding support can help in the safe construction with reduced lining amount. However, even with only circular excavation (no yielding support), the support requirement significantly decreases. The choice of circular excavation and yielding support in these case depends upon the designer and engineer since circular excavation is difficult for smaller tunnels in terms of to and fro movement of vehicles during construction process. Providing circular excavation with yielding support for σ_{cm}/P_0 value less than 0.1 results in greater stability with less liner for weaker section. This solution has been successfully implemented in case

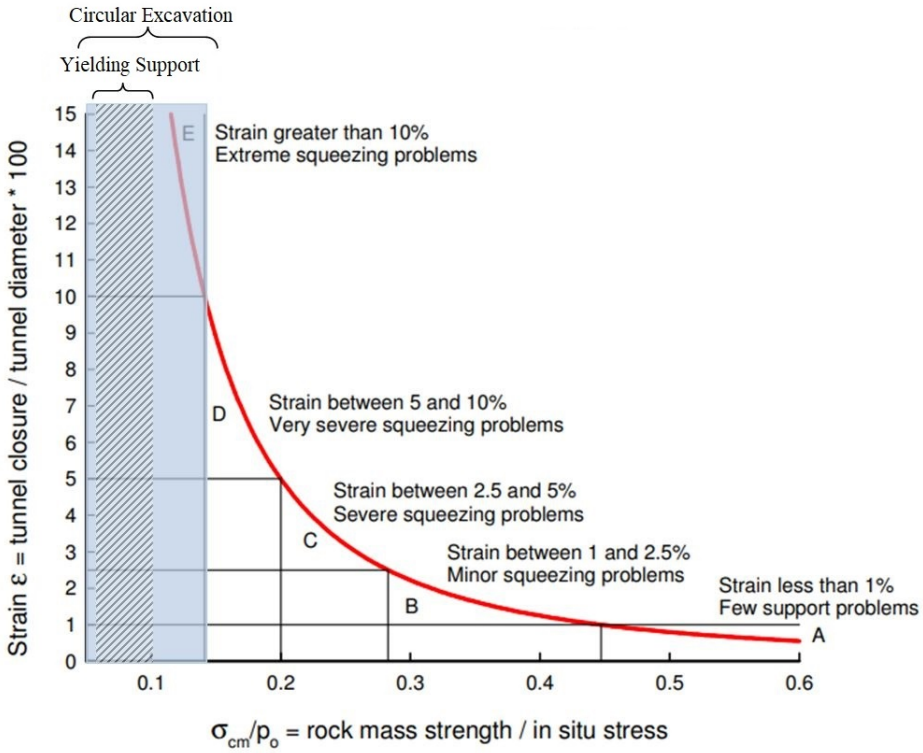

Figure 5.22: Region for circular excavation and yielding support (with changes made in the original chart from Figure 2.12).

of Chameliya headrace tunnel and Yacambu-Quibot tunnel of Venezuela. These findings have been shown in Figure 5.22. *(The σ_{cm}/P_0 for the sections can be calculated from Table 5.2).*

Chapter VI
Conclusion

This study focuses on the study of weak rock mass from the case histories of Lesser Himalayan Region of Nepal. Tunnelling in weak rocks have always been a challenge and due to lack of proper design and analysis several instances of failure of sections have been reported. Due to the presence of weak rock mass with high overburden, squeezing and collapse of tunnel sections are frequently encountered. The common practice in the country is to design the tunnel supports based on empirical methods such as the Rock Quality Index *(Q-system)* and Rock Mass Rating *(RMR)*. These methods although provide a good classification solution of the rock masses, they have in many instances proved to be inadequate in terms of support design. The most widely used method, the Q-system, is changed as per the demand of the rock mass and the experience of the designer while construction of underground structure in the Himalayan region. Due to presence of faults and discontinuities and due to the frequent seismic activities in the region, the empirical methods have failed in many occasions since they were originally designed for hard and brittle rocks where problems of rock squeezing and ground water flow are seldom encountered.

Since the country is moving forward in the development of underground structures, it is essential to develop a support guideline to address the problems of the region. Thus an approach has been made to establish a supporting guideline, especially for the weak rock mass, by use of numerical analysis and results in this study. By use of the commercially available software *RS2*, detail study has been carried out for the weak rock of three different tunnels from the Lesser Himalayas in terms of excavation support and stability. Based on the support elements used for construction in the region, a criteria has been set for the amount of support to be used for weak class of rocks. Two-dimensional modelling has been done for the purpose and considering the stability of weak rocks, forepoling, which commonly requires three-dimensional study, has also been modeled by two-dimensional approach. The major conclusions of the study are summarized below:

1. The Rock Mass Classification approaches provide a good basis for rock classification however, the support recommendation provided by these approaches have proved to be inadequate in many instances, especially for the weak rock class. Due to lack of a proper guideline, the support for such class of rocks is done based on the experience and judgment of the engineer and the designer which could lead to under or over support of the section.

2. The ground stress re-distributes around an underground opening after its excavation resulting in tangential stress around its boundary. This stress concentrates as the radius of opening decreases as shown by Figure 2.9b and Figure 2.10. This results in the high concentration of stress in the bottom corners of a horse-shoe or inverted D shaped opening (Figure 5.12a). This can result in the failure of the corners in the opening which can be remedied by either increasing the radius around the corners or by providing greater lining in the location.

3. On comparing the supporting effects of the shotcrete with steel beam composite (S&S) and shotcrete with *RRS* composite (R&S), it was seen that the *RRS* beam takes higher moment than the steel beam for the same load and ground conditions. This results in the shotcrete element taking greater load in case of S&S composite. As the spacing of the beams decreases, the moment and load acting on the beam also increases. Also, as the ground disturbances increases *(Disturbance factor D)*, the load over the support element increases as shown by the Figure 3.4a and 3.4b. It was also seen that when both the supports show safe behavior for a given load, the (R&S) composite shows higher bending moment capacity suggesting that the support combination could lead to oversupport of section.

4. Face support is essential during excavation of the weak rocks and this can be achieved by use of forepoles or spiling bolts. However, during numerical modeling, 3D modeling is required to study its effects on the ground. Since 2D modeling is preferred for the design of underground excavation for its time efficiency, a methodology has been developed for modeling the forepole in two-dimensional plain strain model as shown in Figure 3.11. Here, the rock mass above the crown has been improved as suggested by Hoek (2001, 2004) to impart the supporting effect of the forepoles.

5. A methodology has been developed for numerical modeling of weak grounds in two-dimensional model and given in Figure 5.4. This methodology allows ground stress relaxation determined from the *LDP* (Vlachopoulos & Diederichs, 2009) before installation of support. Installation sequence of support plays an important role in the stability of the underground excavation and this has been achieved in the numerical model by providing liners sequentially in different stages. This methodology can be adopted for modeling rock mass during the design of tunnel in weak rock mass.

6. It was seen that the bending moment over the boundary of the excavation differs greatly when the support is provided throughout the boundary as a closed ring and while providing different supports in the walls and invert (Figure 5.9) which

led to complete failure of the invert (where the moment was maximum). For a weak rock mass, it is essential to provide a ring of support in the excavation in order to prevent the failure of the rock mass.

7. Yielding support provide a safe and economic support for extremely squeezing ground. The support behaves robust enough to provide safe support for the construction at the same time it behaves flexibly to allow the ground to deform further allowing greater ground stress relaxation. It was seen that allowing 0.2-0.3 m of additional closure for the weak rock mass results in the safe excavation and support. This corresponds to 3-4% of strain closure in liners after its installation and before it starts to take the ground load.

8. Circular excavation or yielding support can be provided to rock mass whose σ_{cm}/P_0 ratio is less than 0.15. Further for value of $\sigma_{cm}/P_0 < 0.1$, providing yielding support with circular excavation reduces the amount of liner required for the stability of the section. This has been summarized in the chart in Figure 5.22.

9. Finally support recommendations have been provided for the extremely and exceptionally rock mass (< 0.1) with inclusion of steel beams and concrete lining. Forepoles are also included for the stability of the sections constructed in such rock mass. These have been summarized in Table 5.6. and shown in Figure 5.21.

Further Study

This study has made an approach to provide a support guideline for extremely and exceptionally poor rock mass (as classified by the Q system). Based on eight different sections from three hydropower tunnels in the Lesser Himalayas Region, support has been defined using the common support elements used during construction in the Himalayas. The recommended supports have proved to be safe from the analysis done using finite element method (two-dimensional modeling). However, additional case studies should be taken into study for more precise guidelines. Additionally, three dimensional study should be carried out to accurately study the behavior of the support elements and the ground stress during excavation.

References

Agarwal, R. K., & Boshkov, S. H. (1968, December). Stresses and displacements around a circular tunnel in a three-layered medium. *International Journal of Rock Mechanics and Mining Sciences*, *6*, 519-528.

Aksoy, C. O. (2008). Review of Rock Mass Rating Classification: Historial developments, applications, and restritions. *Journal of Mining Sciences*, *44*(1), 51-63.

Aydan, O., Akagi, T., & Kawamoto, T. (1993). The squeezing potential of rocks around tunnels: Theory and prediction. *Rock Mechanics and Rock Engineering*, *26*(2), 137-163. doi: 10.1007/BF01023620

Barla, G. (1970, August). The distributinoo of stress around a single underground opening in a layered medium under gravity loading. *International Journal of Rock Mechanics and Mining Sciences*, *9*, 127-154.

Barton, N. (1995). The influence of joint properties in modelling jointed rock masses. In 8^{th} *iSRM Congress. Keynote Lecture* (p. 1023-1032). Tokyo.

Barton, N. (2015, September). Forty years with the Q-system – Lessons and Developments. Hung Hom, Hong Kong.

Barton, N., & Grimstad, E. (2004, October). The Q-system following thirty years of development and application in tunnelng projects. In W. Schubert (Ed.), *Eurock2004 &53rd geomechanics colloquim.* Salzburg, Austria.

Barton, N., Lien, R., & Lunde, J. (1974). Engineering classification of rock masses for the design of tunnel supports. In *NGI Publication No. 106* (p. 48). Oslo: Norwegian Geotechnical Institute.

Barton, N., Lien, R., & Lunde, J. (1975). Estimation of support requirements for underground excavations. In *Xvith symposium of rock mechanics* (p. 163-177). Minneapolis.

Basnet, C. B. (2013). *Evaluation on the squeezing phenomenon at the headrace tunnel of Chameliya Hydroelectric Project, Nepal* (Master's thesis, Norwegian University of Science and Technology, Trondheim). Retrieved from `http://hdl.handle.net/11250/236161`

Bhasin, R., & Grimstad, E. (1996). The use of stress-strength relationship in the assessment of tunnel stability. In *Proceesings of the recent advances in tunnelling technology* (p. 183-196). New Delhi, India.

Bhattarai, P., Karki, B., Karki, S., & Shrestha, R. (2018, October). *Assessment and numerical modelling of selected hydropower tunnels in lesser himalayas with hydraulic design.* `http://rmlab.ku.edu.np/wp-content/uploads/2019/09/BE_Thesis_2018.pdf`. (Bachelor Thesis)

Bieniawski, Z. T. (1973). Engineering classification of jointed rock masses. *Transactions of the South African Institute of Civil Engineers*, *15*(12), 335-344.

Bieniawski, Z. T. (1974). Geomechanics classification of rock masses and its application in tunnelling. In *Proceedings in third international congress on rock mechanics* (p. 27-32). Denver.

Bieniawski, Z. T. (1976). Rock mass classification in rock engineering. In A. Balkema (Ed.), *Proceedings symposium on exploration for rock engineering* (p. 97-106). Rotterdam.

Bieniawski, Z. T. (1978). Determining rock mass deformability, experience from case histories. *International Journal of Rock Mechanics and Mining Sciences & Geomechanics Abstracts*, *15*, 237-247.

Bieniawski, Z. T. (1979). The geomechanics classification in rock engineering applications. In *Proceedings of the* 4^{th} *congress of the international society for rock mechanics* (p. 41-48). Montreux.

Bieniawski, Z. T. (1984). *Rock mechanics design in mining and tunnelling.* Rotterdam: A.A. Balkema.

Bieniawski, Z. T. (1988). Rock mass classification as a design aid in tunnelling. *Tunnels and Tunnelling*, *20*(7), 19-22.

Bieniawski, Z. T. (1989). *Engineering rock mass classification.* John Wiley and Sons.

Bieniawski, Z. T. (1993). Classification of rock masses for engineering: The RMR system and future trends. In *Comprehensive Rock Engineering* (Vol. 3, p. 553-573). New York: Peramon Press.

Bray, J. W. (1967). A study of jointed and fractured rock. Theory of limit equilibrium. *Felsmechanik und ingeneurgeologie (Rock mechanics and engineering geology)*, *5*, 197-216.

Cai, M., & Kaiser, P. K. (2006). Visualization of rock mass classification systems. *Geotechnical and Geological Engineering*, *24*, 1089-1102. (`https://doi.org/10.1007/s10706-005-7464-x`)

Cai, M., Kaiser, P. K., Tasaka, Y., & Minami, M. (2007). Determination of residual strength parameters of jointed rock masses using the GSI system. *International Journal of Rock Mechanics and Mining Sciences*, *44*, 247-265.

Cai, M., Kaiser, P. K., Uno, H., Tasaka, Y., & Minami, M. (2004). Estimation of rock mass deformation modulus and strength of jointed hard rock masses using the GSI system. *International Journal of Rock Mechanics and Mining Sciences*, *41*, 3-19.

Carranza-Torres, C., & Diederichs, M. S. (2009). Mechanical analysis of circular liners with particular reference to composite supports. for example, liners consisting of shotcrete and steel ribs. *Tunnelling and Underground Space Technology*, *24*, 506-532.

Carranza-Torres, C., & Fairhurst, C. (2000). Application of convergence confinement method of tunnel design to rock masses that satisfy the Hoek Brown failure criteria. *Tunnelling and Underground Space Technology*, *15*, 187-213.

CCC. (2002). *Civil Construction Report: Khimti I hydropower project* (Tech. Rep. No. Volume I). Civil Construction Company.

Chhushyabaga, B., Karki, S., & Khadka, S. S. (2020). Fault induced problems in hydropower tunnels in nepal: A case study. *Lowland Technology International*, *21*(4), 255-267.

Deere, D. U. (1968). Rock mechanics in engineering practice. In K. Stagg & O. Zienkiewicz (Eds.), (p. 1-20). London: Wiley.

Deere, D. U., & Deere, D. W. (1988). Rock classification systems for engineering purposes. In L. Kirkaldie (Ed.), (p. 91-101). West Conshohocken, PA: ASTM International. (`https://doi.org/10.1520/STP48465S`)

Dhakal, S. (2014). Contemporary environmental issues and methods in Nepal. In (p. 100-109). Kirtipur: Central Department of Environmental Sciences (CDES), Tribhuwan University.

Dwivedi, R. D., Singh, M., Viladkar, M. N., & Goel, R. K. (2013a). Estimation of support pressure during tunnelling through squeezing grounds. *Engineering Geology*, *168*, 9-22.

Dwivedi, R. D., Singh, M., Viladkar, M. N., & Goel, R. K. (2013b). Prediction of tunnel deformation in squeezing grounds. *Engineering Geology*, *161*, 55-64.

Gartoula, G. (2019, November). *Nepali Times.* Retrieved April 17, 2021, from `https://www.nepalitimes.com/uncategorized/nepals-first-and-forgotten-tunnel/`

Goel, R., & Jethwa, J. (1991). Prediction of support pressure using RMR classification. In *Proceedings in indian geotechnial conference* (p. 203-205). Surat, India.

Goel, R. K. (1994). *Correlations for predicting support pressures and closures in tunnels.* (Doctoral dissertation, Nagpur University)

Goel, R. K., Jethwa, J. L., & Paithankar, A. G. (1995a). Indian experience with Q and RMR systems. *Tunnelling and Underground Space Technology*, *10*(1), 97-109.

Goel, R. K., Jethwa, J. L., & Paithankar, A. G. (1995b). Tunnelling through the young Himalayas - A case history of the Maneri-Uttarkashi power tunnel. *Engineering Geology*, *39*(1-2), 31-44.

Goodman, R. E. (1989). *Rock mechanics.* New York: John Wiley & Sons.

Heidbach, O., Rajabi, M., Reiter, K., Ziegler, M., & Team, W. (2016). *World Stress Map Database Release 2016.* Retrieved April 15, 2021, from `https://doi.org/10.5880/WSM.2016.001`

Hoek, E. (1998). Reliability of Hoek-Brown estimates of rock mass properties and their impact on design. *International Journal of Rock Mechanics and Mining Sciences*, *35*(1), 63-68.

Hoek, E. (2001). Big tunnel in bad rocks-2000 Terzaghi lecture. *ASCE Journal of Geotechnical and Geoenvironmental Engineering*, *127*(9), 726-740.

Hoek, E. (2004). *Numerical modelling for shallow tunnels in weak rock.* Retrieved May 11, 2021, from `https://www.rocscience.com/assets/resources/learning/papers/Numerical-Modelling-for-Shallow-Tunnels-in-Weak-Rock.pdf`

Hoek, E. (2006). Empirical estimation of rock mass modulus. *International Journal of Rock Mechanics and Mining Sciences*, *43*, 203-215.

Hoek, E. (2007). Practical Rock Engineering. In (chap. Rock mass properties). RocScience.

Hoek, E., & Briceno, R. G. (2009). Overcoming squeezing in the Yacambú-Quibor tunnel, Venezuela. *Rock Mechanics and Rock Engineering*, *42*(2), 389-418.

Hoek, E., & Brown, E. T. (1980). *Underground excavation in rock.* London: CRC Press.

Hoek, E., & Brown, E. T. (1997). Practical estimates of rock mass strength. *International Journal of Rock Mechanics and Mining Science*, *34*(8), 1165-1186.

Hoek, E., Carranza-Torres, C., & Corkum, B. (2002). Hoek-Brown failure criterion-2002 edition. In *Proceedings of the Fifth North American Rock Mechanics Symposium* (p. 267-273). Toronto.

Hoek, E., Carter, T. G., & Diederichs, M. S. (2013). Quantification of the geological strength index chart. In 47^th *us rock mechanics/geomechanics symposium.* (`https://www.rocscience.com/assets/resources/learning/hoek/2013-Quantification-of-the-GSI-Chart.pdf`)

Hoek, E., Kaiser, P. K., & Bawden, W. F. (1995). *Support of Underground Excavation in Hard Rock.* London: CRC Press.

Hoek, E., & Marinos, P. (2000). Predicting tunnel squeezing problems in weak heterogeneous rock masses. *Tunnels and Tunnelling International*, *32*(11), 45-51.

Hussain, S., Rehman, Z. U., Mohammad, N., Tahir, M., Khan, S., Khan, S. W., ... Gul, A. (2018). Numerical modeling for engineering analysis and designing of optimum support systems for headrace tunne. *Advances in Civil Engineering*, *2018*. Retrieved from `https://doi.org/10.1155/2018/7159873`

Hydro-Solutions. (n.d.). *History of Projects.* Retrieved June 26, 2018, from `http://hydrosolutions.com.np/wp-content/uploads/2017/10/history-projects.pdf`

IHA. (n.d.). *Nepal-Jhimruk: Case Studies.* Retrieved June 26, 2018, from `https://www.hydropower.org/sediment-management-case-studies/`

nepal-jhimruk

ISRM. (1978). Suggested methods for the quantitative description of discontinuities in rock mass. *International Journal of Rock Mechanics, Mining Sciences & Geomechanics Abstracts*, *15*, 319-368.

Janin, J. P., Dias, D., Emeriault, F., Kastner, R., Bissonnais, H. L., & Guilloux, A. (2015). Numerical back-analysis of the southern Toulon tunnel measurements: A comparison of 3D and 2D approaches. *Engineering Geology*, *195*, 42-52.

Jimenez, R., & Recio, D. (2011). A linear classifier for probabilistic prediction of squeezing conditions in Himalayan tunnels. *Engineering geology*, *121*, 101-109.

Karki, S., Chhushyabaga, B., & Khadka, S. S. (2020). An overview of design and construction practices of himalayan hydropower tunnels. *Journal of Physics: Conference Series*, *1608*. doi: 10.1088/1742-6596/1608/1/012008

Karki, S., Karki, B., Chhushyabaga, B., & Khadka, S. S. (2020). Design and analysis of squeezing ground hydropower tunnel in the himlaya through a case study. *Lowland Technology International*, *21*(4), 268-278.

Khadka, S. S., Karki, S., Chhushyabaga, B., & Maskey, R. K. (2019). Assessment and numerical analysis of hydropower tunnel in lesser himalayan region of Nepal- a case study. *Journal of Physics: Conf. Series*, *1266*.

Khakda, S. S. (2019). *Tunnel closure analysis of hydropower tunnels in lesser himalayan region of Nepal through case studies* (Doctoral dissertation, Kathmandu University). Retrieved from http://rmlab.ku.edu.np/wp-content/uploads/2019/09/PhD-Thesis_Fulltext.pdf

Kirsch, E. G. (1898). Die Theorie der Elastizität und die Bedürfnisse der festigkeitslehre. *Zeitschrift des Vereines deutscher Ingenieure*, *42*, 797-807.

Laubscher, D. H. (1977). Geomechanics classification of jointed rock masses-mining applications. *Transactions of the Institution of Mining and Metallurgy*.

Laubscher, D. H. (1984). Design aspects and effectiveness of support system in different mining conditions. *Transactions of the Institution of Mining and Metallurgy*.

Lorig, L. J., & Varona, P. (2013). *Ground support 2013* (Y. Potvin & B. Brady, Eds.). Perth: Australian Centre for Geomechanics. (ISBN 978-0-9806154-7-0)

Marinos, P., & Hoek, E. (2000). GSI — A geologically friendly tool for rock mass strength estimation. In *Proceedings of the geoengineering 2000 conference.* Melbourne, Australia.

Mendive, I. G., Sterin, U., Rellan, G., Sfriso, A. O., & Fuentealba, M. (2016, August). Arenal Deeps: Application of numerical methods to 2d and 3d stability analyses of underground excavations. In *EUROCK 2016.* Turkey: ISRM. Retrieved from https://dxi97tvbmhbca.cloudfront.net/upload/user/image/IMendive_ASfriso_Arenal_Deeps_20162019112818280041.pdf

Moldovan, R. A., & Popa, A. (2012). Finite element modelling for tunneling excavation. *Acta Technica Napocensis: Civil Engineering & Architecture*, *55*(1), 98-114.

NEA. (n.d.). *Generation, Operation and Maintenance.* Retrieved June 12, 2018, from `https://www.nea.org.np/generation/index.php?page=powerhouse&pid=16`

NEA. (1997). *Upgraded feasibility report,Chameliya Hydroelectric Project, Nepal* (Tech. Rep.). Nepal Electricity Authority.

NEA. (2004). *Kaligandaki "A" hydroelectric project* (Tech. Rep.). Nepal Electricity Authority.

NGI. (2015, May). *Rock mass classification and support design.* Oslo.

Nilsen, B., & Palmstrom, A. (2000). *Engineering geology and rock engineering. handbook no. 2.* Oslo, Norway: Norwegian Group for Rock Mechanics (NBG).

NTS. (2017). *The principles of Norwegian tunnelling Pub No. 26.* Oslo, Norway.

Palmstrom, A., & Broch, E. (2006). Use and misuse of rock mass classification system with particular reference to the Q-system. *Tunnels and Underground Space Technology*, *21*, 575-593.

Palmstrom, A., & Singh, R. (2001). The deformation modulus of rock masses: comparisons between in situ tests and indirect estimates. . *Tunnelling and Underground Space Technology*, *16*, 115-131.

Panthi, K. K. (2004). Tunnelling challenges in Nepal. *Proceedings in Norwegian National Tunnelling Conference*, 4.1-4.15.

Panthi, K. K. (2006). *Analysis of engineering geological uncertainties related to tunnelling in himalayan rock mass conditions* (Doctoral dissertation, Norwegian University of Science and Technology, Trondheim). Retrieved from `https://core.ac.uk/download/pdf/30862108.pdf`

Panthi, K. K. (2008). Underground space for infrastructure development and engineering geological challenges in tunneling in Himalayas. *Hydro Nepal Journal of Water Energy and Environment*.

Panthi, K. K. (2012). Evaluation of rock bursting phenomena in a tunnel in the Himalayas. *Bulletin of Engineering Geology and the Environment*, *71*, 761-769.

Panthi, K. K., & Nilsen, B. (2007). Uncertainty analysis of tunnel squeezing for two tunnel. *International Journal of Rock Mechanics & Mining Science*, *44*, 67-76.

Panthi, K. K., & Shrestha, P. K. (2018). Estimating tunnel strain in the weak and schistose rock mass influenced by stress anisotrophy: An evaluation based on three tunnel cases from Nepal. *Rock Mechanics and Rock Engineering*, *51*, 1823-1838.

Plamstrom, A. (2000). Recent development in rock support estimates by the RMi.

Journal of Rock Mechanics and Tunnelling Technology(1), 1-24.

Pop, V., Pop, M., & Cosobea, P. (2013). Variation of stress concentration around rectangular holes. Influence of joints types between the sides of a rectangular holes. *Acta Technica Napocensis: Civil Engineering & Architecture*, *57*(2).

Ribacchi, R. (2000). Mechanical tests on pervasively jointed rock material: insight into rock mass behaviour. *Rock Mechanics and Rock Engineering*, *33*(4), 243-266.

RocScience. (n.d.). Material Strength Parameters in RS2 [Computer software manual]. (`https://www.rocscience.com/help/rs2/phase2_model/strength_parameters.htm?agt=index`)

Russo, G., Kalamaras, G. S., & Grasso, P. (1998). A discussion on the concepts of geomechanical classes, behaviour categories, and technical classes for an underground project. *Gallerie e grandi opere soterranee*, *54*, 40-51.

Schijve, J. (2009). Fatigue of structures and materials. In (p. 59-88). Dordrecht: Springer. (`https://doi.org/10.1007/978-1-4020-6808-9_3`)

Shah, S. (2016). *Underground Excavation at Chameliya Hydroelectric Project: Case Study.* Retrieved from `https://www.scribd.com/document/312725160/Sanjiv-Shah-Underground-Excavations-at-CHEP`

Shrestha, G. L. (2005). *Stress induced problems in himalayan tunnels with special reference to squeezing* (Doctoral dissertation, Norwegian University of Science and Technology, Trondheim). Retrieved from `http://hdl.handle.net/11250/248703`

Shrestha, P. K., & Panthi, K. K. (2013). Analysis of the plastic deformatoin behavior of schist and schistose mics gneiss at Khimti headrace tunnel, Nepal. *Bulletin of Engineering Geology and the Environment*, *73*(3), 759-773. doi: 10.1007/s10064-013-0533-0

Shrestha, P. K., & Panthi, K. K. (2014a). Assessment of the effect of stress anisotropy on tunnel deformation in the Kaligandaki project in the Nepal Himalaya. *Bulletin of Engineering Geology and the Environment*, *74*, 815-826. Retrieved from `https://doi.org/10.1007/s10064-014-0641-5`

Shrestha, P. K., & Panthi, K. K. (2014b). Groundwater effect on faulted rock mass: An evaluation of Modi Khola pressure tunnel in the Nepal Himalaya. *Rock Mechanics and Rock Engineering*, *47*, 1021-1035.

Singh, Jethwa, J. L., Dube, A. K., & Singh, B. (1992). Correlation between observed support pressure and rock mass quality. *Tunnelling and Underground Space Technology*, *7*(1), 59-74.

Singh, B., & Goel, R. (2006). *Tunnelling in weak rocks* (Vol. 5). Elsevier.

Singh, B., Goel, R. K., Jethwa, J. L., & Dube, A. K. (1997). Support pressure assessment in arched underground openings through poor rock masses. *Engineering*

Geology, *48*, 59-81.

Singh, R., & Gahrooee, D. (1989). Application of rock mass weakening coefficient for stability assessment of slopes in heavily jointed rock mass. *International Journal of Surface Mining, Reclamation and Environment*, 207-219.

Sofiano, A. I., & Nomikos, P. P. (2006). Equivalent Mohr-Coulomb and generalized Hoek-Brown srength parameters for supported axisymmetric tunnels in plastic or brittle rocks. *International Journal of Rock Mechanics & Mining Sciences*, *43*, 683-704.

Terzaghi, K. (1946). Rock tunnelling with steel supports. In R. Proctor & T. White (Eds.), (p. 271). Youngstown, OH: Commercial Shearing & Stamping Co.

Ulusay, R. (1991). *Geotechnical evaluations and deterministic design consideration from pit-wall slopes at Eskihisar (Yatagan-Mugla) strip coal mine* (Unpublished doctoral dissertation). Middle East Technical University, Ankara, Turkey.

Upreti, B. (1999). An overview of the stratigraphy and tectonic of the Nepal himalaya. *Journal of Asian Earth Sciences*, *17*, 577-606.

Vlachopoulos, N., & Diederichs, M. S. (2009). Improved Longitudinal Profiles for Convergence Confinement Analysis of Deep Tunnels. *Rock Engineering and Rock Mechanics*, *42*, 131-146.

Vlachopoulos, N., & Diederichs, M. S. (2014). Appropriate uysed and practical limitations of 2D numerical analysis fo tunnels and tunnel support response. *Geotechnical and Geological Engineering*, *32*(2), 469-488.

Wawersik, W. R., & Fairhurst, C. (1970). A study of brittle rock fracture in laboratory compression experiments. *International Journal of Rock Mechanics and Mining Sciences & Geomechanics Abstracts*, *7*(5), 561-575. doi: https://doi.org/10.1016/0148-9062(70)90007-0

Zhang, L. (2017). Chapter 5 - Rock Masses. In L. Zhang (Ed.), *Engineering properties of rocks* (Second ed., p. 137-171). Butterworth-Heinemann. Retrieved from `https://www.sciencedirect.com/science/article/pii/B9780128028339000055` doi: https://doi.org/10.1016/B978-0-12-802833-9.00005-5

Appendix A:

Empirical approach of rock mass classification

A.1 Estimation of Support Pressure

Barton, Lien, and Lunde (1975); Barton et al. (1975) obtained the empirical relation for the ultimate support pressure (Equation (A.1)) by plotting the support capacity against rock mass quality (Q) for 200 underground openings.

$$\left.\begin{aligned} p_v &= (0.2/J_r)Q^{-1/3} \\ p_h &= (0.2/J_e)Q_w^{-1/3} \end{aligned}\right\} \tag{A.1}$$

where the term p_v is the ultimate roof pressure in MPa, p_h is the ultimate wall pressure in MPa, J_w is the Joint Water Reduction Factor (Table B.13) and Q_w is the wall factor obtained as given in Table A.1.

Further, Barton et al. (1974) suggested that if the number of joint sets is less than three, the support pressure is then expresses as given in Equation A.2.

$$\left.\begin{aligned} p_v &= \frac{0.2J_n^{1/2}}{3J_r}Q^{-1/3}[MPa] \\ p_h &= \frac{0.2J_n^{1/2}}{3J_r}Q_w^{-1/3}[MPa] \end{aligned}\right\} \tag{A.2}$$

For tunnelling in poor rock masses, Bhasin and Grimstad (1996) provided the relation (A.3) for estimating the support pressure. They utilized the data from Singh et al. (1992) and R. K. Goel et al. (1995a) including case studies from Scandinavian tunnels for development of the equation.

$$p_v = \frac{40B}{J_r}Q^{-1/3}[kPa] \tag{A.3}$$

Singh et al. (1992) proposed Equation A.4 for estimating the short term pressure

Table A.1: Wall factor for various ranges of Q value (Barton et al., 1974)

Range of Q	**Wall factor Q_w**
> 10	5.0 Q
0.1–10	2.5 Q
< 0.1	1.0 Q

based on Q values of 30 instrumented tunnels.

$$p_v = \frac{0.2}{J_r} Q_i^{-0.33} * f * f' * f'', [MPa] \tag{A.4}$$

$$f = 1 + (H - 320)/800 \geq 1 \tag{A.5}$$

$$f'' = log(9.5t^{0.25}) \tag{A.6}$$

where Q_i=5Q is the short term rock mass quality, p_v is the short term roof support pressure, f is the correction factor for overburden (Equation (A.5)), f' is the correction factor for tunnel closure (Table A.2), f" is the correction factor for time after excavation (Equation (A.6)) and H is the overburden above crown. t in Equation (A.6) is time in months after support installation. The correction factor f and f' was verified by R. K. Goel, Jethwa, and Paithankar (1995b) for the Maneri-Uttarkashi tunnel. Incorporating these correction factors, Singh et al. (1992) proposed relation (A.7) for ultimate tunnel support pressure (p_{ult}) after about 100 years.

$$p_{ult} = \frac{0.2}{J_r} * Q^{-1/3} * f * f', [MPa] \tag{A.7}$$

Table A.2: Correction factor f' for tunnel closure (Singh et al., 1992)

S.N.	**Rock Condition**	**Support System**	**Tunnel Closure** (u_a/a),%	**Correction factor (f')**
1	Non-squeezing $(H < 350Q^{0.33})$	–	< 1	1.0
2	Squeezing $(H > 350Q^{0.33}, J_r/J_a < 0.5)$	Very Stiff	$< 2\%$	> 1.8
3	-do-	Stiff	2–4%	0.85
4	-do-	Flexible	4–6%	0.70
5	-do-	Very Flexible	6–8%	1.15
6	-do-	Extremely Flexible	$> 8\%$	1.8

Tunnel closure depends significantly on method of excavation. In extreme squeezing ground conditions, heading and benching method may lead to tunnel closure > 8%.
Tunnel closures more than 4% of tunnel span should not be allowed, otherwise support pressures are likely to build up rapidly due to failure of rock arch. In such cases, additional rock anchors should be installed immediately to arrest the tunnel closure within a limiting value of 4% of width. Steel ribs with struts may not absorb more than 2% tunnel closure. Thus, SRFS is suggested as an immediate support at the face to be supplemented with steel arches behind the face in situations where closures are encountered.
The minimum spacing between the parallel tunnels is 5B center to center in squeezing ground, where B is the width of tunnel.

Similarly, using data from 25 different tunnel sections, R. K. Goel (1994); R. K. Goel et al. (1995a); B. Singh et al. (1997) developed two separate equations for tunnel sections under non-squeezing and squeezing ground conditions (Equation (A.8) and

Equation (A.9) respectively).

$$p_v(el) = \left[\frac{0.12H^{0.1} * a^{0.1}}{N^{0.33}}\right] - 0.038[MPa] \tag{A.8}$$

$$p_v(sq) = \left[\frac{f(N)}{30}\right] * 10^{\left[\frac{H^{0.6}{}_{*}a^{0.1}}{50*N^{0.33}}\right]}, [MPa] \tag{A.9}$$

where $p_v(el)$ is the short term roof pressure in non-squeezing ground conditions, $p_v(sq)$ is the short term roof pressure in squeezing ground conditions, *f(N)* is the correction factor for tunnel closure (Table A.3), H and a is the overburden and tunnel radius in meters and N is the rock mass number given by $RQD/J_n * J_r/J_a * J_w$.

Dwivedi et al. (2013a) analyzed the 52 tunnel sections along the Himalayan region including 16 tunnel sections from Lesser Himalayan region of Nepal. These sections have high in-situ stress, poor rock mass quality being excavated in squeezing ground. They developed a dimensionally correct empirical correlation for assessment of support pressure in tunnels which are excavated in squeezing ground conditions (Equation (A.10)). The correlation uses the concept of 'joint factor' as a measure of rock mass quality, allowable closure, depth and radius of opening as the governing parameters. The predicted results have been compared with the results obtained via existing approaches, discussed above, based on rock mass quality (Q) and rock mass number (N). It was observed that the proposed correlation fits better the collected data with a correlation coefficient of 0.92.

$$P_s = 9.23 * 10^{-3} * \sigma_v \left(\frac{J_f^3 \sigma_h^{0.1}}{10^7 \sigma_{ci}^{0.1}(d^{0.2} + J_f/1434)}\right)^{1.7} \tag{A.10}$$

Table A.3: Correction factor for tunnel closure (R. K. Goel et al., 1995a)

S.N.	Degree of squeezing	Normalized Tunnel Closure (%)	f(N)
1	Very mild squeezing ($275*N^{0.33}*B^{-0.1} < H < 360*N^{0.33}*B^{-0.1}$)	1–2	1.5
2	Mild Squeezing ($360*N^{0.33}*B^{-0.1} < H < 450*N^{0.33}*B^{-0.1}$)	2–3	1.2
3	Mild to moderate squeezing ($450*N^{0.33}*B^{-0.1} < H < 540*N^{0.33}*B^{-0.1}$)	3–4	1.0
4	Moderate squeezing ($540*N^{0.33}*B^{-0.1} < H < 630*N^{0.33}*B^{-0.1}$)	4–5	0.8
5	High squeezing ($630*N^{0.33}*B^{-0.1} < H < 800*N^{0.33}*B^{-0.1}$)	5–7	1.1
6	Very high squeezing ($800 * N^{0.33} * B^{-0.1} < H$)	> 7	1.7

Tunnel closure depends significantly on the method od excavation. In highly squeezing ground condition heading and benching method of excavation may lead to tunnel closure > 8%

where, P_s is ultimate support pressure in MPa, J_f is the joint factor, σ_v is the vertical in-situ stress, σ_{ci} is the uniaxial compressive strength of intact rock in MPa, σ_h is horizontal in-situ stress in MPa and d is the radial tunnel deformation ($= u/a * 100$, u is the radial tunnel deformation and a is the tunnel radius).

A.2 Estimation of tunnel deformation

Based on measured tunnel closures from 60 tunnel sections, correlations have been developed for predicting tunnel closures in non-squeezing and squeezing ground conditions R. K. Goel (1994) given in Equation (A.11) and Equation (A.12) respectively.

$$\text{Non-Squeezing} \qquad \frac{u_a}{a} = \frac{H^{0.6}}{28 * N^{0.4} * K^{0.35}}\% \tag{A.11}$$

$$\text{Squeezing} \qquad \frac{u_a}{a} = \frac{H^{0.8}}{10 * N^{0.3} * K^{0.6}}\% \tag{A.12}$$

where u_a/a is the normalized tunnel closure in percent, K is the effective support stiffness($= p_v.a/u_a$), H is the tunnel depth and a is the tunnel radius.

Similarly, Dwivedi et al. (2013b) predicted the tunnel closure by analyzing 63 tunnel sections including 37 tunnel sections from Lesser Himalayan region of Nepal. The dimensionally correct empirical correlation (Equation (A.13)) has been developed with correlation factor of 0.94 to predict tunnel deformation for squeezing ground.

$$\left.\begin{aligned} \text{Using } J_f \qquad \frac{u_p}{a} &= \frac{5 * 10^{-10} * \sigma_v * J_f^3}{K + 0.5} + 0.0052 \\ \text{Using Q} \qquad \frac{u_p}{a} &= \frac{0.0191 * \sigma_v * Q^{-0.2}}{K + 1} + 0.0025 \end{aligned}\right\} \tag{A.13}$$

where u_p is the predicted radial deformation of tunnel in m, a is the radius of tunnel in m, J_f is the joint factor, σ_v is the vertical in-situ stress in MPa, K is the support stiffness in MPa, and Q is the rock mass quality.

Panthi and Shrestha (2018) also developed relation for estimating the initial and final convergence values (Equation (A.14) and (A.15))of tunnels based on case histories of Himalayan region. This relation also incorporates the stress anisotrophy, which is the case in almost all underground excavations.

$$\varepsilon_{IC} = 3065 * \left(\frac{\sigma_v * (1 + k)/2}{2G * (1 + P_i)}\right)^{2.13} \tag{A.14}$$

$$\varepsilon_{FC} = 4509 * \left(\frac{\sigma_v * (1 + k)/2}{2G * (1 + P_i)}\right)^{2.09} \tag{A.15}$$

Table A.4: Classification of the degree of squeezing (Aydan et al., 1993)

Class No.	Squeezing Degree	Theoretical Expression	Comments in tunnel behavior
1	No-squeezing	$\epsilon_\theta^a/\epsilon_\theta^e \leq 1$	The rock behaves elastically and the tunnel will be stable as the face effect ceases.
2	Light-squeezing	$1 < \epsilon_\theta^a/\epsilon_\theta^e \leq \eta_p$	The rock exhibits a strain-hardening behavior. As a result, the tunnel will be stable and the displacement will converge as a dace effect ceases.
3	Fair-squeezing	$\eta_p < \epsilon_\theta^a/\epsilon_\theta^e \leq \eta_s$	The rock exhibits a strain-softening behaviior and the displacement will be larger. However, it will converge as the face effect ceases.
4	Heavy-squeezing	$\eta_s < \epsilon_\theta^a/\epsilon_\theta^e \leq \eta_f$	The rock exhinits a strain-softening behavior at much higher rate. Subsequently displacement will be larger and it will not take to converge as the face effect ceases.
5	Very heavy-squeezing	$\eta_f < \epsilon_\theta^a/\epsilon_\theta^e$	The rock flows which will result in the colapse in the medium and the displacement will be very large and it will be necessary to re-excavate the opening and install heavy supports.

A.3 Semi-empirical approach

Apart from the semi-empirical method given by Hoek and Marinos (2000) (Section 2.4.1), there exists another method of classifying rock mass based on the squeezing potential given by Aydan et al. (1993). Aydan et al. (1993) proposed to relate the strength of intact rock σ_{ci} to the overburden pressure γH in which the uniaxial compressive strength of intact rock σ_{ci} and of the rock mass σ_{cm} are the same. The fundamental concepts of the method based on the analogy between the stress-strain responses of the rock in laboratory testing and tangential stress-strain response around tunnels. ased on a closed form analytical solution, which has been developed for computing the strain level ϵ_θ^a around a circular tunnel in a hydrostatic stress field, five different degree of squeezing are defined as shown in Table A.4 with some comments on expected tunnel behavior.

A.4 Squeezing Assessment

To differentiate squeezing from non squeezing ground, researchers have provided several empirical relations. The relation is mostly based on the rock mass classification numbers which is used to determine a critical overburden depth. If the rock cover above a section is grater than the critical overburden, then the rock mass above the section is determined as squeezing ground else it is classified as non-squeezing ground.

As given in Equations (2.15), (2.16) and (2.17) by Singh et al. (1992), R. K. Goel et al. (1995a) and Jimenez and Recio (2011) respectively, the critical overburden is a factor of rock quality number (rock mass number in case of Equation (2.16)). Figure A.1, A.2 and A.3 shows the graphical plot of the same relations provided by the respective authors for differentiating squeezing rocks for their selected tunnel sections. The criteria given by Jimenez and Recio (2011) is more suitable for the Himalayan

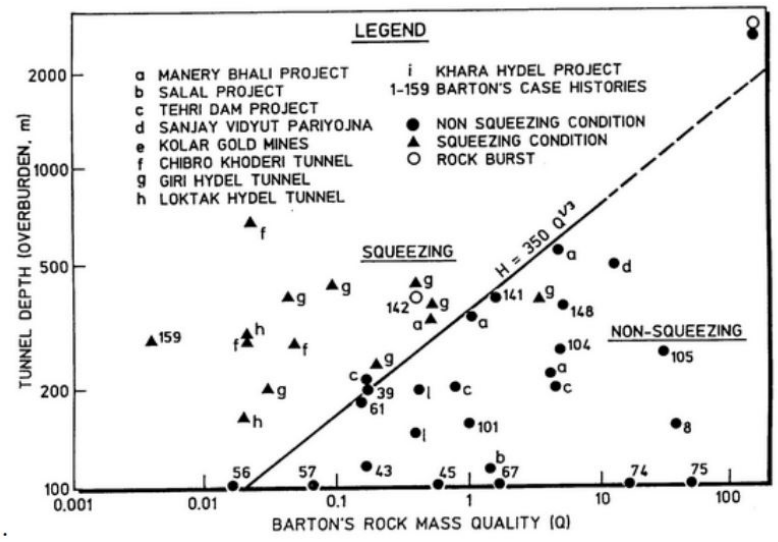

Figure A.1: Prediction of squeezing by Singh et al. (1992).

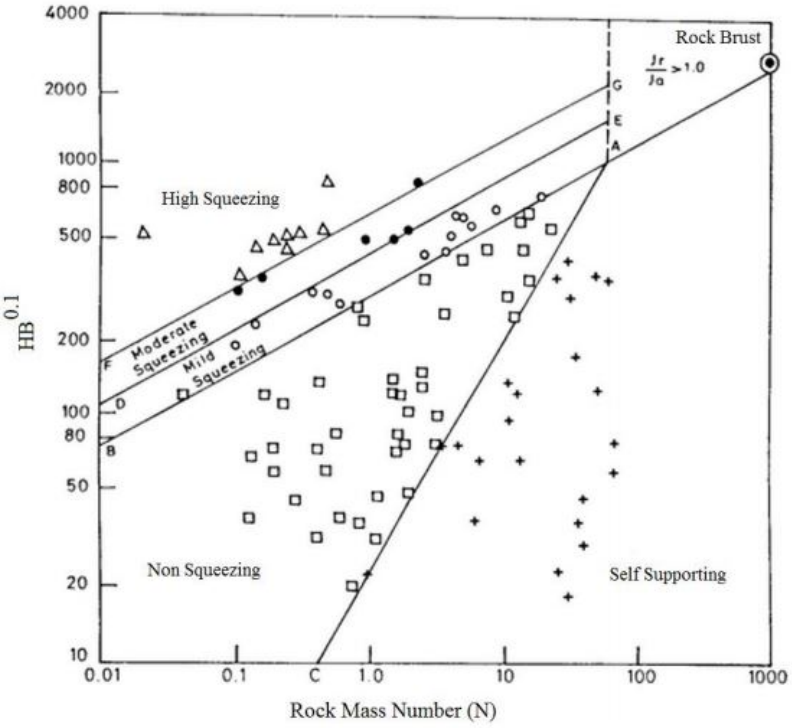

Figure A.2: Prediction of squeezing by R. K. Goel et al. (1995a).

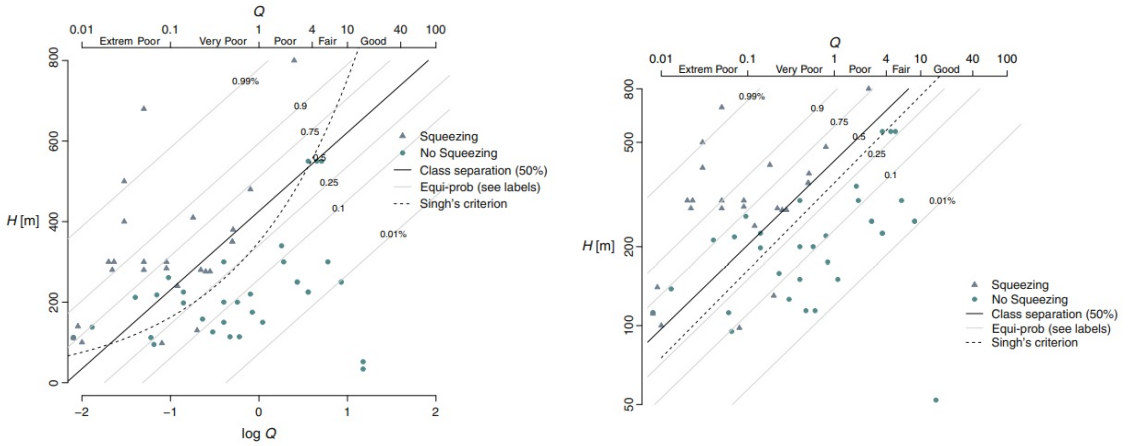

(a) semi-log plot

(b) log-log plot

Figure A.3: Prediction of squeezing by Jimenez and Recio (2011).

region since he developed the criteria by taking case studies from the Himalayan tunnels. Figure A.3 shows the plot developed by Jimenez and Recio (2011) where he compares the results with the criteria given by Singh et al. (1992) which shows that the criteria given by Singh et al. (1992) might sometimes fail to correctly classify the rock mass compared to Jimenez and Recio (2011).

Appendix B:
Ratings for rock mass classifications

B.1 Terzaghi Rock Mass Classification

Table B.1: Rock classes given by Terzaghi (Terzaghi, 1946)

Rock Class	Type of rock	Definition	Remarks
I	Hard and intact	The rock is unweathered. It contains neither joints nor hair cracks. If fractured, it breaks across intact rock. After excavation the rock may have some popping and spalling failures from the roof. At high stresses spontaneous and violent spalling of rock slabs may occur from the sides or the roof. The unconfined compressive strength is equal to or more than 100 MPa.	Light lining required only if spalling or popping occurs.
II	Hard stratified and schistose	The rock is hard and layered. The layers are usually widely separated. The rock may or may not have planes of weakness. In this type of rock, spalling is quite common.	Light support mainly for protection against spalling. Load may change erratically from point to point.
III	Massive moderately jointed	A jointed rock. The joints are widely spaced. The joints may or may not be cemented. It may also contain hair cracks, but the huge blocks between the joints are intimately interlocked so that vertical walls do not require lateral support. Spalling may occur.	
IV	Moderately blocky and seamy	Joints are less spaced. Blocks are about 1m in size. The rock may or may not be hard. The joints may or may not be healed, but the interlocking is so intimate that no side pressure is exerted or expected.	No side pressure.
V	Very blocky and seamy	Closely spaced joints. Block size is less than 1m. it consists of almost chemically intact rock fragments that are entirely separated from each other and imperfectly interlocked. Some side pressure of low magnitude is expected. Vertical walls may require supports.	Little or no side pressure.
VI	Completely crushed but chemically intact	Comprises chemically intact rock having the character of a crusher-run aggregate. There is no interlocking. Considerable side pressure is expected on tunnel supports. The block size could be a few centimeters to 30 cm.	Considerable side pressure. Softening effects of seepage toward bottom of tunnel requires either continuous support for lower ends of ribs or circular ribs.
VII	Squeezing rock – moderate depth	Squeezing is a mechanical process in which the rock advances into the tunnel opening without perceptible increase in volume. Moderate depth is a relative term and could be 150 to 1000 m.	Heavy side pressure, invert struts required. Circular ribs are recommended.
VIII	Squeezing rock — great depth	The depth may be more than 150 m. the maximum recommended tunnel depth is 1000 m.	
IX	Swelling rock	Swelling is associated with volume change and is due to chemical change of the rock usually in the presence of moisture or water. Some shales absorb moisture from air and swell. Rocks containing swelling minerals such as montmorillonite, illite, kaolinite, etc. can swell and exert heavy pressure on rock supports.	Circular ribs are required. In extreme cases, use of yielding support recommended.

B.2 Rock Mass Rating (RMR)

The six parameters used in the RMR system along with their ratings (Bieniawski, 1989) includes:

1. **Uniaxial Compressive Strength (UCS):** The UCS values are obtained from the laboratory experiments on rock cores. Dependent upon the values obtained, the ratings for different types of rocks are given in Table B.2.

2. **Rock Quality Designation (RQD):** Defined by Deere in 1964, RQD is an index of assessing rock quality quantitatively and is defined in Section 2.2.2. The ratings for corresponding RQD values is given in Table B.3.

3. **Joint or Discontinuity Spacing:** It is known that the presence of joints and discontinuities reduces the strength of rock mass and the spacing of the joint is one of the factors that affects it. Thus, it is important to measure the linear distance between two joints for all joint sets. Table B.4 shows the rating for the most critically orientated joint or discontinuity. If more than one discontinuity set is present and the spacing of discontinuities of each set varies, the unfavorably oriented set with lowest rating is considered.

4. **Joint Condition:** The condition of joint include the roughness of discontinuity surfaces, their separation, length or continuity, weathering of wall rock or the planes of weakness and infill materials. Table B.5 gives the rating value for the different joint condition and Table 10 provides a guideline for classification of the discontinuity.

5. **Groundwater Condition:** The rate of inflow of water per 10 m length should be determined or if actual water pressure data are available, they should be expressed in terms of ratio of seepage water pressure to major principal stress. Or the general condition can be described as dry, damp, wet, dripping or flowing and based on these, the ratings for various conditions should be selected as per Table B.7.

6. **Joint Orientation:** Orientation means the strike and dip of the excavation. The strike should be recorded in reference to magnetic north and the dip angle is the angle between the horizontal and discontinuity plane taken in a direction in which the plane dips. The alignment of the excavation should also be recorded since the influence of the strike and dip of discontinuity is considered with respect to it. To determine whether the orientation is favorable or not, Table B.8 should be referred and based on the favorability, the adjustment of the rating is done based on Table 2.3.

Table B.2: Rating of strength of intact rocks.

Qualitative Description	**Compressive Strength (MPa)**	**Point Load Strength (MPa)**	**Rating**
Extremely Strong	> 250	8	15
Very Strong	100–250	4–8	12
Strong	50–100	2–4	7
Medium Strong	25–50	1–2	4
Weak	5–25	*Use of UCS is preferred*	2
Very Weak	1–5	–	1
Extremely Weak	< 1	–	0
Materials with compressive strength less than 1 MPa would be regarded as soil			

Table B.3: Rating for RQD values.

Qualitative Description	**RQD (%)**	**Rating**
Excellent	90–100	20
Good	75–90	17
Fair	50–75	13
Poor	25–50	8
Very Poor	< 25	3

Table B.4: Rating for discontinuity spacing.

Description	**Spacing (m)**	**Rating**
Very Wide	> 2	20
Wide	0.6–2	15
Moderate	0.2–0.6	10
Close	0.06–0.2	8
Very Close	< 0.06	5

Table B.5: Rating for condition of discontinuity.

Description	**Joint Separation (mm)**	**Rating**
Very rough and unweathered, wallrock tught and discontinuous, no separation	0	30
Rough and slightly weathered, wall rock surface separation < 1 mm	< 1	25
Slightly rough and moderate to highly weathered, wall rock surface separation < 1 mm	< 1	20
Slickensided wall rock surface, or 1–5 mm thick gouge, or 1–5 mm wide continuous discontinuity	1–5	10
5 mm thick soft gouge, 5 mm wide continuous discontinuity	> 5	0

Table B.6: Guideline for classification of discontinuity condition.

Parameter*	**Ratings**				
Discontinuity Length (persistence/continuity)	< 1m 6	1–3 m 4	3–10 m 2	10–20 m 1	> 20m 0
Separation (aperture)	None 6	< 0.1mm 5	0.1–1.0 mm 4	1–5 mm 1	> 5mm 0
Roughness of discontinuity surface	Very Rough 6	Rough 5	Slightly Rough 3	Smooth 1	Slickensided 0
Infilling (gouge)	None	*Hard fillings*		*Soft fillings*	
		< 5 mm	> 5 mm	< 5 mm	> 5 mm
	6	4	2	2	0
Weathering discontinuity surface	Unweathered 6	Slightly weathered 5	Moderately weathered 3	Highly weathered 1	Decomposed 0

** some conditions are mutually exclusive. For example, if infilling is present, it is irrelevant what the roughness may be, since its effect will be overshadowed by the influence of the gouge. In such cases use Table B.5 directly.*

Table B.7: Rating for groundwater condition.

Inflow per 10 m tunnel length (L/min)	None	< 10	10–25	25–125	> 125
Ratio of joint water pressure to major principal stress	0	0–0.1	0.1–0.2	0.2–0.5	> 0.5
General description	Completely Dry	Damp	Wet	Dripping	Flowing
Rating	15	10	7	4	0

Table B.8: Characterization of discontinuity orientation related to underground excavation.

Strike	**Dip**		
	$0 - 20^0$	$20 - 45^0$	$45 - 90^0$
Across the axis	Fair	Favorable for drive with dip Unfavorable with drive against dip	Very favorable with drive with dip Fair with dive against dip
Parallel to tunnel axis	Fair	Fair	Very favorable

Table B.9: Guidelines for excavation and support of rock tunnels in accordance to RMR.

Rock Mass Class (RMR value range)	**Excavation**	**Supports**		
		Rock bolts (20 mm diameter, fully grouted)	**Conventional shotcrete**	**Steel Sets**
Very Good Rock *81-100*	Full face; 3 m advance	Generally, no support required except for occasional spot bolting		
Good Rock *61-80*	Full face; 1.0–1.5 m advance; complete support 20 m from face	Locally, bolts in crown 3m long, spaced 2.5 m with occasional wire mesh	50 mm in crown where required	None
Fair Rock *41-60*	Heading and bench; 1.5–3 m advance in heading; commence support after each blast; complete support 10 m from face	Systematic bolts 4 m long, spaced 1.5–2.0 m in crown and walls with wire mesh in crown	50–100 mm in crown and 30 mm in sides	None
Poor Rock *21-40*	Top heading and bench; 1.0–1.5 m advance in top heading; install support concurrently with excavation 10 m from face	Systematic bolts 4–5 m long, spaced 1–1.5 m in crown and wall with wire mesh	100–150 mm in crown and 100 mm in sides	Light to medium ribs spaced 1.5 m where required
Very Poor Rock < 20	Multiple drifts; 0.5–1.5 m advance in top heading; install support concurrently with excavation with excavation; shotcrete as soon as possible after blasting	Systematic bolts 5–6 m long, spaced 1–1.5 m in crown and walls with wire mesh; bolts inverts	150–200 mm in crown, 150 mm in sides and 50 mm on face	Medium to heavy ribs spaced 0.75 m with steel lagging and forepoling if required; close invert

B.3 Rock Quality Index (Q)

B.4 Geological Strength Index (GSI)

The chart for the selection of *GSI* value was first developed by Hoek and Brown (1997) and in order to later quantify the value, Cai et al. (2004) made slight changes in the chart by giving scale for Block Volume and Joint Condition Factor in the same chart (Figure B.1). The six parameters that define the Q-system along with their values for different types of rock conditions (NGI, 2015) are as follows:

1. **Rock Quality Designation (RQD):** The RQD is defined in Section 2.2.2 which classifies the rock in value ranging from 0 to 100. If 0 is used in the Q formula, it will give a Q value of 0 and therefore all RQD values between 0 and 10 are increased to 10 when calculating the Q value i.e. for calculating Q value the minimum value of RQD is 10.

2. **Joint Set Number (J_n):** Joints within a joint set will be nearly parallel to one another and will display a characteristic joint spacing. Joints that do not occur systematically or that have a spacing of several meters are called random joints. However, the effect of spacing strongly depends on the span or height of the underground opening. If more than one joint belonging to a joint set appears in the underground opening, it has an effect on the stability and should be regarded as a joint set. The Joint set number can be selected from Table B.10.

3. **Joint Roughness Number (J_r):** Joint friction depends on the nature of the joint wall surfaces, if they are undulating, planar, rough or smooth. The joint roughness number describes these conditions and is estimated from Table B.11, or Figure B.2. All joint sets at a location must be evaluated with regards to J_r. When calculating the Q-value, the J_r-value for the most unfavorable joint set concerning stability of the excavation must be used, i.e., use J_r of the joint set where shear is most likely to occur. In Figure B.2, there are two scales to describe the roughness:

    - The rough, smooth and slickenside refer to small structures in a scale of centimeters or millimeters. This can be evaluated by running a finger along the joint wall, small scale roughness will then be felt.
    - Large scale roughness is measured on a decimeter to meter scale and is measures by laying a meter-long ruler on the joint surface to determine the large-scale roughness amplitude. Stepped, undulating and planar are used to describe the large-scale roughness.

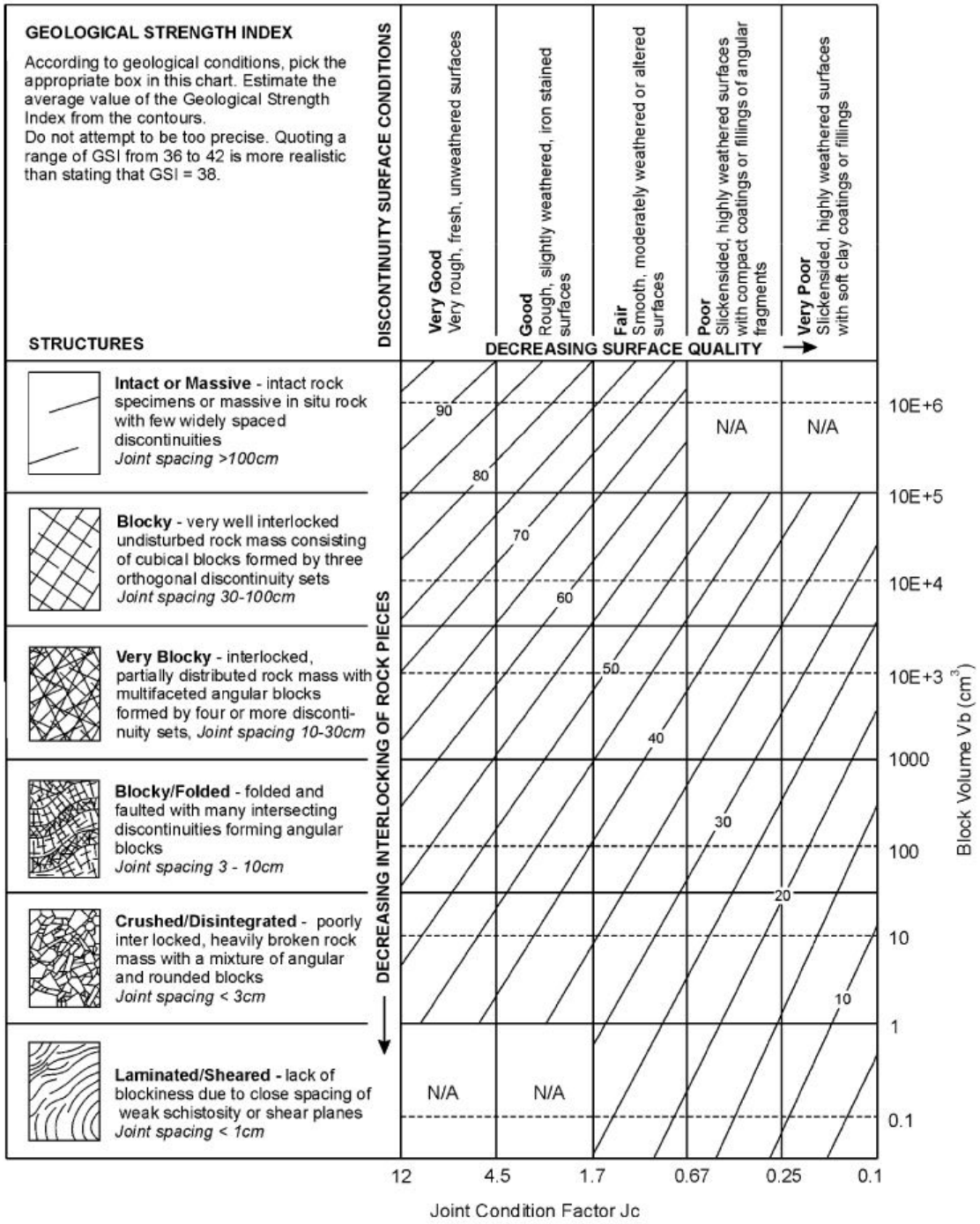

Figure B.1: Estimate of GSI based on visual inspection of geological conditions (Cai et al., 2004)

4. **Joint Alteration Number (J_a):** Joint infill is also a determining factor for joint friction. When considering the joint infill, two factors are important: thickness and strength, these factors depend on the material composition. The joint infill is divided into three categories: a, b and c based on thickness and degrees of the rock wall contact when sheared. For smooth joints, one millimeter of filling could be enough to prevent rock wall contact. However, for rough and undulating joints, several millimeters or in some cases centimeters, may be required. All joint sets at a given location must be evaluated. When calculating the Q value, the J_a value for the most unfavorable joint set regarding the excavation stability must be used i.e., the joint set where shear is most likely to occur. Table B.12 gives the J_a value for the three different categories defined above.

5. **Joint Water Reduction Factor (J_w):** Joint water may soften or wash out the mineral infill and thereby reduce the friction on the joint planes. Water pressure may reduce the normal stress on the joint walls and cause the blocks to shear more easily. A determination of the joint water reduction factor is based on inflow and water pressure observed in an underground opening. The lowest J_w-values ($Jw < 0.2$) represent large stability problems. Table B.13 gives the value of J_w for different groundwater condition.

6. **Stress Reduction Factor (SRF):** In general, *SRF* describes the relation between stress and rock strength around an underground opening. The effects of stresses can usually be observed in an underground opening as spalling, slabbing, deformation, squeezing, dilatancy and block release. However, some time may pass before the stress phenomena are visible. Whereas intensive spalling and rock burst may occur immediately after excavation, slower deformations like growth of new joints or plastic deformation of weak rock masses may take several days, weeks or months after excavation to form. In such cases an *SRF*-value determined from mapping the underground opening immediately after excavation may be incorrect. In order to determine *SRF*, the category must be determined first before the parameter value can be determined from the description given in Table B.14. The stress situation is classified in four categories in accordance with Table B.14

    - Weakness zones that intersect the underground opening which may or may not be able to transfer stresses in the surrounding rock mass.
    - Competent rock with stability problems due to high stresses or lack of stresses.
    - Squeezing rock with plastic deformation of incompetent rock under the

influence of moderate or high rock stresses.

- Swelling rock; chemical swelling activity depending on the presence of water.

Table B.10: Joint set number.

A	Massive, no or few joints	0.5–1.0
B	One joint set	2
C	One joint set plus random joint	3
D	Two joint sets	4
E	Two joint sets plus random joint	5
F	Three joint sets	9
G	Three joint sets plus random joint	12
H	Four or more joint sets, random heavily jointed 'sugar-cube', etc.	15
I	Crushed rock, earth like	20
Note:	i *For tunnel intersection use* $3 * J_n$ ii *For portals use* $2 * J_n$	

Based on the obtained Q value and the calculated *ESR* values (Equation (2.3) and Table 2.5), the support required for different rock class are determined from the chart given in Figure B.3

Table B.11: Joint roughness number.

a) **b)**	**Rock-wall contact, and** **Rock-wall contact before 1 cm of shear movement**	
A	Discontinuous joints	4
B	Rough or irregular joints	3
C	Smooth, undulating	2
D	Slickensided, undulating	1.5
E	Rough, irregular, planar	1.5
F	Smooth, planar	1
G	Slickensided, planar	0.5
Note:	*i) Description refers to small scale features and intermediate scale features in that order*	
c)	**No rock-wall contact when sheared**	
H	Zone containing clay minerals thickn enough to prevent rock-wall contact when sheared	1
Note:	*ii) Add 1 if the mean spacing of the relevant joint set is greater than 3 m (dependent on the size of the underground opening)* *iii) J_r =0.5 can be used for planar slickensided joints having lineations, provided the lineations are oriented in the estimated sliding direction*	

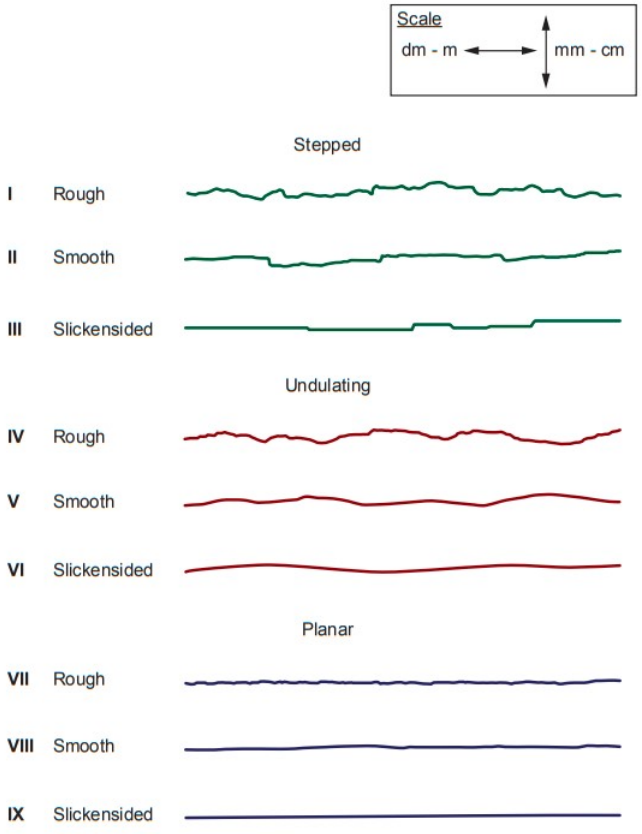

Figure B.2: Examples of Joint wall surface.

Table B.12: Joint alteration number.

a)	**Rock-wall contact (no mineral fillings, only coatings)**		
A	Tightly healed, hard, non-softening, impermeable fillings		0.75
B	Unaltered joint walls, surface staining only	$25-35^0$	2
C	Slightly altered joint walls. Non-softening minerals coatings; sandy particles, clay-free disintegrated rock, etc.	$25-30^0$	3
D	Silty or sandy clay coatings, small clay fraction	$20-25^0$	3
E	Softening or low friction clay mineral coatings, i.e. kaolinite or mica. Also, chlorite, talc gypsum, graphite, etc., and small quantities of swelling clays	$8-16^0$	4
b)	**Rock-wall contact before 10cm shear (thin mineral fillings)**		
F	Sandy particles, clay-free disintegrated rock, etc.	$25-30^0$	4
G	Strongly over-consolidated, non-softening, clay minerals fillings (continuous, but <5 mm thickness)	$16-24^0$	6
H	Medium or low over-consolidated, non-softening, clay mineral fillings (continuous, but <5 mm thickness)	$12-16^0$	8
I	Swelling-clay fillings, i.e., montmorillonite (continuous, but <5 mm thickness). Value of J_a depends on percent of swelling clay size particles	$6-12^0$	8–12
c)	**No rock-wall contact when sheared (thick mineral fillings)**		
J	Zones or bands of disintegrated or crushed rock. Strongly over-consolidated	$16-24^0$	6
K	Zones or bands of clay, disintegrated or crushed rock. Medium or low over-consolidated or softening fillings	$12-16^0$	8
L	Zones or bands of clay, disintegrated or crushed rock. Swelling clay. J_a depends on percent of swelling clay-size particles	$6-12^0$	8–12
M	Thick continuous zones or bands of clay. Strongly over-consolidated	$12-16^0$	10
N	Thick, continuous zones or bands of clay. Medium to low over-consolidation	$12-16^0$	13
O	Thick, continuous zones or bands with clay. Swelling clay. J_a depends on percent of swelling clay-size particles	$6-12^0$	13–20

Table B.13: Joint water reduction factor.

A	Dry excavation or minor inflow (humid or a few drips)	1.0
B	Medium inflow, occasional outwash of joint fillings (many drips/ 'rain')	0.66
C	Jet inflow or high pressure in competent rock with unfilled joints	0.5
D	Large inflow or high pressure, considerable outwash of joint fillings	0.33
E	Exceptionally high inflow or water pressure decaying with time. Causes outwash of materials and perhaps cave in	0.2–0.1
F	Exceptionally high inflow or water pressure continuing without noticeable decay. Causes outwash of material and perhaps cave in	0.1–0.05
Note:	i *Factors C to F are crude estimates. Increase J_w if the rock is drained or grouting is carried out*	
	ii *Special problems caused by ice formation are not considered*	

Table B.14: Stress Reduction Factor.

a)	**Weak zones intersecting the underground opening, which may cause loosening of rock mass**			**SRF**
A	Multiple occurrences of weak zones within a short section containing clay or chemically disintegrated, very loose surrounding rock (any depth), or long sections with incompetent (weak) rock (any depth). For squeezing, see L and M			10
B	Multiple shear zones within a short section in competent clay-free rock with loose surrounding rock (any depth)			7.5
C	Single weak zones with or without clay or chemical disintegrated rock (depth $\leq$ 50 m)			5
D	Loose, open joints, heavily jointed or "sugar cube", etc. (any depth)			5
E	Single weak zones with or without clay or chemical disintegrated rock (depth $>$ 50 m)			2.5
Note:	i *Reduce these values of SRF by 25–50% if the weak zones only influence but do not intersect the underground opening*			
b)	**Competent, mainly massive rock, stress problems**	σ_c/σ_1	σ_θ/σ_c	**SRF**
F	Low stress, near surface, open joints	$>$ 200	$<$ 0.01	2.5
G	Medium stress, favorable stress condition	200–10	0.01–0.3	1
H	High stress, very tight structure. Usually favorable to stability. May also be unfavorable to stability dependent on the orientation of stresses compared to jointing/weakness planes*	10–5	0.3–0.4	0.5–22.5*
I	Moderate spalling and/or slabbing after $>$ 1 hour in massive rock	5–3	0.5–0.65	5–50
J	Spalling or rock burst after a few minutes in massive rock	3–2	0.65–1	50–200
K	Heavy rock burst and immediate dynamic deformation in massive rock	$<$ 2	$>$ 1	200-400
Note:	ii *For strongly anisotropic virgin stress field (if measured): when* $5 \leq \sigma_1/\sigma_3 \leq 10$*, reduce* σ_c *to 0.75* σ_c*. When* $\sigma_1/\sigma_3 > 10$*, reduce* σ_c *to 0.5* σ_c*, where* σ_c *= Unconfined Compression Strength,* σ_1 *and* σ_3 *are the major and minor principal stresses, and* σ_θ *= maximum tangential stress* iii *When the depth of the crown below the surface is less than the span; suggest SRF increase from 2.5 to 5 for such cases (see F)*			
c)	**Squeezing rock: plastic deformation in incompetent rock under the influence of high pressure**		σ_θ/σ_c	**SRF**
L	Mild squeezing rock pressure		1–5	5–10
M	Heavy squeezing rock pressure		$>$ 5	10–20
Note:	iv *Determination of squeezing rock conditions must be made according to relevant literature*			
d)	**Swelling rock: chemical swelling activity depending on the presence of water**			**SRF**
N	Mild swelling rock pressure			5–10
O	Heavy swelling rock pressure			10–15

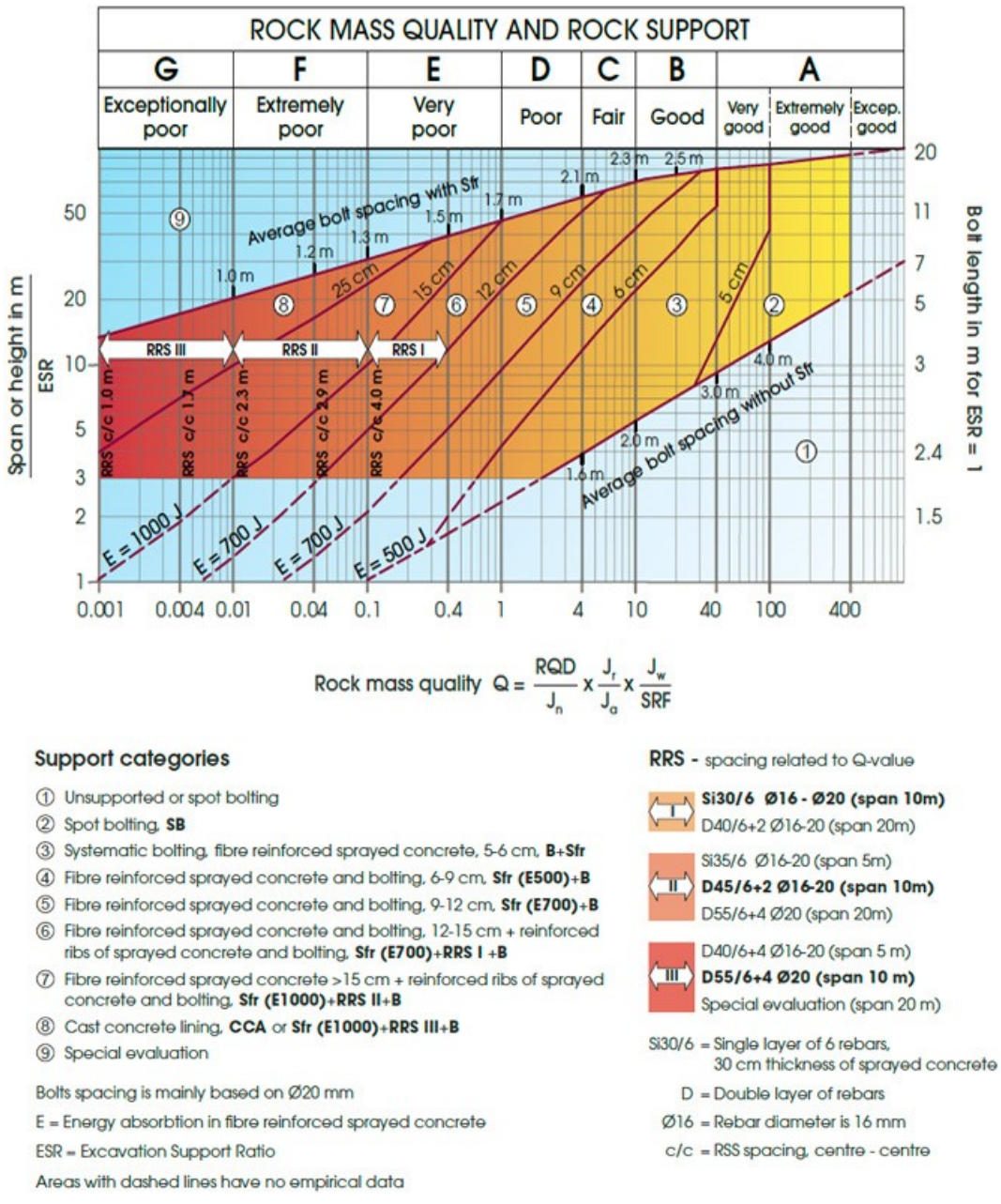

Figure B.3: Permanent support recommendation based on Q value (NGI, 2015)

Appendix C:
Rock Mass Parameter selection guidelines

Appearance of rock mass	Description of rock mass	Suggested value of D
	Excellent quality controlled blasting or excavation by Tunnel Boring Machine results in minimal disturbance to the confined rock mass surrounding a tunnel.	D = 0
	Mechanical or hand excavation in poor quality rock masses (no blasting) results in minimal disturbance to the surrounding rock mass. Where squeezing problems result in significant floor heave, disturbance can be severe unless a temporary invert, as shown in the photograph, is placed.	D = 0 D = 0.5 No invert
	Very poor quality blasting in a hard rock tunnel results in severe local damage, extending 2 or 3 m, in the surrounding rock mass.	D = 0.8
	Small scale blasting in civil engineering slopes results in modest rock mass damage, particularly if controlled blasting is used as shown on the left hand side of the photograph. However, stress relief results in some disturbance.	D = 0.7 Good blasting D = 1.0 Poor blasting
	Very large open pit mine slopes suffer significant disturbance due to heavy production blasting and also due to stress relief from overburden removal. In some softer rocks excavation can be carried out by ripping and dozing and the degree of damage to the slopes is less.	D = 1.0 Production blasting D = 0.7 Mechanical excavation

Figure C.1: Guidelines for estimating disturbance factor D (Hoek et al., 2002)

Table C.1: Field estimate of Uniaxial Compressive Strength (UCS) (Hoek, 2007)

Grade*	Term	Uniaxial Comp. Strength (MPa)	Point Load Index (MPa)	Field estimate of strength	Examples
R6	Extremely Strong	>250	>10	Specimen can only be chipped with a geological hammer	Fresh basalt, chert,diabase, gneiss, granite, quartzite
R5	Very Strong	100–250	4–10	Specimen requires many blows of a geological hammer to fracture it	Amphiobolite, sandstone, basalt, gabbro, gneiss, granodiorite, limestone, marble, rhyolite, tuff
R4	Strong	50–100	2–4	Specimen requires more than one blow of a geological hammer to fracture it	Limestone, marble, phyllite, sandstone, schist, shale
R3	Medium Strong	25–50	1–2	Cannot be scraped or peeled with a pocket knife, specimen can be fractured with a single blow from a geological hammer	Claystone, coal, concrete, schist, shale, siltstone
R2	Weak	5–25	**	Can be peeled with a pocket knife with difficulty, shallow indentation made by firm blow with a point of geological hammer	Chalk, rocksalt, potash
R1	Very Weak	1–5	**	Crumble under firm blows with point of a geological hammer, can be peeled by a pocket knife	Highly weathered or altered rock
R0	Extremely Weak	0.21–1	**	Indented by thumbnail	Stiff fault gouge

* Grade according to Brown (1981)
** Point load tests on rocks with a UCS below 25 MPa are likely to yield highly ambiguous results.

Table C.2: Average Uniaxial Compressive strength (q_c) of a varity of rocks. measured on 50 mm diameter samples (Plamstrom, 2000)

Type of rock	q_c **[MPa]**	**Type of rock**	q_c **[MPa]**	**Type of rock**	q_c **[MPa]**
Andesite (I)	150	Gneiss (M)	130	Sandstone (S, M)	< 100 >
Amphibolite (M)	< 160 >	Greenschist (M)	< 75 >	Serpentine (M)	135
Augen Gneiss (M)	160	Greenstone (M)	110	Shale (S, M)	95
Basalt (I)	160	Greywacke (M)	80	Siltstone (S, M)	< 80 >
Clay Schist (S, M)	55	Limestone (S)	90	Slate (M)	< 190 >
Diorite (I)	140	Marble (M)	< 100 >	Syenite (I)	150
Dolerite (I)	200	Micagneiss (M)	90	Tuff (S)	< 25 >
Dolomite (S)	< 100 >	Micaquartzite (M)	85	Ultrabasic (I)	160
Gabbro (I)	240	Micaschist (M)	< 80 >	Clay (hard)	0.7
Granite (I)	160	Phyllite (M)	< 80 >	Clay (stiff)	0.2
Granitic Schist (M)	100	Quartzite (M)	< 190 >	Clay (soft)	0.03
Granodiorite (I)	160	Quartzitic Phyllite (M)	100	Silt, sand (approx.)	0.0005
Granulite (M)	< 90 >	Rhyolite (I)	85		

(I): Igneous, (M): Metamorphic, (S): Sedimentary, <>: Large variation

Table C.3: Values of constant m_i for intact rock, by rock group (Hoek, 2007)

Rock type	Class	Group	Texture			
			Coarse	**Medium**	**Fine**	**Very Fine**
SEDIMENTARY	Clastic		Conglomerates* (21±3) Breccias (19±5)	Sandstones (17±4)	Siltstones (7±2) Greywackes (18±3)	Claystones (4±2) Shales (6±2) Marls (7±2)
	Non-Clastic	Carbonates	Crystalline Limestone (12±3)	Sparitic Limestone (10±2)	Micritic Limestone (9±2)	Dolomites (9±3)
		Evaporites		Gypsum (8±2)	Anhydrite (12±2)	
		Organic				Chalk (7±2)
METAMORPHIC	Non Foliated		Marble (9±3)	Homfels (19±4) Metasandstone (19±3)	Quartzites (20±3)	
	Slightly Foliated		Migmatite (29±3)	Amphibolites (26±6)		
	Foliated**		Gneiss (28±5)	Schists (12±3)	Phyllites (7±3)	Slates (7±4)
IGNEOUS	Plutonic	Light	Granite (32±3) Granodiorite (29±3)	Diorite (25±5)		
		Dark	Gabbro (27±3) Norite (20±5)	Dolerite (16±5)		
	Hypabyssal		Porphyries (20±5)		Diabase (15±5)	Peridotite (25±5)
	Volcanic	Lava		Rhyolite (25±5) Andesite (25±5)	Dacite (25±3) Basalt (25±5)	Obsidian (19±3)
		Pyroclastic	Agglomerate (19±3)	Breccia (19±5)	Tuff (13±5)	

*Conglomerates and breccias may present a wide range of m_i values depending on the nature of the cementing material and the degree of cementation, so they may range from values similar to sandstone to values used for fine grained sediments.
**These values are for intact rock specimens tested normal to bedding or folation. The value of m_i will be significantly different if failure occurs along a weakness plane.

Table C.4: Guideline for selection of Modulus Ratio (MR) values based on Deere (1968) and Palmstrom and Singh (2001)

Rock type	Class	Group	Texture			
			Coarse	**Medium**	**Fine**	**Very Fine**
SEDIMENTARY	Clastic		Conglomerates (300–400) Breccias (230–350)	Sandstones (200–350)	Siltstones (350–400) Greywackes (350)	Claystones (200–300) Shales (150–250*) Marls (150–200)
	Non-Clastic	Carbonates	Crystalline Limestone (400-600)	Sparitic Limestone (600–800)	Micritic Limestone (800–1000)	Dolomites (350–500)
		Evaporites		Gypsum (350**)	Anhydrite (350**)	
		Organic				Chalk (1000+)
METAMORPHIC	Non Foliated		Marble (700–1000)	Homfels (400–700) Metasandstone (200–300)	Quartzites (300–450)	
	Slightly Foliated		Migmatite (350–400)	Amphibolites (400–500)	Gneiss (350–750*)	
	Foliated*			Schists (250–1100*)	Phyllites/ Mica Schists (300–800*)	Slates (400–600*)
IGNEOUS	Plutonic	Light	Granite+ (300–550)	Diorite+ (300–350) Granodiorite+ (400–450)		
		Dark	Gabbro (400–500) Norite (350–400)	Dolerite (300–400)		
	Hypabyssal		Porphyries (400**)		Diabase (300–350)	Peridotite (250–300)
	Volcanic	Lava		Rhyolite (300–500) Andesite (300–500)	Dacite (350–450) Basalt (250–450)	
		Pyroclastic	Agglomerate (400–600)	Volcanic Breccia (500**)	Tuff (200–400)	

*Highly anisotropic rocks: the value of MR will be significantly different if normal strain and/or loading occurs parallel (high MR) or perpendicular (low MR) to a weakness plane. Uniaxial test loading direction should be equivalent to field application.
+Felsic Granitoids: Coarse Grained or Altered (high MR), fined grained (low MR).
**No data available, estimated on the basis of geological logic.

Appendix D:
Equations for the analysis of arches made of composite sections

The original document of this appendix is provided in the full paper Carranza-Torres and Diederichs (2009) and is provided here for the reference of readers. Here, a demonstration of the equations for the analysis of composite sections is provided.

Another assumption of the analysis presented here is that the two units '1' and '2' in the composite section are rigidly attached to each other so that if a thrust N is applied to the section, both units '1' and '2' contract axially by the same amount; similarly, if a bending moment M is applied to the section, both units rotate in the same amount (a similar analysis is made for shear forces Q in regard to the resulting distortion of the composite section).

Since the equations involved vary depending on whether the formulation is for thick or for thin shells, the equations for each of these formulations will be discussed separately.

D.1 Analysis of thick sections

The equilibrium condition requires that the total bending moment M along the width b of section is in balance with the bending moments acting on the units '1' and '2' i.e.

$$M = n(M_1 + M_2) \tag{D.1}$$

The relationship between bending moment M and radial displacements u_r and first derivative of the rotation φ with respect to θ is

$$u_r + \frac{d\varphi}{d\theta} = -\frac{MR^2}{K} \tag{D.2}$$

where,

$$\varphi = \frac{du_r}{d\theta} \tag{D.3}$$

The condition that rotations and displacements of the units '1' are the same as the rotations and radial displacements of the units '2', and therefore equal to the rotation and radial displacement of the equivalent section of flexibility coefficient K_{eq}, implies that the following equality holds (see Eq. (D.2)):

$$\frac{M_1}{K_1} = \frac{M_2}{K_2} = \frac{M}{K_{eq}} \tag{D.4}$$

Considering Eq. (D.1) and the equality of the two terms on the left side in expression (D.4), the bending moments M_1 and M_2 transmitted to the units '1' and '2' result

to be,

$$M_1 = \frac{MK_1}{n(K_1 + K_2)} \tag{D.5}$$

$$M_2 = \frac{MK_2}{n(K_1 + K_2)} \tag{D.6}$$

Considering the equality of the two terms on the right side in expression ((D.4)), the flexibility coefficient of the equivalent section consistent with the conditions stated above is,

$$K_{eq} = n(K_1 + K_2) \tag{D.7}$$

The distribution of shear forces are directly 'linked' to the distribution of bending moments. In view that the total shear force Q must be in balance with the shear forces acting on units '1' and '2', then the following equation applies:

$$Q = n(Q_1 + Q_2) \tag{D.8}$$

Thus, the relationship between shear force and radial displacement and rotation (as defined by Eq. ((D.3))) is

$$\frac{du_r}{d\theta} + \frac{d^2\varphi}{d\theta} = \frac{QR^3}{K} \tag{D.9}$$

With the condition that displacements and rotation (and their derivatives respect to the variable θ) are the same for units '1' and '2', and thus the same as for the equivalent section of flexibility K_{eq}, the following equality must hold:

$$\frac{Q_1}{K_1} = \frac{Q_2}{K_2} = \frac{Q}{K_{eq}} \tag{D.10}$$

As with the case of the corresponding equations for bending moments (Eqs. (D.1) and (D.4)), it can be easily shown that the shear forces Q_1 and Q_2 transmitted to units '1' and '2' results to be

$$Q_1 = \frac{QK_1}{n(K_1 + K_2)} \tag{D.11}$$

$$Q_2 = \frac{QK_2}{n(K_1 + K_2)} \tag{D.12}$$

It can be also be shown that the equivalent stiffness K_{eq} in the rightmost side of Eq. (D.10) that is in agreement with Eqs. (D.11) and (D.12) above must also satisfy the Eq. (D.7).

Similarly to the case of bending moment and shear force in Eq. (D.1), the equilibrium condition also requires that the total thrust N along the width b is in balance

with the thrust acting on the units '1' and '2', i.e.,

$$N = n(N_1 + N_2) \tag{D.13}$$

The relationship between thrust N and bending moment M, and the radial displacement u_r and the first derivative of the tangential displacement u_θ with respect to θ is,

$$u_r + \frac{du_\theta}{d\theta} = \frac{M - NR}{D} \tag{D.14}$$

A similar analysis as done with bending moments and shear forces can be done for thrust. The condition that displacements of the units '1' and '2' are the same, and also same as the displacements of the equivalent section of compressibility coefficient D_{eq}, implies that the following equality holds (see Eq. (D.14)):

$$\frac{M_1 - N_1 R}{D_1} = \frac{M_2 - N_2 R}{D_2} = \frac{M - NR}{D_{eq}} \tag{D.15}$$

From Eqs. (D.13) and (D.15), it can be shown that the thrust N_1 and N_2 transmitted to the units '1' and '2' are,

$$N_1 = \frac{N}{n}\frac{D_1}{(D_1 + D_2)} + \frac{M}{nR}\frac{D_2 K_1 - D_1 K_2}{(D_1 + D_2)(K_1 + K_2)} \tag{D.16}$$

$$N_2 = \frac{N}{n}\frac{D_2}{(D_1 + D_2)} - \frac{M}{nR}\frac{D_2 K_1 - D_1 K_2}{(D_1 + D_2)(K_1 + K_2)} \tag{D.17}$$

and the compressibility coefficient of the equivalent section consistent with the conditions stated above results,

$$D_{eq} = n(D_1 + D_2) \tag{D.18}$$

D.2 Analysis of thin sections

The analysis of thin sections is analogous to that of thick sections presented above. In what follows, a step-by-step demonstration is omitted and only the final results are summarized.

For the case of thin sections, the analysis of bending moment yields exactly the same results as for thick sections, i.e., the bending moments M_1 and M_2 transmitted to the units '1' and '2' are,

$$M_1 = \frac{M K_1}{n(K_1 + K_2)} \tag{D.19}$$

$$M_2 = \frac{M K_2}{n(K_1 + K_2)} \tag{D.20}$$

and the flexibility coefficient of the equivalent section, consistent with the conditions

stated above, results

$$K_{eq} = n(K_1 + K_2) \tag{D.21}$$

Also, the analysis of shear forces yield exactly the same results as for thick sections, i.e., the shear forces Q_1 and Q_2 transmitted to the units '1' and '2' are,

$$Q_1 = \frac{QK_1}{n(K_1 + K_2)} \tag{D.22}$$

$$Q_2 = \frac{QK_2}{n(K_1 + K_2)} \tag{D.23}$$

For the case of thin sections, the analysis of thrust yields simpler expressions than for thick sections, i.e., the thrust N_1 and N_2 transmitted to the units '1' and '2' are now,

$$N_1 = \frac{ND_1}{n(D_1 + D_2)} \tag{D.24}$$

$$N_2 = \frac{ND_2}{n(D_1 + D_2)} \tag{D.25}$$

while the compressibility coefficient of the equivalent section is still the same as for the case of thick sections, i.e.,

$$D_{eq} = n(D_1 + D_2) \tag{D.26}$$

D.3 Properties of the equivalent section

It was shown that the compressibility coefficient D_{eq} and flexibility coefficient K_{eq} of the equivalent section are the same whether the thick or thin formulations are considered—compare Eqs. (D.18) and (D.26), Eqs. and (D.7) and (D.21), respectively.

The equivalent section has a height t_{eq} and width b, so if it is considered that this equivalent section is characterized by a Young's modulus E_{eq}, then the compressibility and flexibility coefficients can be written as

$$D_{eq} = E_{eq} t_{eq} b \tag{D.27}$$

$$K_{eq} = E_{eq} \frac{t_{eq}^3 b}{12} \tag{D.28}$$

Solving for the variables t_{eq} and E_{eq} in the set of Eqs. (D.27) and (D.28), considering

also the Eqs. (D.7) and (D.18)—or (D.21) and (D.26)—one gets

$$t_{eq} = \sqrt{12\frac{K_1 + K_2}{D_1 + D_2}} \tag{D.29}$$

$$E_{eq} = \frac{n(D_1 + D_2}{bt_{eq}} \tag{D.30}$$

Eqs. (D.29) and (D.30) are the same Eqs. (3.1) and (3.2) discussed in Section 3.1.2.

Publications

- **Karki, S.**, Chhushyabaga, B., & Khadka, S.S. (2020) An Overview of Design and Construction practices of Himalayan Hydropower tunnels. Journal of Physics: Conference Series 1608 https://iopscience.iop.org/article/10.1088/1742-6596/1608/1/012008/pdf
- Chhushyabaga, B., **Karki, S.** & Khadka, S.S. (2020) Tunnel Support Design in Fault Zone in Hydropower Project in the Himalaya: A case study. Journal of Physics: Conference Series 1608 https://iopscience.iop.org/article/10.1088/1742-6596/1608/1/012009/pdf
- **Karki, S.**, Karki, B., Chhushyabaga, B. & Khadka, S.S. (2020). Design and Analysis of Squeezing Ground Hydropower Tunnel in the Himalaya through a Case Study. Lowland Technology International 21(4). 268-278 https://cot.unhas.ac.id/journals/index.php/ialt_lti/article/view/726
- Chhushyabaga, B., **Karki, S.** & Khadka, S.S. (2020). Fault induced problem in hydropower tunnels in Nepal: A Case Study. Lowland Technology International 21(4). 255-267 https://cot.unhas.ac.id/journals/index.php/ialt_lti/article/view/725
- Khadka, S.S., **Karki, S.**, Chhushyabaga, B. & Maskey, R. (2019). Assessment and Numerical Analysis of Hydropower Tunnel in Lesser Himalayan Region of Nepal - A Case Study. Journal of Physics: Conference Series 1266 https://iopscience.iop.org/article/10.1088/1742-6596/1266/1/012015/pdf